

**CATALYTIC ACTIVITY ENHANCEMENT OF NANO CALCIUM
OXIDE CATALYST VIA THERMAL HYDRATION-DEHYDRATION
TREATMENT FOR BIODIESEL PRODUCTION**

By

CHOOI CHEE YOONG

A dissertation submitted to the Department of Chemical Engineering,
Lee Kong Chian Faculty of Engineering Science,
Universiti Tunku Abdul Rahman,
in partial fulfillment of the requirements for the degree of
Master of Engineering Science Structure A
Sept 2021

ABSTRACT

CATALYTIC ACTIVITY ENHANCEMENT OF NANO CALCIUM OXIDE CATALYST VIA THERMAL HYDRATION-DEHYDRATION TREATMENT FOR BIODIESEL PRODUCTION

CHOOI CHEE YOONG

The reaction rate of biodiesel production at moderate temperature can be accelerated by developing green heterogeneous nanocatalyst from waste source with desired catalytic properties besides offering environmental friendly downstream process with minimum waste generation. This research focused in deducing kinetic mechanism, rate-limiting step and developed kinetic rate law specifically for the biodiesel production catalyzed by green CaO nanocatalyst derived from waste cockle shell via thermal hydration-dehydration treatment. In addition, the CaO nanocatalyst preparation method via thermal hydration-dehydration related parameters (hydration duration, recalcination temperature and recalcination duration) were studied and optimized. The transesterification reaction catalyzed by CaO nanocatalyst followed the Langmuir-Hinshelwood kinetic mechanism with surface reaction as the rate-limiting step. The relatively low activation energy (3786.7 J/mol) for transesterification reaction offered by the CaO nanocatalyst had speed up the reaction rate to 27.3% FAME yield / hr. The optimum condition for the thermal hydration-dehydration treatment used to develop nano CaO catalyst were at 6 h of hydration duration, 650 °C of recalcination temperature and 3 h of recalcination duration. 82 % of biodiesel yield was obtained at moderate temperature of 60 °C and at 5 h reaction time during the transesterification of

palm oil catalysed by the nano CaO. SEM, BET and TPD results proved the CaO nanocatalyst with the existence of large surface area (13.9113 m²/g) and high pore volume (0.0318 cm³/g) that are rich in vacant active sites (1046.46 μmol CO₂/g) and the pore diameter (33.17 nm) were accessible to reactants (triglycerides, methanol) and products (FAME, glycerol).

ACKNOWLEDGEMENTS

I would like to thank everyone who had contributed to the successful completion of this project. I would like to express my gratitude to the University Tunku Abdul Rahman (UTAR), Malaysia for the financial support in project funding through UTAR Research Fund (Project no.: IPSR/RMC/UTARRF/2018-C1/S01).

Additionally, i would like to express my gratitude to my research main supervisor, Dr. Sim Jia Huey for her invaluable advice, guidance and her enormous patience throughout the development of the research. And, I would like to express my gratitude to my research co-supervisor, Dr. Tee Shiau Foon for her invaluable advice in instrumental analysis and Dr. Lee Zhi Hua for her guidance in the writing of dissertation.

In addition, I would also like to express my gratitude to my loving parents and friends who had helped and given me encouragement in completing this report. Without them, I would have not resolved my problems which I had faced during my research work and report writing.

APPROVAL SHEET

This dissertation/thesis entitled “CATALYTIC ACTIVITY ENHANCEMENT OF NANO CALCIUM OXIDE CATALYST VIA THERMAL HYDRATION-DEHYDRATION TREATMENT FOR BIODIESEL PRODUCTION” was prepared by CHOOI CHEE YOONG and submitted as partial fulfillment of the requirements for the degree of Master of Engineering Science Structure A at Universiti Tunku Abdul Rahman.

Approved by:

SIM JIA HUEY

Date: 8/9/2021

Supervisor: SIM JIA HUEY

Department of Chemical Engineering
Lee Kong Chian Faculty of Engineering Science
Universiti Tunku Abdul Rahman

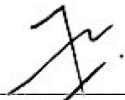


(ChM. Ts Dr Tee Shiau Foon)

Date: 8 September 2021

Co-supervisor

Department of Chemical Engineering
Lee Kong Chian Faculty of Engineering Science
Universiti Tunku Abdul Rahman



(Dr. Lee Zhi Hua)

Date: 9 September 2021

Co-supervisor

Department of Chemical Engineering
Lee Kong Chian Faculty of Engineering Science
Universiti Tunku Abdul Rahman

LEE KONG CHIAN FACULTY OF ENGINEERING SCIENCE

UNIVERSITI TUNKU ABDUL RAHMAN

Date: 8/9/2021 _____

SUBMISSION OF DISSERTATION

It is hereby certified that CHOOI CHEE YOONG (ID No: 1806692) has completed this dissertation entitled “Catalytic Activity Enhancement Of Nano Calcium Oxide Catalyst Via Thermal Hydration-Dehydration Treatment For Biodiesel Production” under the supervision of Dr. Sim Jia Huey (Supervisor) from the Department of Chemical Engineering, Lee Kong Chian Faculty of Engineering Science, Dr. Lee Zhi Hua (Co-Supervisor) from the Department of Chemical Engineering, Lee Kong Chian Faculty of Engineering Science, and Dr. Tee Shiau Foon (Co-Supervisor) from the Department of Chemical Engineering, Lee Kong Chian Faculty of Engineering Science.

I understand that University will upload softcopy of my dissertation in pdf format into UTAR Institutional Repository, which may be made accessible to UTAR community and public.

Yours truly,



(CHOOI CHEE YOONG)

DECLARATION

I hereby declare that the dissertation is based on my original work except for quotations and citations which have been duly acknowledged. I also declare that it has not been previously or concurrently submitted for any other degree at UTAR or other institutions.

Name 

Date 8/9/2021

TABLE OF CONTENTS

ABSTRACT	ii
ACKNOWLEDGEMENTS	iv
APPROVAL SHEET	v
SUBMISSION OF DISSERTATION	vi
DECLARATION	vii
TABLE OF CONTENTS	viii
LIST OF TABLES	xii
LIST OF FIGURES	xv

CHAPTER

1	INTRODUCTION	1
	1.1 Background	1
	1.1.1 World energy consumption	1
	1.1.2 Renewable energy	3
	1.1.3 Biodiesel	4
	1.2 Problem Statement	4
	1.3 Research Aims and Objectives	7
	1.4 Scope of study	8
2	LITERATURE REVIEW	9
	2.1 Commercialized biodiesel production	9
	2.2 Catalyst for biodiesel production	10
	2.2.1 Homogeneous catalyst for biodiesel production	11
	2.2.2 Heterogeneous catalyst for biodiesel production	14
	2.2.3 Acid catalyst	17
	2.2.4 Base catalyst	18

2.3	Nano catalyst	20
2.4	Current research trend of works	21
2.4.1	Nano CaO	21
2.4.2	Thermal decomposition of CaO	22
2.4.3	Nano-CaO Preparation via Thermal-Hydration-Dehydration	23
2.4.4	Factors related to thermal hydration-dehydration treatment	25
2.5	Characterisation of catalyst	28
2.5.1	Thermogravimetric analysis (TGA) for Calcite	28
2.5.2	FTIR analysis of Treated CaO	29
2.5.3	X-ray Diffraction (XRD) Analysis	32
2.5.4	Surface Morphology Analysis via Scanning Electron Microscopy (SEM)	34
2.5.5	Brunauer-Emmett-Teller (BET) analysis	36
2.5.6	Basicity Analysis via Temperature Programmed Desorption (TPD)	37
2.6	Kinetic study of transesterification process	37
2.7	Kinetic study of CaO catalyst	41
2.7.1	Eley-Rideal Kinetics	41
2.7.2	Langmuir-Hinshelwood-Hougen-Watson (LHHW)	42
2.8	Factors that affecting the biodiesel production	45
2.8.1	Dosage of catalyst	45
2.8.2	Reaction time	46
2.8.3	Reaction temperature	47
2.8.4	Alcohol to oil molar ratio	47
3	METHODOLOGY AND WORK PLAN	49
3.1	Project Workflow	49
3.2	Materials and Equipment	52
3.3	Catalyst Preparation	53
3.3.1	CaO catalyst prepared via calcination treatment	53

	3.3.2 Catalyst prepared via thermal hydration and dehydration method	54
3.4	Optimization of thermal-hydration-dehydration treatment	55
3.5	Transesterification reaction of palm oil	56
3.6	Gas chromatography analysis for biodiesel	58
3.7	Characterisation of catalyst	60
	3.7.1 Thermogravimetric & Differential Thermal Analyser (TGS/DTA)	60
	3.7.2 Fourier Transform Infrared (FT-IR)	61
	3.7.3 X-ray Diffraction (XRD)	61
	3.7.4 Scanning Electron Microscopy (SEM) and Energy Dispersive X-ray (EDX)	62
	3.7.5 Temperature Programmed Desorption (TPD)	62
	3.7.6 Brunauer-Emmett-Teller (BET) analysis	63
	3.7.7 High Resolution Transmission Electron Microscopy (HRTEM)	63
3.8	Experimental work for verification of kinetic model	64
4	RESULTS AND DISCUSSION	65
4.1	Catalyst Characterization	65
	4.1.1 Thermogravimetric (TGA) analysis	65
	4.1.2 Fourier Transform Infrared (FT-IR) Analysis	68
	4.1.3 X-ray Diffraction (XRD) Analysis	71
	4.1.4 Scanning Electron Microscopy (SEM) analysis	80
	4.1.5 Energy Dispersive X-ray (EDX) Analysis	85
4.2	Analysis on sintering effects	92
	4.2.1 Temperature Programmed Desorption (TPD) Analysis	93
	4.2.2 Brunauer-Emmett-Teller (BET) Analysis	94
	4.2.3 High Resolution Transmission Electron Microscopy (HRTEM) analysis	99

4.3	Optimization of thermal hydration-dehydration treatment	101
4.3.1	Effect of Hydration duration	102
4.3.2	Effect of Recalcination temperature	104
4.3.3	Effects of Recalcination duration	106
4.3.4	Optimization study	108
4.3.5	Comparison of optimized nano CaO catalyst (6_650_3) with literature	109
4.4	Kinetic mechanism of transesterification reaction catalysed by optimized nano CaO catalyst	113
4.4.1	Derivation of kinetic rate equation:	116
4.4.2	Verification of kinetic equation with experimental data	118
4.4.3	Activation energy and pre-exponential factor	120
5	CONCLUSION AND RECOMMENDATION	123
5.1	Conclusion	123
5.2	Recommendation	124
	REFERENCES	125
	APPENDICES	139

LIST OF TABLES

Table		Page
2.1	Biodiesel production from different types of homogeneous catalysts	13
2.2	Differences between homogeneous and heterogeneous catalysts	15
2.3	Summary of biodiesel production from different types of heterogeneous catalysts	16
2.4	Comparison between acid catalyst with base catalyst	19
2.5	Decomposition temperature and duration for different samples (Lesbani et al., 2016)	23
2.6	Parameters effects study for thermal hydration-dehydration treatment	27
2.7	Surface morphologies of CaO derived from different catalyst sources	35
2.8	Rate constant and activation energy for different catalyst and oil feedstock	40
2.9	Derivation of formula based on Eley-Rideal Kinetics.	41
2.10	Derivation of formula based on Langmuir-	43

Hinshelwood-Hougen-Watson (LHHW).

2.11	Summary of factors and the range of the study for biodiesel production	45
3.1	Materials for biodiesel production	52
3.2	Equipment needed for the research	52
3.3	Denotation of the catalyst samples	56
3.4	Reaction condition for biodiesel production	57
3.5	Type of FAME and their retention time	59
3.6	Reaction condition for kinetic studies	64
4.1	Average crystalline size of different samples	74
4.2	Average crystalline size of different samples	79
4.3	Average weightage of elemental compound in different samples	88
4.4	Average weightage of different parameters	89
4.5	Total basicity of catalysts	93
4.6	BET data for CaO catalyst prepared via calcination treatment, and nano CaO catalyst prepared via thermal hydration-dehydration treatment (6_650_3, 6_950_3 and 6_650_5)	96
4.7	Optimized condition based on the characterization	108

studies and biodiesel yield obtained at 5 h reaction time

- 4.8 Comparison of optimized nano CaO catalyst to synthesized catalyst by other researchers with palm oil as oil feedstock 111

LIST OF FIGURES

Figures		Page
1.1	Global energy consumption from year 2009 to 2019 (Looney, 2020)	1
1.2	Global shares among the fuel types (BP, 2018)	2
2.1	Standard FTIR spectrum of calcium carbonate (CaCO ₃) (WebBook, 2018)	30
2.2	FTIR spectrum of calcium hydroxide (Ca (OH) ₂) (Khachani et al., 2014)	31
2.3	FTIR spectrum of calcined eggshell (CaO) (Nomura et al., 2019)	32
2.4	Standard diffractogram of calcium carbonate (CaCO ₃ , calcite)	33
2.5	Standard diffractogram of CaO.	34
2.6	Standard diffractogram of calcium hydroxide (Ca (OH) ₂)	34
3.1	Research flow diagram	49
3.2	Catalyst preparation from cockle shell to CaO catalyst prepared via calcination treatment and then to nano CaO catalyst prepared via thermal hydration-dehydration treatment	54

3.3	Experimental set-up for biodiesel production	58
4.1	Decomposition of cockle shell	65
4.2	Derivative weight for decomposition of cockle shell	66
4.3	Decomposition of hydrated CaO	67
4.4	Derivative weight for thermal decomposition of hydrated CaO	67
4.5	FT-IR spectra of (a) raw cockle shell, (b) CaO catalyst prepared via calcination treatment, (c) hydrated CaO and (d) nanosized CaO catalyst prepared via thermal hydration-dehydration treatment	69
4.6	XRD analysis of (a) raw cockle shell, (b) CaO catalyst prepared via calcination treatment, (c) hydrated CaO and (d) nano CaO catalyst prepared via thermal hydration-dehydration treatment	73
4.7	XRD analysis for effects of hydration duration	75
4.8	XRD analysis for effects of recalcination temperature	76
4.9	XRD analysis for effects of recalcination duration	76
4.10	Structure of (a) raw cockle shell; (b) CaO catalyst prepared via calcination treatment; (c) hydrated CaO; and (d) nanosized CaO	80

4.11	Effects of hydration duration (a) 3 h; (b) 4 h; (c) 5 h; and (d) 6 h to nano CaO catalyst	83
4.12	Effects of recalcination temperature (a) 650 °C; (b) 750 °C; (c) 850 °C; (d) 950 °C to nano CaO catalyst	84
4.13	Effects of recalcination duration (a) 2 h; (b) 3 h; (c) 4 h and (d) 5 h to nano CaO catalyst	85
4.14	HRTEM analysis of (a) CaO catalyst prepared via calcination treatment, (b) 6_650_3, (c) 6_950_3 and (d) 6_650_5	99
4.15	Preliminary run for transesterification reaction.	101
4.16	The relationship of biodiesel yield and the duration of hydration for 5 h reaction time	103
4.17	The relationship of biodiesel yield and the recalcination temperature for 5 h reaction time	105
4.18	The relationship of biodiesel yield and the recalcination duration	107
4.19	Plot of $\ln \frac{C_{TG0}}{C_{TG}}$ versus time	119
4.20	Arrhenius plot of transesterification reaction catalysed by nano CaO catalyst	121

CHAPTER 1

INTRODUCTION

1.1 Background

1.1.1 World energy consumption

In recent years, the total world energy consumption is increasing gradually. During 2019, the total world energy consumption is marked at approximately 13946 million tonnes of oil equivalent (MTOE). Figure 1.1 shows the global energy consumption from 2009 to 2019.

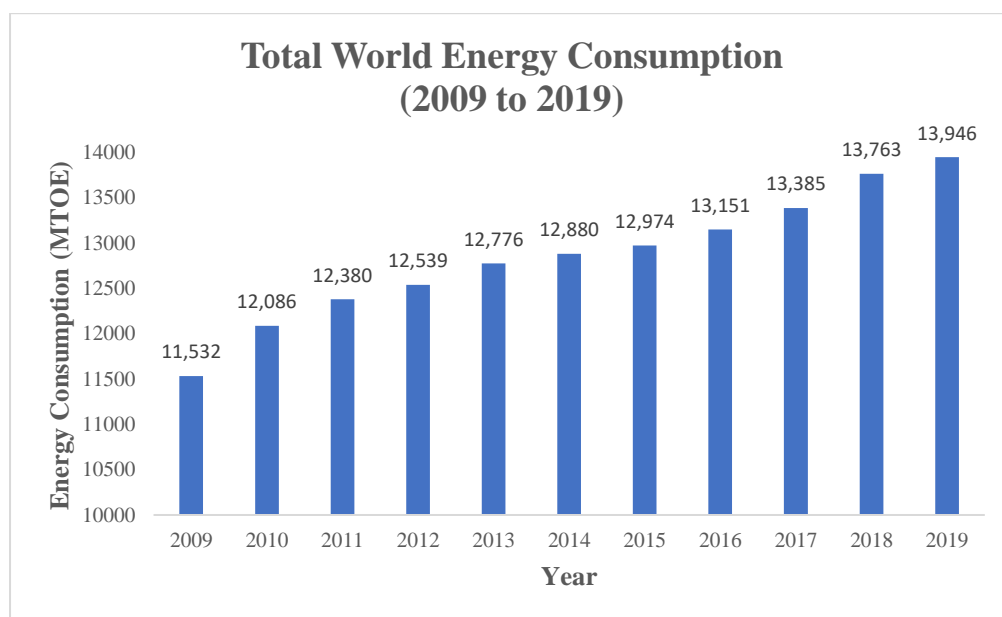


Figure 1.1: Global energy consumption from year 2009 to 2019 (Looney, 2020)

The increment of the world energy consumption is likely to grow by 1.3 % from the year 2017 to 2040 due to the emerging economies whereby

major growth of 50 % in energy consumption is attributed to industries, approximate 30 % of growth is due to construction and around 20% from transportation (Looney, 2020). Figure 1.2 presents the shares among the fuel types where crude oil is still the main energy source among all types of fuels, followed by natural gas and coal. Looney (2020) claimed that renewable energy is the fastest growing fuel source while the demand for the coal in the market may fall to 21 % and replace by natural gas during 2040. Nonetheless, the oil and gas industries are predicted to supply more than half of the global energy source in the future. As the consumption of the energy increased, the depletion of the non-renewable sources is accelerated, especially liquid fuels. In order to ensure a sustainable energy supply in the future, the search for promising renewable fuel for substitution is a must.

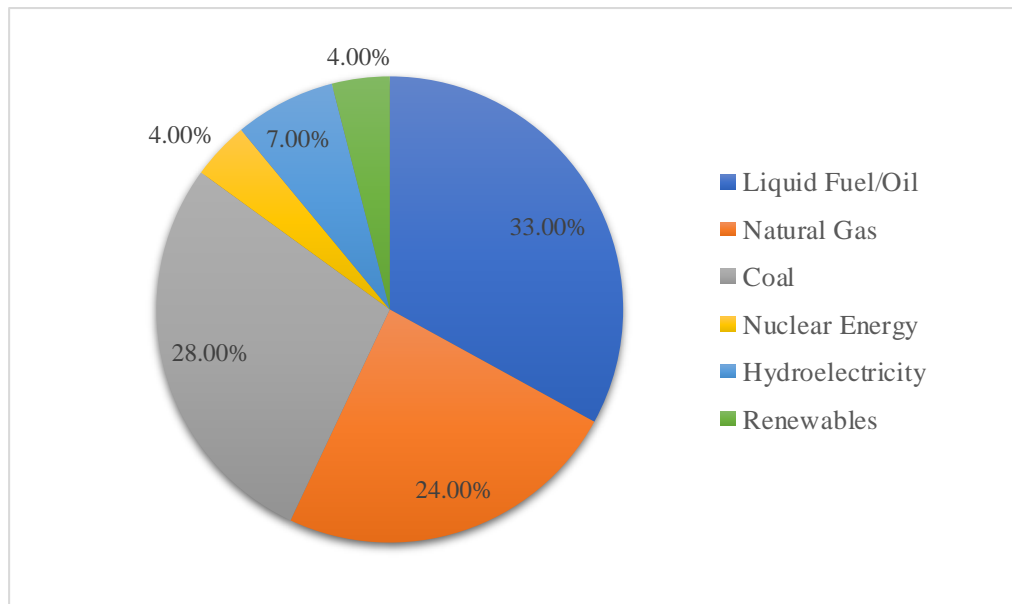


Figure 1.2: Global shares among the fuel types (Looney, 2020).

1.1.2 Renewable energy

Renewable energy can bring down the dependency on non-renewable resources and also provide an alternative solution to reduce the releasing of greenhouse gases (Badriyah, 2018). Thus, renewable energy resources had been discovered such as nuclear energy, hydroelectricity and wind energy to replace the fossil fuels since renewable energy resources are originated from the natural cycles that infinite and never exhausted (Leung *et al.*, 2010; Ahmad *et al.*, 2011; Borges *et al.*, 2012). In terms of economic, renewable energy resources help in stabilize energy prices even though the upfront investments to build the renewable facilities are high compared to fossil fuels (Union of Concerned Scientists, 2018).

Besides that, there is a new megatrend called the energy transition megatrend which was firstly initiated by Germany. Nowadays, many countries have followed the footstep of Germany and implement the process of undergoing energy transition which transitioning from fossil fuel to more clean and sustainable energy (Samah, 2018). In 2017, the global renewable energy generation capacity had increased by 178 GW which become the strongest year even for new capacity additions and bringing the global total capacity to approximately 2200 GW (Adib REN *et al.*, 2018).

1.1.3 Biodiesel

Among the renewable energy resources, biodiesel is a promising fuel to replace the crude oil. Biodiesel is a sustainable renewable resource non-toxic, and environmentally friendly compound. The biodiesel emission contains of neutral carbon dioxide, and zero nitrogen oxides (NO_x), sulphur oxides (SO_x), and particulates (Borges *et al.*, 2012; Cheirsilp *et al.*, 2013). Compared to fossil fuels, the utilization of biodiesel as the fuel reduces the emission of carbon monoxide, unburned hydrocarbons, particulate matters and net carbon dioxide emission per life cycle by a significant amount (Ezebor *et al.*, 2014) which prove that the application of biodiesel can reduce the negative impacts of fossil fuels to the environment.

Besides, Ahmad *et al.* (2011) reported that biodiesel can be applied in the conventional diesel engine with simple modification. In comparison, biodiesel gives higher lubricity and durability than conventional diesel fuel due to the absence of sulphur (Dehkhoda *et al.*, 2010). Besides, the raw materials that needed for biodiesel production such as palm oil and calcium-based compound are available in Malaysia which give advantage to the production of biodiesel (Yusuf *et al.*, 2011).

1.2 Problem Statement

Rapid growth of human population and industrialization has caused the fast diminishing of energy resources. Biodiesel, a renewable resource has the

massive potential to replace non-renewable resource of crude oil. However, biodiesel is still unable to substitute the crude oil as primary energy source due to the comparatively higher selling price of biodiesel. The expensive production cost of biodiesel is partly due to the difficulties in developing cheap catalyst materials with excellent catalyst properties. Numerous studies have shown that calcium oxide (CaO) catalyst derived from different waste resources such as egg-shell (Mosaddegh *et al.*, 2014), chicken manure (Maneerung *et al.*, 2016) and abalone shell (G.Y. Chen *et al.*, 2016), possess good catalytic activity with biodiesel yield ranging between 80% - 90%.

However, the catalytic performance of these catalysts is considered low in terms of the reaction time. It is reported that waste shell derived CaO required more than 6 h to achieve high biodiesel yield and thus the catalyst has low commercial value. This low catalytic activity is due to low basicity and reduced surface area of waste shell derived CaO catalyst. As a result, the production of biodiesel can be enhanced by developing nano sized CaO catalyst. The high surface area to volume ratio of the nano size catalyst will increase the conversion of biodiesel greatly. According to Reddy *et al.* (2006), low biodiesel conversions (approximately 2%) of biodiesel was found when the commercial CaO catalyst with low surface area ($1 \text{ m}^2/\text{g}$) was used in the process. When the reaction was replaced with a nanocrystalline CaO catalyst ($90 \text{ m}^2/\text{g}$), the biodiesel conversion was found to be 99% under the same conditions. This has proven that the surface area of the catalyst plays the major role in determining the conversion of biodiesel.

Nano catalyst can be developed by using a top-down or bottom-up approach (Islam *et al.*, 2007). Top-down approach refers to the bulk material where it is being broken down into smaller particles by mechanical grinding (Schmidt, 2001), thermal breakdown (Zhang *et al.*, 2003) or chemical breakdown (Garrigue *et al.*, 2004) while bottom-up approach is carried out via reaction or agglomeration such as sol-gel method, template-directed, precipitation and microemulsion. In this study, nano-sized CaO catalyst will be produced from waste cockle shells and, thermal hydration-dehydration technique is chosen to enhance the basicity and surface area of the CaO catalyst even though bottom-up approach will give uniform and well-defined structure on the catalyst (Zahmakiran *et al.*, 2011). This is because the thermal hydration-dehydration method exhibits the lowest operating cost compared to bottom-up methods which requires expensive chemical precursors and critical reaction conditions (Nadagouda *et al.*, 2006).

In this research, important parameters of thermal hydration-dehydration treatment such as hydration duration, recalcination temperature and recalcination duration were optimized towards the most favourable catalyst properties where the CaO catalyst expected in nano size (within the range of 1 to 100 nm) with high yield of biodiesel in relatively short reaction time. The physical and chemical properties of waste cockle shell, CaO catalyst prepared via calcination treatment, hydrated CaO and nano CaO catalyst prepared via thermal hydration-dehydration treatment were investigated using various instruments; X-ray diffractometry (XRD), scanning electron microscopy (SEM), energy dispersive X-ray spectroscopy (EDX),

temperature-programmed desorption (TPD), Brunauer–Emmett–Teller (BET) and High-Resolution Transmission Electron Microscopy (HRTEM). The catalytic performance of the nano CaO catalysts were compared based on the yield of biodiesel from the transesterification reaction of palm oil-based cooking oil. Lastly, a kinetic mechanism for transesterification process that catalysed by nano CaO catalyst derived from waste cockle shells was developed and verified with experimental data.

1.3 Research Aims and Objectives

The research aims to enhance the catalytic activity of nano CaO catalyst via thermal hydration-dehydration treatment for the biodiesel production. The objectives of this research are listed in the following:

1. To optimize the catalytic activity of nano CaO catalyst prepared via thermal hydration-dehydration treatment for biodiesel production by varying the hydration duration, recalcination duration and recalcination temperature during the synthesis.
2. To characterize the physical and chemical properties of waste cockle shell, CaO catalyst prepared via calcination, hydrated CaO catalyst and nano scale CaO catalyst prepared via thermal hydration-dehydration treatment.

3. To deduce the kinetic mechanism and subsequently formulate kinetic model for the transesterification reaction catalysed by nano CaO catalyst for biodiesel production.

1.4 Scope of study

The scopes of this research are in line with the objectives of the research. Firstly, CaO catalyst was produced by calcination of waste cockle shell. The catalyst produced was treated via the thermal-hydration-dehydration treatment. The effects of hydration duration, recalcination temperature and recalcination duration was studied and optimized. The performance of the CaO catalyst prepared via calcination treatment and nano CaO catalyst were compared by transesterification reaction of palm cooking oil. The physical and chemical properties of raw cockle shell, CaO catalyst prepared via calcination treatment, hydrated CaO and nano CaO catalyst prepared via thermal hydration-dehydration treatment were characterised by using various instruments such as Thermogravimetric analysis (TGA), X-ray diffractometry (XRD), scanning electron microscopy (SEM), energy dispersive X-ray (EDX) spectroscopy, Brunauer-Emmett-Teller (BET) analysis, temperature-programmed desorption (TPD) and High-Resolution Transmission Electron Microscopy (HRTEM). Kinetic mechanism was deduced for the transesterification of palm oil catalysed by optimized nano CaO catalyst.

CHAPTER 2

LITERATURE REVIEW

2.1 Commercialized biodiesel production

Nowadays, biodiesel is produced by esterification and transesterification reactions from edible and non-edible vegetable oils or animal fats with primary alcohols in the presence of an acid- or base-catalyst (Ejikeme *et al.*, 2010). Homogeneous alkaline catalyst transesterification is more favourable in commercial biodiesel production as base catalyst gives a high Fatty Acid Methyl Ester (FAME) yield in a short reaction time and having a simple set up for the reaction (Thanh *et al.*, 2012). Nevertheless, the poor-quality oil feedstocks containing high amount of free fatty acids need to be removed as it will react with base catalyst to form soap as by-product during the reaction.

According to Thanh *et al.* (2012), the conventional way to carry out biodiesel production on the industrial scale is mechanical stirring method with a batch reactor since the operation is simple and low cost. However, longer reaction duration is required to obtain high yield of FAME and the separation of biodiesel from the reaction mixture is difficult. In order to solve the problems, the ultrasonic irradiation and co-solvent methods have been discovered and applied for the biodiesel production on the industrial scale. With these innovative methods, the reaction duration is being shorten and the

raw material consume efficiently. The catalysts that used in biodiesel production will be further discussed in section 2.2.

2.2 Catalyst for biodiesel production

In the production of biodiesel, transesterification reaction and esterification can be proceeded either with catalyst or without catalyst. Catalyst is a substance that reduces the activation energy for a chemical reaction which increased the yield of main product and decrease the duration of reaction time. Without the catalyst, the reaction will occur in slower rate. A fast reaction rate can be achieved without catalyst, yet, supercritical methanol and co-solvent has to be used where the transesterification and esterification reaction can be completed in 10 minutes at the operating temperature of 623 K (Cao *et al.*, 2005) and the esterification reaction itself can be completed under the conditions of 453 K to 493 K (Santacesaria *et al.*, 2020).

In the absence of catalyst, the operation cost for biodiesel production will be expensive since more consideration has to be taken for developing the unit operations to maintain the operating conditions during the transesterification reactions (Atabani *et al.*, 2012). With the utilization of catalysts in transesterification reaction, milder operating condition is needed to achieve the favourable reaction rate and biodiesel yield as the activation energy of the reaction reduced (Yoo *et al.*, 2010). Besides, the incorporation of catalyst in biodiesel production will be greener to the environment and cost effective.

According to Yoo *et al.* (2010), a better yield of biodiesel was obtained as catalyst is applied during the production. There are three different kind of catalyst that utilized in transesterification process and esterification process which are acid (Balat, 2007), alkali (Talebian-Kiakalaieh *et al.*, 2013), and enzyme catalyst (Canakci *et al.*, 1999). Among the catalysts, alkali and acid catalysts are most common compared to enzyme catalysts (Leung *et al.*, 2010). Enzyme catalysts are not commercially used due to the long duration of chemical reaction and expensive cost although it can reduce the soap formation during the biodiesel production and having simple purification work step (Leung *et al.*, 2010). In general, the catalyst is grouped by its phase with the reactants. For the catalyst that having same phase as reactants, it is homogenous while different phase from reactants is classified as heterogeneous.

2.2.1 Homogeneous catalyst for biodiesel production

Homogeneous acid catalysts used for biodiesel production are sulphuric acid or phosphoric acid while homogeneous base catalysts are potassium hydroxide or sodium hydroxide. Some problems may arise during the transesterification reaction that accompanied with homogeneous catalysts although it have better catalytic performance compared to heterogeneous catalysts (Karmakar *et al.*, 2010).

The recovery of catalysts involves a series of work step such as, neutralization of the acidic or basic catalyst, tremendous amount of wastewater, and the

drying process need to be applied as the biodiesel is having high moisture content at the end of separation process. As a result, the operation cost was increased and the duration of the production will be longer which shows the catalyst not feasible (Borugadda *et al.*, 2012; N. Kumar *et al.*, 2013). Table 2.1 shows the types of homogeneous catalysts that used for biodiesel production.

Table 2.1: Biodiesel production from different types of homogeneous catalysts

Oil	Catalyst	Alcohol to oil molar ratio	Process duration(min)	Process temperature (K)	Yield (%)	Reference
Palm fatty acid	H ₂ SO ₄	7.2 :1	120	343	99.6	(Chongkhong <i>et al.</i> , 2009)
Waste Cooking Oil (WCO)	KOH	6:1	60	343	98.2	(Agarwal <i>et al.</i> , 2012)
Castor oil	KOH	9 :1	30	333	95.0	(Keera <i>et al.</i> , 2018)
Rapeseed oil	1-butyl-3-methylimidazolium imidazolid	6 :1	60	333	95.0	(Luo <i>et al.</i> , 2013)
Cottonseed oil	NaOH	6 :1	60	323	95.0	(Shankar <i>et al.</i> , 2017)

2.2.2 Heterogeneous catalyst for biodiesel production

Similar to homogeneous catalyst, the heterogeneous catalyst can be acidic or basic. The types of heterogeneous acid catalysts include sulphated metal oxides and sulphated zeolites whereas heterogeneous alkali catalyst includes calcium oxide and magnesium oxide. By comparing homogeneous catalysts to heterogeneous catalysts, operating with heterogeneous catalysts are having cheaper operation cost, simpler separation process and the catalyst are more environmentally friendly (Yaakob *et al.*, 2013). Table 2.2 shows the differences between homogeneous and heterogeneous catalysts.

Nonetheless, there are some disadvantages with heterogeneous catalysts such as slower reaction rate, higher difficulty in catalyst preparation works and the operating conditions are more energy intensive (Atadashi *et al.*, 2011; Sharma *et al.*, 2011). Table 2.3 shows the studies on the application of various types of heterogeneous catalysts in biodiesel production by researchers.

Table 2.2: Differences between homogeneous and heterogeneous catalysts.

Factors	Catalyst		References
	Homogeneous	Heterogeneous	
Rate of reaction	Fast with high conversion	Moderate conversion	(Atadashi <i>et al.</i> , 2011)
Recovery of catalyst	Catalyst unrecoverable, must be neutralized leading to waste chemical production	Catalyst can be recovered	(Dwivedi <i>et al.</i> , 2011)
Processing methodology	Limited used of continuous methodology	Continuous fixed bed operation possible	(Atadashi <i>et al.</i> , 2011)
Presence of water/Free Fatty Acid	Sensitive	Not sensitive	(Karmakar <i>et al.</i> , 2010)
Catalyst reusability	Not possible	Possible	(Yaakob <i>et al.</i> , 2013)
Operation cost	Comparatively costly	Potentially cheaper	(N. Kumar <i>et al.</i> , 2013)

Table 2.3: Summary of biodiesel production from different types of heterogeneous catalysts.

Oil	Catalyst	Alcohol to oil molar ratio	Process temperature (K)	Process duration (min)	Yield (%)	Reference
Waste Cooking Oil	ZS/Si	1:18	473	600	98.0	(Jacobson et al., 2008)
Palm Oil	CaO/Al ₂ O ₃	12:1	338	378	95.0	(Zabeti <i>et al.</i> , 2010)
Soybean	K/BC-Fe ₂ O ₃	8:1	333	60	98.0	(Liu <i>et al.</i> , 2018)
Crude palm kernel oil	SO ₄ ²⁻ /ZrO ₂	6 :1	473	60	90.3	(Kumar Naik <i>et al.</i> , 2008)
Canola oil	Nano-g- Al ₂ O ₃	15 :1	338	480	97.7	(Boz <i>et al.</i> , 2009)
Sunflower oil	WO ₃ /ZrO ₂	20 :1	473	300	97	(Sunita <i>et al.</i> , 2008)

2.2.3 Acid catalyst

Generally, acid catalyst is more favourable than base catalyst for the production of biodiesel. It is because the acid catalyst can act as the esterification reagents and the solvent during the biodiesel production (Balat, 2007). During the acid catalysis process, the free fatty acid was converted into alkyl esters or biodiesel as final product (Lam *et al.*, 2010). Thus, the production involved only a single step since the esterification and transesterification reaction can occur simultaneously.

Moreover, the water content and free fatty acid content would not affect the performance of acid catalysts, hence, the feed stocks with free fatty acid content greater than 1 % can be used (Clark *et al.*, 1981). Nevertheless, there are some shortcomings during the application of acid catalyst. Long reaction time was required for the acid catalysts to achieve the favourable yield of biodiesel as the reaction rate was slower compared to base catalysis process (Nye *et al.*, 1983).

Additionally, there would be high acid content in the product stream with the usage of acid catalyst. The acid content can lead to serious corrosion and environmental problems (Loterio *et al.*, 2005). As a result, these would cause an additional operation cost for the treatment of acidic wastewater before discharging to the environment.

2.2.4 Base catalyst

Compared to acid catalyst, base catalyst has higher accessibility, shorter reaction time and lower operation cost (Talebian-Kiakalaieh *et al.*, 2013). Mandolesi de Araújo *et al.* (2013) claimed that homogeneous alkali catalysts such as sodium methoxide (Bhuiya *et al.*, 2016), sodium hydroxide (NaOH) and potassium hydroxide (KOH) are frequently used to catalyse the transesterification reaction. Researchers reported that there was no formation of water during the transesterification reaction that catalysed with base catalyst (Sharma *et al.*, 2008).

However, the performance of base catalyst would be affected by the saponification reaction when the reaction contains sufficient amount of water and free fatty acids. The base catalyst would react with free fatty acids (FFA) and form the soap and thus resulted in low biodiesel yield. Besides, the formation of emulsions tends to increase the difficulty in the purification of the biodiesel at the end of transesterification. In order to avoid the saponification reaction, the feed stock for the transesterification reaction need to undergo pre-treatment to ensure the water content to be approximately zero and free fatty acid content below 1 % (Marchetti *et al.*, 2007; Enweremadu *et al.*, 2009; Zhang *et al.*, 2014). A comparison of acid catalyst and base catalyst has been shown in Table 2.4.

Table 2.4: Comparison between acid catalyst with base catalyst

Type of catalyst	Advantages	Disadvantages
Acid catalyst	<p>Immune to free fatty acid and water content in the feedstock (Lotero <i>et al.</i>, 2005) and saponification reaction is inhibited.</p> <p>Waste cooking oil can be used as feedstock (Lam <i>et al.</i>, 2010).</p> <p>Esterification and transesterification can be carried out simultaneously (Lam <i>et al.</i>, 2010).</p>	<p>Slower reaction (Sharma <i>et al.</i>, 2008).</p> <p>Formation of salt can cause corrosion problem (Leung <i>et al.</i>, 2010).</p> <p>Higher reaction conditions and longer duration compared to base catalyst (Leung <i>et al.</i>, 2010).</p>
Base catalyst	<p>No formation of water during transesterification reaction (Atadashi <i>et al.</i>, 2013).</p> <p>Faster reaction rate than acid catalyst (Atadashi <i>et al.</i>, 2013).</p> <p>Lower activation energy and mild reaction condition for the process (Lam <i>et al.</i>, 2010).</p>	<p>Sensitive to free fatty acid content and water content in the feedstock (Lam <i>et al.</i>, 2010).</p> <p>Saponification will occur simultaneously as free fatty acid content greater than 1 % which lead to low biodiesel yield (Lam <i>et al.</i>, 2010).</p> <p>High difficulty in purification step (Atadashi <i>et al.</i>, 2013) and generate high amount of wastewater (Leung <i>et al.</i>, 2010).</p>

2.3 Nano catalyst

In general, the materials with one or more geometrical dimension that is within the range of 1 to 100 nm will be classified as nanomaterials (Bensebaa, 2013). Nano catalyst is important to the industry as the characteristic of the catalyst can be further enhanced when the catalyst is present in nanosized. It is because the smaller the size of catalyst, the greater the surface to volume ratio. The improved pore sizes and larger surface area in nano catalyst would lead to the increased number in active sites (Banković-Ilić *et al.*, 2017). Therefore, nano catalysts are expected to have high catalytic activity and selectivity approximately 100 %, longer lifespan and reduce the activation energy require in the chemical reaction. Moreover, mild reaction condition was applied to the process that catalysed by nano catalyst (Philippot *et al.*, 2012).

Nanoparticles can be synthesized through two different methods either physical method or the chemical method. The physical method involves a higher capital costs compared to chemical approach due to the physical method is high energy dependency (Bensebaa, 2013). Normally, nano catalysts can be formed by using a top-down or bottom-up approach (Islam *et al.*, 2007). In terms of top-down approach, the bulk material was being broken down into smaller particles by mechanical grinding (Schmidt, 2001), thermal breakdown (Zhang *et al.*, 2003) or chemical breakdown (Garrigue *et al.*, 2004) which may cause non-uniform characteristics among the broken particles (Ahmad *et al.*, 2011). On contrary, the bottom-up approach needs reaction or agglomeration of suitable starting molecules with or without structure-

directing agents (Yilmaz *et al.*, 2009) such as sol-gel method, template-directed, precipitation and microemulsion. In comparison, bottom-up approach is more commonly applied (Zahmakiran *et al.*, 2011) due to its well-defined and uniform structure of the catalysts in terms of size, shape and surface composition (El-Sayed, 2004) even though the approach involves critical reaction conditions with the expensive precursors and structure directing agents (Nadagouda *et al.*, 2006).

2.4 Current research trend of works

Researchers had discovered different solid catalysts in nano size. For instance, amorphous alumina powder (Amini *et al.*, 2013), $K_2O/\gamma-Al_2O_3$ (Han *et al.*, 2009), Fe_3O_4 (Tamilmagan *et al.*, 2015), $Ca/Al/Fe_3O_4$ (Tang *et al.*, 2012), $Cs-Ca/SiO_2-TiO_2$ (Feyzi *et al.*, 2015), $K_2CO_3/Al-Ca$ (Sun *et al.*, 2014) and others. In comparison, the calcium-based compounds are more favourable to be utilized in transesterification of different oil feedstocks as it only requires mild reaction conditions and results in high yield of biodiesel (Kesic *et al.*, 2016).

2.4.1 Nano CaO

Based on researchers, CaO has the potential to act as catalyst in the biodiesel production under mild reaction conditions (Chen *et al.*, 2014). In comparison, nano size CaO has a simple preparation work steps than other solid catalysts. According to Banković-Ilić *et al.* (2017), there are two major steps in catalyst preparation works, which are the preparation of the nano CaO and the

activation of the nano CaO. Several ways can be used during the preparation works such as thermal decomposition, impregnation and precipitation. At last, calcination is normally applied to activate the catalytic activity of nano CaO.

2.4.2 Thermal decomposition of CaO

Thermal decomposition defines that the fresh raw material will be decomposed and thus increased the active sites on the surface under high temperature condition. Normally, the efficiency of the catalyst is measured by the number of basic sites in the catalyst.

Generally, CaO is unstable substance under normal condition and the CaO compound can be obtained through the decomposition of calcium carbonate. Due to the instability of CaO at room temperature, carbon dioxide in the air and water would tend to poison the basic sites of CaO and thus reduces the catalytic activity of CaO. Moreover, the number of active sites on the surface of the CaO is dependent on the calcination environment and temperature. As the calcination temperature increased, there would be decomposition of undesired substances and formation of active sites on the particle surface (Hattori, 1995).

According to Smith *et al.* (2013), when the calcination temperature of calcium carbonate fall within the range of 350 °C to 550 °C, the structure of calcium carbonate remained unchanged which gave no effect to the biodiesel yield. When temperature beyond 670 °C, decomposition of calcium carbonate

and the formation of CaO occurred simultaneously (Muciño *et al.*, 2014). Roschat *et al.* (2012) claimed a complete transformation of calcium carbonate (CaCO₃) to CaO need a long calcination duration. However, prolonged calcination duration would lead to sintering effects which reduced the surface area of the catalyst and led to negative impact to catalytic performance (Micic *et al.*, 2015). Table 2.5 shows the temperature and duration of decomposition for different waste shell to obtain calcium oxide (Lesbani *et al.*, 2016).

Table 2.5: Decomposition temperature and duration for different samples (Lesbani *et al.*, 2016)

Sample	Decomposition temperature (°C)	Time of decomposition (h)
Mollusk	900	2.5
Freshwater mussel shell	900	4
Oyster shell	1000	3
Crab shell	800	2
Waste egg shell	1000	2
Snail shell	700	3
Fish bone	1000	3

2.4.3 Nano-CaO Preparation via Thermal-Hydration-Dehydration

Recently, different treatment methods were proposed by researchers to improve the catalytic performance of CaO catalyst. The surface morphology and the basicity of the nano CaO catalysts are dependent on its precursor. For example, relatively higher biodiesel yield in the biodiesel production was

observed when CaO catalyst was obtained from calcining calcium hydroxide rather than from calcining calcium carbonate (Cho *et al.*, 2009).

According to Yoosuk, Udomsap and Puttasawat (2011), the hydration-dehydration technique was applied subsequently to improve the catalytic activity of CaO catalyst by increasing its basicity and specific surface area. This treatment had generated a nanosized of CaO with large number of basic sites and large surface area to volume ratio that further enhanced the biodiesel yield. Thus, thermal hydration-dehydration treatment had its potential to improve the catalytic activity of CaO catalyst.

During the hydration process (eq 2.2), the calcined CaO was refluxed in water for a certain period of time. After that, the hydrated CaO is dried and undergo recalcination (eq 2.3) for the catalyst activation purpose:

Thermal decomposition of CaO:



Hydration of CaO:



Dehydration of Ca (OH)₂:



During the reflux of calcined catalyst, there was a transformation of oxide structures into hydroxide structures which increased the volume of the grains. Therefore, there would be cracking on the surface of the sample when the particles expanded. During the recalcination, the water molecules that bonded with CaO would detach from the lattice surface and the crystallites were fractionated and resulted in nanosized crystallites. The evolution of water molecules can help to enhance the total porosity and pore diameter in the catalyst (Yoosuk *et al.*, 2011; Asikin-Mijan *et al.*, 2015).

2.4.4 Factors related to thermal hydration-dehydration treatment

During the synthesis of catalyst via thermal hydration-dehydration, three factors of hydration duration, recalcination temperature and recalcination duration significantly influence the catalytic performance of CaO catalyst. Table 2.6 shows the research studies on the effect of the factors and the corresponding range of the factors used.

The catalytic performance can be estimated by determining the basicity of CaO catalyst. According to Asikin-Mijan, Taufiq-Yap and Lee (2015), the basicity of CaO catalyst is directly proportional to the hydration duration. The catalysts were prepared under different hydration duration of 1 h, 3 h, and 6 h

and the basicity were determined by using TPDRO analysis and they found that basicity increased with the hydration duration which can then enhance the catalytic performance of CaO catalyst.

For the recalcination temperature, Roschat *et al.* (2018) reported that there was a total weight loss around 25 wt% for hydrated CaO when the recalcination temperature reached 400 °C. This is due to the decomposition of calcium hydroxide and evolution of water molecules. A small weight loss approximately 0.5 wt% was occurred subsequently when the temperature was ranging from 450 °C to 650 °C which indicated that the CO₂ were removed from CaCO₃ to CaO. In result, the minimum recalcination temperature is set at 650 °C. Similarly, Ljupkovic *et al.* (2014) found that the weight percentage of the hydroxide in the calcined CaO (under 500 °C) sample is around 10 to 15 %, and the carbonate content approximately 5 %. As the calcination temperature higher than 500 °C, there were much lower amounts of the hydroxide and carbonate in the samples. In other word, as the recalcination temperature increased the lower the weight percentage of hydroxide and carbonate.

The calcination duration can be a factor to affect the crystalline size of the catalyst. According to Reli *et al.* (2012), as the calcination duration increased under the same calcination temperature, an increase in crystalline size was observed. This also indicated that the specific surface area of the catalyst (under BET analysis) reduced simultaneously. The calcination

Table 2.6: Parameters effects study for thermal hydration-dehydration treatment

Factors	Catalyst	Parameters	Biodiesel Yield (%)	References
Hydration duration	CaO derived from calcite	6 h	95.7	(Yoosuk <i>et al.</i> , 2011)
	CaO derived from commercial CaCO ₃	6 h	95	(Roschat <i>et al.</i> , 2018)
Recalcination temperature	Commercial CaO	700 °C to 800 °C	-	(Micic <i>et al.</i> , 2015b)
	Nano CaO derived from chemical precursors	900 °C	96.2	(Harsha <i>et al.</i> , 2017)
Recalcination duration	CaO derived from waste shell	2 to 4 h	92 to 94	(Viriya-empikul <i>et al.</i> , 2012)
	TiO ₂ /kaolinite composite	1 to 3 h	-	(Reli <i>et al.</i> , 2012)

duration was recommended within 2 h; thus, the prolonged calcination duration is not favourable to the catalyst as it indirectly cause a reduction to the amount of active site expose to the reaction environment.

2.5 Characterisation of catalyst

2.5.1 Thermogravimetric analysis (TGA) for Calcite

The suitable calcination temperature for calcium compounds were determined by using Thermogravimetric analysis and differential thermal analysis (TGA-DTA). TGA-DTA can detect the trend of a sample mass as a function of temperature and/or time. During the test, the measurements of these changes are made using a thermobalance and programmed heating rate in an enclosed system with a controlled atmosphere. The analysis was usually conducted under a flow of nitrogen and the major phase of calcium compound in the eggshell was converted into nano crystal CaO within calcination temperature of 600 °C to 900 °C (Mosaddegh *et al.*, 2014).

During the calcination, there was a mass loss due to the decomposition of calcite and released of carbon dioxide. There are three important decomposition for calcium-based catalyst during recalcination which are detachment of the physisorbed water molecules from the sample surface, dehydroxylation (removal of hydroxide) and decarbonization (removal of carbon) processes (Ljupkovic *et al.*, 2014). Micic *et al.* (2015) reported that there were two endothermic processes were observed in thermogram, first

reaction was occurred at 450 °C and the second reaction was occurred at 650 °C (Vujicic *et al.*, 2010). The calcium hydroxide break into the calcium hydroxide-calcium oxide CaO interphase during the first endothermic process while the evolution of the water molecules occurred in second endothermic process (Micic *et al.*, 2015).

According to Khachani *et al.* (2014), removal of water molecules from Ca(OH)₂ were observed between temperatures 390 and 480°C, with an endothermic peak at temperature of 462 °C. The mass retained is about 24 %, near to the value expected for formation of CaO. When the temperature increased and above 600°C, a second mass reduction is occurred due to decarbonation process of CaCO₃.

2.5.2 FTIR analysis of Treated CaO

FTIR analysis can use to identify different phases of organic and inorganic compounds. Calcium carbonate has different phases, for example, calcite and aragonite due to the differences in their carbonate ions. Carbonate ions and similar molecules have four normal modes of vibration peaks such as symmetric stretching, out of plane bending, doubly degenerate planar asymmetric stretching and doubly degenerate planar bending (Wang *et al.*, 2010). The FTIR spectra can show the differences between the untreated CaCO₃ and calcined CaCO₃ (Maneerung *et al.*, 2015).

For the raw CaCO_3 , the existence of great peak at 1424.29 cm^{-1} was belong to asymmetric stretching while the minor bands at 873.95 and 711.26 cm^{-1} were responding to the out-of-plane band and in-plane band vibration modes of carbonate (CO_3^{2-}) group, correspondingly (Maneerung *et al.*, 2015). Similar to Rodriguez-garcia (2009), the bands located around 1444 and 877 cm^{-1} are belonging to the two different elongation modes of C—O bonds while the bands present approximately to 2980 , 2875 , 2513 and 794 cm^{-1} are harmonic vibration of these elongation modes. The band at 713 cm^{-1} is related to Ca—O bonds. The minor bands at 2875 cm^{-1} , the first overtone at 2990 cm^{-1} , and the thin and intense band at 1795 cm^{-1} are associated to the carbonate C=O double bonds. The standard spectra for calcium carbonate was showed in the Figure 2.1.

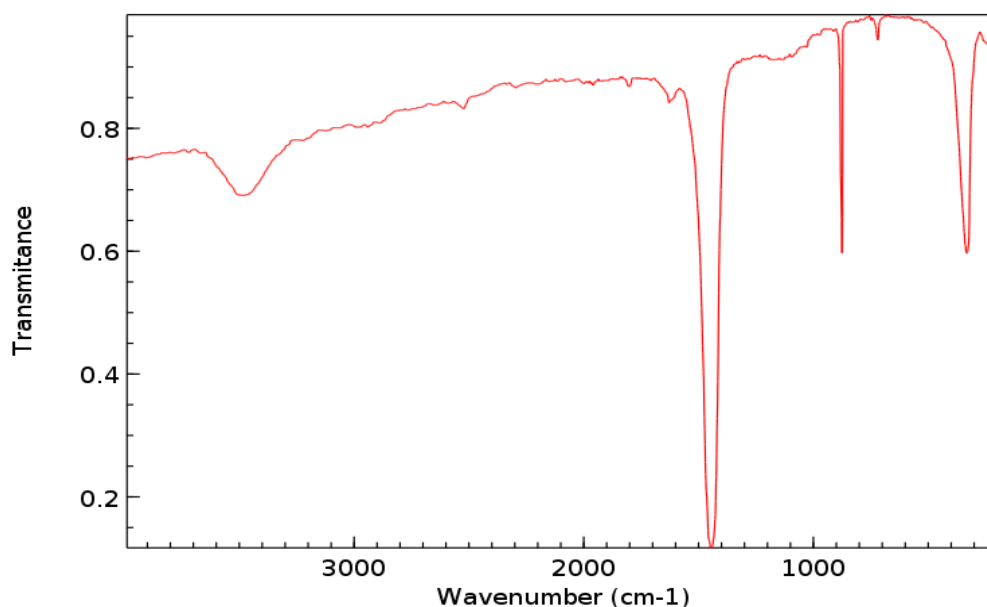


Figure 2.1: Standard FTIR spectrum of calcium carbonate (CaCO_3) (WebBook, 2018)

As the temperature of calcination increasing from $600\text{ }^\circ\text{C}$ to $900\text{ }^\circ\text{C}$, the peaks that related to carbonate (CO_3^{2-}) group were reduced gradually and absent at the highest temperature which indicated the decomposition of

calcium carbonate into CaO. In FTIR spectrum of CaO, the peak located at 3640 cm^{-1} was referred to the hydroxide ions which formed by reaction between CaO with water vapour in the atmospheric air (Putra *et al.*, 2017) and the band at 875 cm^{-1} corresponds to Ca—O bonds (Rodriguez-garcia, 2009). According to Rodriguez-garcia (2009), the band at 1790 cm^{-1} corresponds to C=O bonds while the intense and wide band at 1427 cm^{-1} corresponds to C—O bonds from carbonate due to the carbonation of CaO with carbon dioxide under atmospheric pressure. Figure 2.2 shows the standard FTIR spectrum of calcium hydroxide (Ca (OH)₂) and Figure 2.3 shows the spectrum for calcined egg-shell which chemically is CaO.

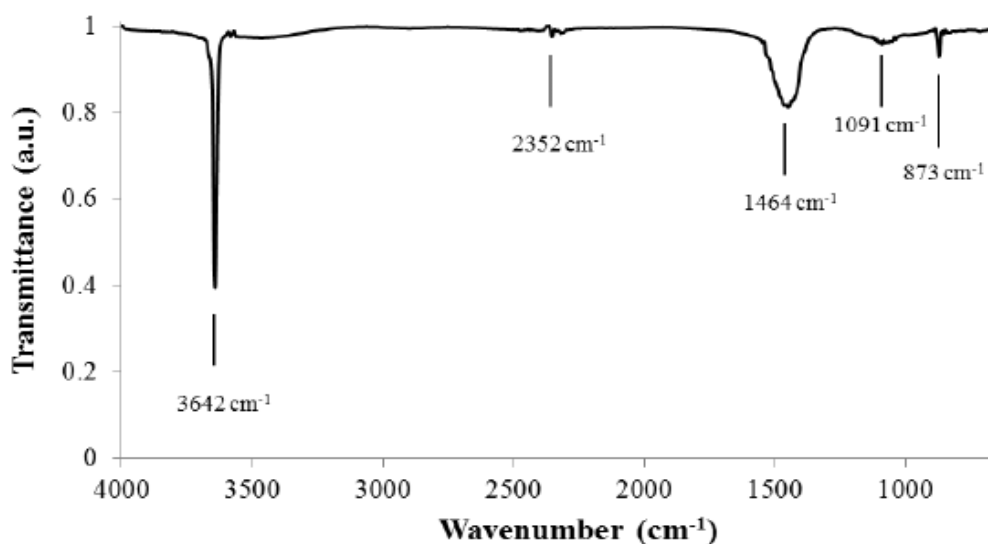


Figure 2.2: FTIR spectrum of calcium hydroxide (Ca (OH)₂) (Khachani *et al.*, 2014)

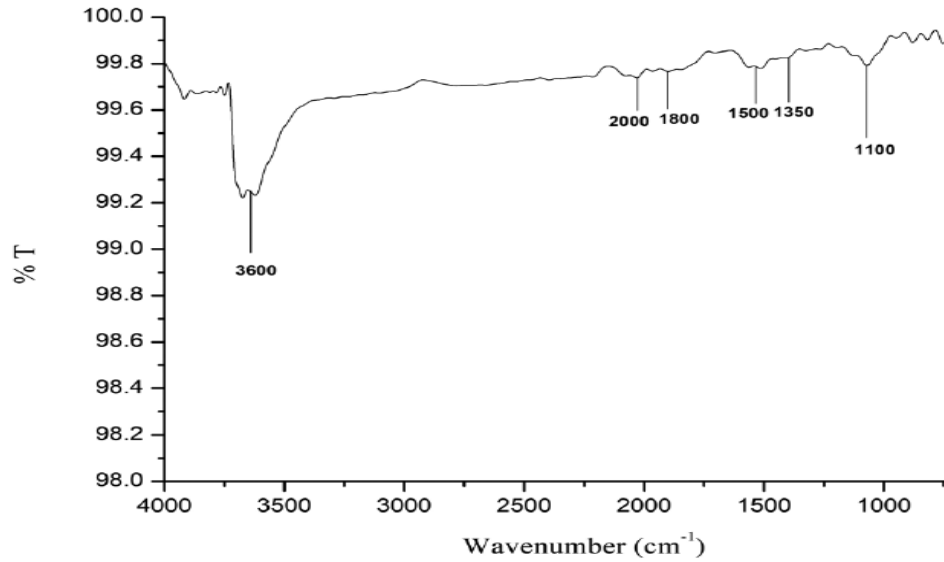


Figure 2.3: FTIR spectrum of calcined eggshell (CaO) (Nomura *et al.*, 2019)

2.5.3 X-ray Diffraction (XRD) Analysis

In order to detect and measure the crystalline size of the components present in the catalyst powder, X-ray diffraction (XRD) method were commonly applied. The crystallite size can be calculated using the Debye-Scherrer equation as follow:

$$L = \frac{K\lambda}{\beta \cos\theta} \quad (2.4)$$

where

K stands for the crystallite shape factor, 0.89

λ stands for the utilized beam wavelength

β stands for the full-width at half-maximum

θ stands for the angle of the maximum diffraction peak or Bragg's angle

According to Roschat *et al.* (2018), the diffractogram of the commercial CaO showed the presence of impurities such as calcium carbonate and calcium hydroxide. These impurities were resulted from the reaction of carbon dioxide and water vapour. Based on the diffractogram for calcined CaO, some of the peaks of CaCO₃ and Ca (OH)₂ were reduced and missing. This indicated that the decomposition of calcium carbonate and calcium hydroxide were occurred during calcination and the peaks that belonged to CaO had increased. Similar results were observed for calcium oxide-based catalyst derived from chicken manure (Maneerung *et al.*, 2016), and eggshell (Putra *et al.*, 2017). Figure 2.4 shows the standard diffractogram of the calcium carbonate (CaCO₃) as calcite phase while Figure 2.5 and Figure 2.6 show the standard diffractogram of CaO and calcium hydroxide (Ca (OH)₂) respectively.

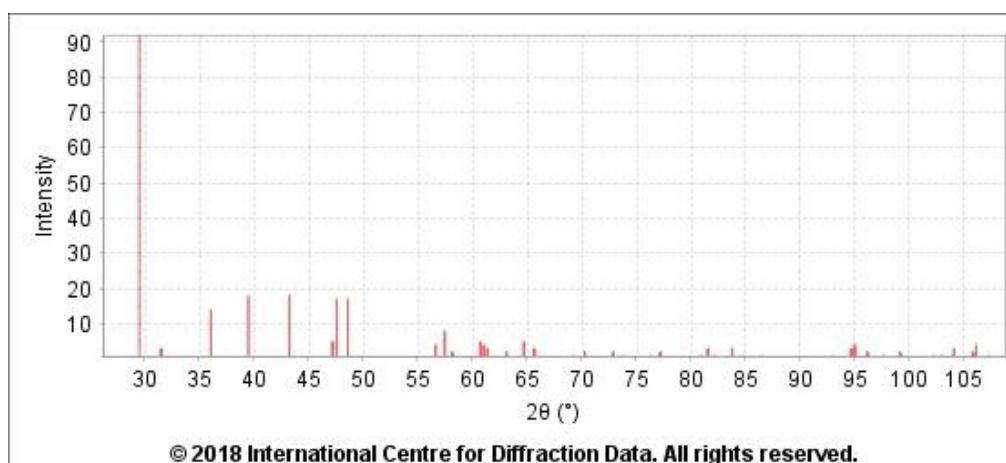


Figure 2.4: Standard diffractogram of calcium carbonate (CaCO₃, calcite)

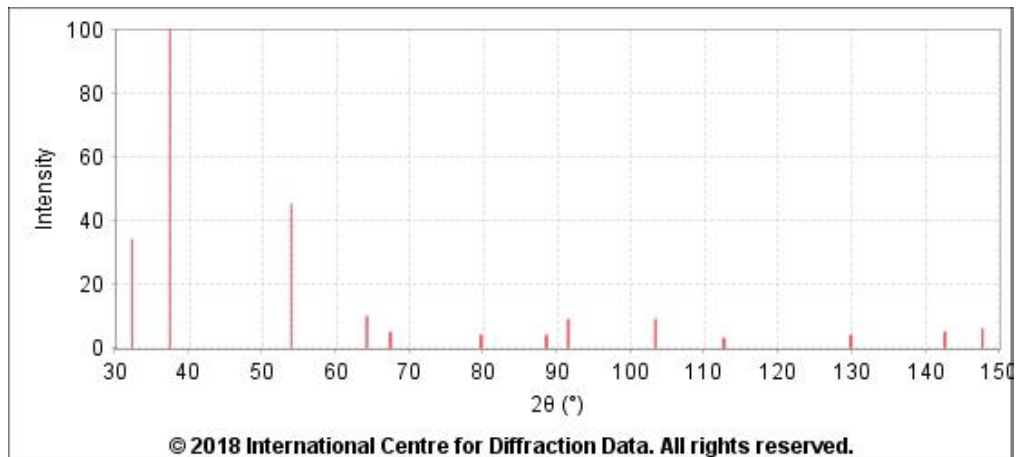


Figure 2.5: Standard diffractogram of CaO.

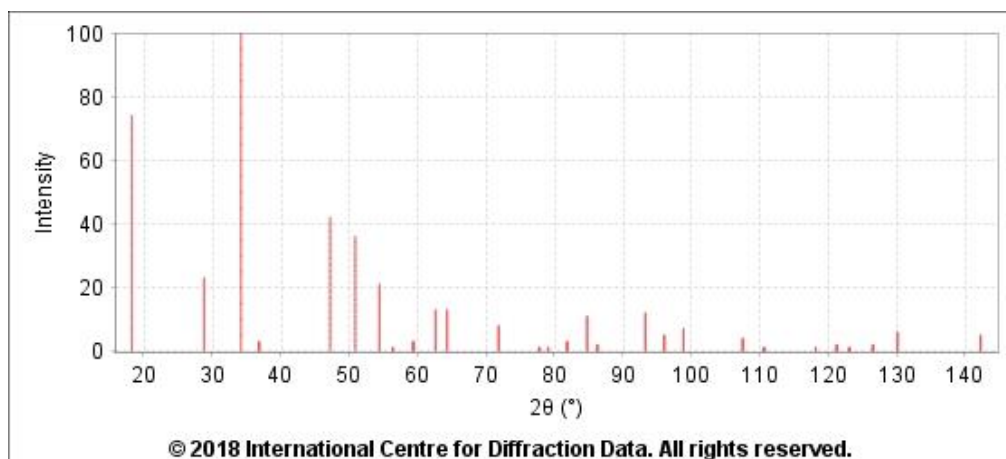


Figure 2.6: Standard diffractogram of calcium hydroxide (Ca(OH)₂)

2.5.4 Surface Morphology Analysis via Scanning Electron Microscopy (SEM)

The surface morphology and size estimation of the catalyst was examined by using SEM. According to Widayat *et al.* (2017), the calcium carbonate and calcium hydroxide can be converted into CaO during the calcination process. The calcined CaO would have a crystalline surface which referred to the active site that take part in the production of biodiesel.

The untreated eggshell was appeared in irregular shape while the thermal treated eggshell appeared in the rod like particles after calcination under 900 °C for 2 h (Putra *et al.*, 2017). Furthermore, the thermal-hydration treated eggshell and thermal-hydration-dehydration treated eggshell appear as porous surface with honey comb shape (Putra *et al.*, 2017). Besides, the untreated fish bones had a granular solid structure in unsymmetrical form while treated fish bones under 1000 °C had smaller in size and more uniform in shape (Lesbani *et al.*, 2016). Similar surface morphology had been found in thermal-hydration-dehydration treated biomass gasification bottom ash (Maneerung *et al.*, 2015). The surface morphologies for thermal hydration-dehydration treated CaO were tabulated in Table 2.7.

Table 2.7: Surface morphologies of CaO derived from different catalyst sources

Catalyst source	Textural properties (SEM)	Reference
Waste egg shell	Spherical shape	(Pandit <i>et al.</i> , 2017)
Waste egg shell	Honey comb like & porous	(Niju <i>et al.</i> , 2014)
Dolomite	Highly textured and rough	(Yoosuk <i>et al.</i> , 2011)
Calcite	Highly textured and very rough	(Yoosuk <i>et al.</i> , 2010)
Fish bone	Smaller in size and uniform in shape	(Lesbani <i>et al.</i> , 2016)

2.5.5 Brunauer-Emmett-Teller (BET) analysis

BET can be used to analyse the surface area, pore volume and pore size of the catalyst. Larger BET surface area indicates higher basicity and catalytic performance of the CaO catalyst (Roschat *et al.*, 2012). This shows that the surface area of the catalyst can influence the catalytic activity as well as the biodiesel production yield (Viriya-empikul *et al.*, 2012). Mekhemer (1998) claimed that the surface area of catalyst may inversely proportional to the calcination temperature while pore size was proportional to the calcination temperature.

Similar trend were found in Raj and Viswanathan (2009). They claimed that the surface area and pore volume of P25 sample had a decreasing trend with increasing of calcination temperature from 500 °C to 900 °C. These data indicated that the P25 sample can only be used for the catalytic processes below 500 °C. In contrast, the pore size showed an increasing trend with the calcination temperature in the mesopore range of 13–23 nm.

On the other hand, Menad *et al.* (2016) reported that as the calcination temperature increased from 300 °C to 700 °C, the BET surface area of and pore volume (micro-porous and meso-porous) of Linde Type A (LTA) zeolite increased, however, reduced when the calcination temperature exceeds 700 °C. The lowest BET surface area among all Linde Type A (LTA) zeolite samples was obtained where the porous is eliminated when the calcination temperature was further increased to 1300 °C (Menad *et al.*, 2016). This shows that high

calcination temperature can lead to sintering effect that reduces the surface area and eliminates the porous of catalyst.

2.5.6 Basicity Analysis via Temperature Programmed Desorption (TPD)

Researchers had run TPD analysis to identify the number of active sites on the treated CaO catalyst. According to Asikin-Mijan *et al.* (2016), with long hydration duration, the catalyst have higher basicity. This indicated that the catalytic performance was enhanced. The catalysts were prepared under different hydration duration of 1 h, 3 h, and 6 h and the basicity of catalysts were 1637, 2067, and 5078 $\mu\text{mol CO}_2/\text{g}$ respectively.

2.6 Kinetic study of transesterification process

Stoichiometrically, the oil to alcohol molar ratio in transesterification process is 3 moles to 1 mole and the products will be 3 moles of fatty acid esters and 1 mole of glycerol. Majority of researchers were conducting kinetic study of biodiesel production by using pseudo first order model. In this model, it assumes the transesterification to be a single step elementary process (Vujicic *et al.*, 2010). The reaction is derived in terms of rate equation as below:

$$r = -\frac{d[TG]}{dt} = k[TG][M]^3 \quad (2.5)$$

where k is the equilibrium rate constant, TG is triglyceride and M represents methanol.

Nevertheless, an excess of methanol is used in the reaction to maintain the forward reaction (Darnoko *et al.*, 2000). This makes the reaction obey to the fourth order rate law and fit the pseudo- first- order kinetics (Singh *et al.*, 2007). Due to the high concentration of methanol, the methanol is considered unchanged in concentration (Birla *et al.*, 2012) and the rate law can be derived as below:

$$r = -\frac{d[TG]}{dt} = k[TG] \quad (2.6)$$

k represents modified rate constant,

$$k = k'[M]^3 \quad (2.7)$$

By integrating the equation,

$$\ln [TG_0] - \ln [TG] = kt \quad (2.8)$$

Applying mass balance,

$$M_E = 1 - \frac{TG}{TG_0} \quad (2.9)$$

where, M_E represents conversion of methyl ester,

$$[TG] = [TG_0] (1 - M_E) \quad (2.10)$$

$$-\ln(1 - M_E) = kt \quad (2.11)$$

From the equation, the rate equation can be estimated. Besides, the activation energy and the pre-exponential factor of the biodiesel production can be investigated by varying the reaction temperature. The activation energy can be found by plotting the graph of $\ln k$ against $1/T$ from the Arrhenius equation (Yadav *et al.*, 2018):

$$k = A e^{\frac{-E_a}{RT}} \quad (2.12)$$

Taking the logarithmic form of Eq. (2.12) the equation can be expressed as:

$$\ln k = \ln A - \frac{E_a}{RT} \quad (2.13)$$

where k represents rate, constants derived from the kinetic model, A is the pre-exponential constant, R is the universal gas constant (8.314 J/mol/K), T is the absolute temperature in kelvin and E_a is the activation energy.

According to Sahani and Sharma (2018), heterogeneous catalytic process is a combination of slow mass transfer, diffusion reactions and the fast

reaction. The transesterification process of Mahua oil was conducted by three different temperatures (45 °C, 55 °C and 65 °C) with respect to different reaction time to observe the trend of kinetics. The rate constants were increasing proportional to the temperature of the biodiesel production which indicates the heat energy can reduce the restriction of mass transfer. By plotting the Arrhenius equation, the activation energy and pre-exponential factor are 34.44 kJ mol⁻¹ and 7.94 min⁻¹ respectively.

Freedman *et al.* (1986) reported that the value of activation energy is normally fall in the range of 33.6–84.0 kJ mol⁻¹ for base-catalysed transesterification reactions. Similar results were obtained by Maneerung *et al.* (2015) for the palm oil feedstock where the activation energy is 83.9 kJ mol⁻¹ which also fall in the feasible range. Table 2.8 summarized the rate constants and the activation energy for different catalysts that used for transesterification reaction with using methanol.

Table 2.8: Rate constant and activation energy for different catalyst and oil feedstock

Oil feedstock	Catalyst	Rate constant (min ⁻¹)	Activation energy (kJ/mol)	Reference
Waste cottonseed	KF/CaO/NiO	0.023	41.2	(Kaur <i>et al.</i> , 2014)
Waste cottonseed	Zn/CaO	0.1	43	(D. Kumar <i>et al.</i> , 2013)
Canola	CaO	0.0921	102.5	(Zhao <i>et al.</i> , 2013)

Table 2.8 (continued): Rate constant and activation energy for different catalyst and oil feedstock

Canola	K ₂ CO ₃ /CaO	-	25.34	(Degirmenbasi <i>et al.</i> , 2015)
--------	-------------------------------------	---	-------	-------------------------------------

2.7 Kinetic study of CaO catalyst

2.7.1 Eley-Rideal Kinetics

In Eley-Rideal kinetics, the elementary step that involved in transesterification was summarized in Table 2.9. The methanol (M) is adsorbed on the vacant site (S) of catalyst, the adsorbed methanol subsequently interacts with TG, DG, MG and results adsorbed diglyceride (DG. S), monoglyceride (MG. S), and glycerol (G.S) respectively, along with FAME in each step. Each of the above step can be rate limiting step. There are two assumptions (Kapil *et al.*, 2011):

- Surface of catalyst is homogenous without the inert species on the surface
- Slowest reaction is assumed as rate limiting step.

Table 2.9: Derivation of formula based on Eley-Rideal Kinetics.

Elementary reaction	Rate equation
$3 S + 3 M \leftrightarrow 3 M. S$	$\frac{k_1 C_M^3 - k_{-1} \left(\frac{k_3 C_{DG} C_{FAME}}{k_2} \right)^3}{\left(1 + \frac{k_3 C_{DG} C_{FAME}}{k_2} + k_3 C_{DG} + k_5 C_{MG} + k_7 C_G \right)^3}$
$M. S + TG \leftrightarrow DG. S + FAME$	$\frac{k_2 C_{TG} - k_{-2} C_{DG} C_{FAME}}{1 + k_1 C_M + k_3 C_{DG} + k_5 C_{MG} + k_7 C_G}$
$DG. S \leftrightarrow S + DG$	$\frac{k_{-3} \left(\frac{k_2 k_1 C_{TG} C_M}{C_{FAME}} \right) - k_3 C_{DG}}{1 + k_1 C_M + \frac{k_2 k_1 C_{TG} C_M}{C_{FAME}} + k_5 C_{MG} + k_7 C_G}$
$M. S + DG \leftrightarrow MG. S + FAME$	$\frac{k_1 k_4 C_M C_{DG} - k_{-4} k_5 C_{MG} C_{FAME}}{1 + k_1 C_M + k_3 C_{DG} + k_5 C_{MG} + k_7 C_G}$

Table 2.9 (continued): Derivation of formula based on Eley-Rideal Kinetics.

MG. S \leftrightarrow MG + S	$\frac{k_{-5}\left(\frac{k_4 k_1 C_{DG} C_M}{C_{FAME}}\right) - k_5 C_{MG}}{1 + k_1 C_M + \frac{k_2 k_1 C_{TG} C_M}{C_{FAME}} + k_5 C_{MG} + k_7 C_G}$
M. S + MG \leftrightarrow G. S + FAME	$\frac{k_1 k_6 C_M C_{MG} - k_{-6} k_7 C_G C_{FAME}}{1 + k_1 C_M + k_3 C_{DG} + k_5 C_{MG} + k_7 C_G}$
G. S \leftrightarrow S + G	$\frac{k_{-7}\left(\frac{k_6 k_1 C_{MG} C_M}{C_{FAME}}\right) - k_7 C_G}{1 + k_1 C_M + \frac{k_6 k_1 C_{MG} C_M}{C_{FAME}} + k_5 C_{MG} + k_3 C_{DG}}$

2.7.2 Langmuir- Hinshelwood-Hougen-Watson (LHHW)

For Langmuir-Hinshelwood model, it assumed that both methanol and triglyceride were adsorbed on the adjacent active sites of catalyst. In the first two steps both methanol and triglyceride are adsorbed adjacently on the catalyst surface, subsequently, the adsorbed methanol (M) and triglyceride (TG) resulted to FAME and adsorbed diglyceride (DG). Therefore, this adsorbed diglyceride (DG) reacts with adsorbed methanol (M) to give fatty acid methyl esters (FAME) and adsorbed monoglyceride (MG). Then adsorbed monoglyceride reacts with adsorbed methanol (M) to produce FAME and glycerol (G). The general reaction steps were summarized in Table 2.10 (Kapil *et al.*, 2011).

Table 2.10: Derivation of formula based on Langmuir-Hinshelwood-Hougen-Watson (LHHW).

Elementary reaction	Rate equation
$3 S + 3 M \leftrightarrow 3 M. S$	$\frac{k_1 C_M^3 - k_{-1} \left(\frac{k_6 k_7 C_{DG} C_{FAME}}{k_3 k_2 C_T} \right)^3}{\left(1 + \frac{k_6 k_7 C_{DG} C_{FAME}}{k_3 k_2 C_{TG}} + k_2 C_{TG} + k_6 C_{FAME} + k_7 C_{DG} + k_9 C_G + k_8 C_{MG} \right)^3}$
$3 S + 3 TG \leftrightarrow 3 TG. S$	$\frac{k_2 C_T - k_{-2} \left(\frac{k_6 k_7 C_{DG} C_{FAME}}{k_3 k_1 C_M} \right)}{\left(1 + \frac{k_6 k_7 C_{DG} C_{FAME}}{k_3 k_1 C_M} + k_1 C_M + k_6 C_{FAME} + k_7 C_{DG} + k_9 C_G + k_8 C_{MG} \right)^3}$
$M. S + TG. S \leftrightarrow DG. S + FAME. S$	$\frac{k_3 C_M C_{TG} - k_{-3} C_{DG} C_{FAME}}{\left(1 + k_1 C_M + k_2 C_{TG} + k_6 C_{FAME} + k_7 C_{DG} + k_9 C_G + k_8 C_{MG} \right)^2}$
$M. S + DG. S \leftrightarrow MG. S + FAME. S$	$\frac{k_4 C_M C_{DG} - k_{-4} C_M C_{FAME}}{\left(1 + k_1 C_M + k_2 C_{TG} + k_6 C_{FAME} + k_7 C_{DG} + k_9 C_G + k_8 C_{MG} \right)^2}$
$M. S + MG \leftrightarrow G. S + FAME. S$	$\frac{k_5 C_M C_{MG} - k_{-5} C_G C_{FAME}}{\left(1 + k_1 C_M + k_2 C_{TG} + k_6 C_{FAME} + k_7 C_{DG} + k_9 C_G + k_8 C_{MG} \right)^2}$
$3 FAME. S \leftrightarrow 3 S + 3 FAME$	$\frac{k_{-6} \left(\frac{k_1 k_2 k_3 C_{TG} C_M}{k_7 C_{DG}} \right)^3 - k_6 C_{FAME}^3}{\left(1 + \frac{k_1 k_2 k_3 C_M C_{TG}}{k_7 C_{DG}} + k_1 C_M + k_2 C_{TG} + k_7 C_{DG} + k_9 C_G + k_8 C_{MG} \right)^3}$
$DG. S \leftrightarrow S + DG$	$\frac{k_{-7} \left(\frac{k_2 k_1 k_3 C_{TG} C_M}{k_6 C_{FAME}} \right) k_6 C_{DG}}{1 + k_1 C_M + k_2 C_{TG} + k_6 C_{FAME} + \frac{k_2 k_1 k_3 C_{TG} C_M}{k_6 C_{FAME}} + k_9 C_G + k_8 C_{MG}}$

Table 2.10 (Continued): Derivation of formula based on Langmuir-Hinshelwood-Hougen-Watson (LHHW).

MG. S \leftrightarrow MG + S	$\frac{k_{-8} \left(\frac{k_6 k_9 C_{FAME} C_G}{k_5 C_M} \right) k_8 C_{MG}}{1 + k_1 C_M + k_2 C_{TG} + k_6 C_{FAME} + \frac{k_6 k_9 C_{FAME} C_G}{k_5 C_M} + k_9 C_G + k_7 C_{DG}}$
G. S \leftrightarrow S + G	$\frac{k_{-9} \left(\frac{k_1 k_5 k_8 C_M C_{MG}}{k_6 C_{FAME}} \right) k_9 C_G}{1 + k_1 C_M + k_2 C_{TG} + k_6 C_{FAME} + \frac{k_1 k_5 k_8 C_M C_{MG}}{k_6 C_{FAME}} + k_8 C_{MG} + k_7 C_{DG}}$

2.8 Factors that affecting the biodiesel production

There are a few factors that affecting the biodiesel production such as dosage of catalyst, reaction time, reaction temperature, and alcohol to oil molar ratio. Table 2.11 shows the factors and the range of the study from researchers.

Table 2.11: Summary of factors and the range of the study for biodiesel production

Factor	Conditions	References
Dosage of catalyst	2 to 9 wt%.	(Chen et al., 2016)
Duration for biodiesel production	from 30 minutes to 210 minutes.	(Chen et al., 2016), (Latchubugata et al., 2018)
Reaction temperature	55 to 70 °C	(Kumar and Ali, 2012), (Zhao, Qiu and Stagg-Williams, 2013).
Methanol to oil ratio	3:1 to 18:1	(Chen et al., 2016)

2.8.1 Dosage of catalyst

The acceleration of transesterification reaction is dependent on the availability of the basic sites on the catalyst (Zhao *et al.*, 2013). The active sites of the catalyst can be increased either enlarge the exposed active sites of the catalyst (Kouzu *et al.*, 2008) or increase the dosage of the catalyst. Nevertheless, the optimum mass of the catalyst is dependent on the type of oil feedstock and the reaction condition (Wen *et al.*, 2010). There would be no significant increment in biodiesel yield even if the dosage of catalyst is greater than its optimal

amount, due to the mass transfer resistant (Kaur *et al.*, 2014) or the occurrence of the saponification reaction (Zhao *et al.*, 2013).

According to Chen *et al.* (2016), the relationship between catalyst dosage and biodiesel yield was observed by altering the catalyst to palm oil mass ratio from 2 to 9 wt%. The biodiesel yields increased proportional to the catalyst loading and around 7 wt%, a drop of biodiesel yield was detected even though the amount of catalyst was increased. It can be explained as that the reaction mixture had become more viscous due to the high amount of catalyst which indicate the increment mass transfer resistant in the heterogeneous reaction system (Bai *et al.*, 2009).

2.8.2 Reaction time

Another factor that affect the biodiesel yield is the duration of transesterification. Chen *et al.* (2016) reported that the performance of the treated CaO catalysts was determined with the reaction time ranging from 30 minutes to 210 minutes. The maximum yield of biodiesel was approximately 96% and the optimum reaction time was around 170 minutes.

Due to the reversibility of the transesterification reaction, a prolonged reaction time can shift the reaction pathway and decreased the biodiesel yield. A similar trend was obtained from Latchubugata *et al.* (2018). The long hour of reaction time may initiate the formation of glycerol in methanol solution and part of the catalyst may reacted with free fatty acids and formed soap.

2.8.3 Reaction temperature

The formation of biodiesel was significantly affected by the reaction temperature even though with the presence of CaO catalyst (Wen *et al.*, 2010). Majority of researchers concluded that the optimum temperature for the transesterification reaction was 65 °C which is the boiling point of methanol at the atmospheric pressure (Kumar *et al.*, 2012). According to Latchubugata *et al.* (2018), the experiments were carried out under a temperature range of 55 to 70 °C. If the temperature exceeds 70 °C, a much lower biodiesel yield was obtained, the methanol would begin to boil at 65 °C, the contact time between methanol and oil was reduced which led to the decrease in biodiesel yield (Zhao *et al.*, 2013).

The oil can also be fully converted into biodiesel at 35 °C, however, a prolonged reaction time is needed which was not feasible for industry application (D. Kumar *et al.*, 2013). For instance, the transesterification reaction can be performed at room temperature, still, 24 h was needed to complete the process (Reddy *et al.*, 2006).

2.8.4 Alcohol to oil molar ratio

Theoretically, the stoichiometric ratio for biodiesel reaction is 3 moles of alcohol to 1 mole of oil molar ratio in order to achieve 100 % conversion. Normally, the transesterification reaction is run in excess of methanol. A high methanol to oil molar ratio was favourable as it can shift the equilibrium

toward the product (Chen *et al.*, 2016). Besides, the excess methanol can compete with the product molecules in order to detach biodiesel molecules from the catalyst surface and regenerate the basic sites (Kaur *et al.*, 2014).

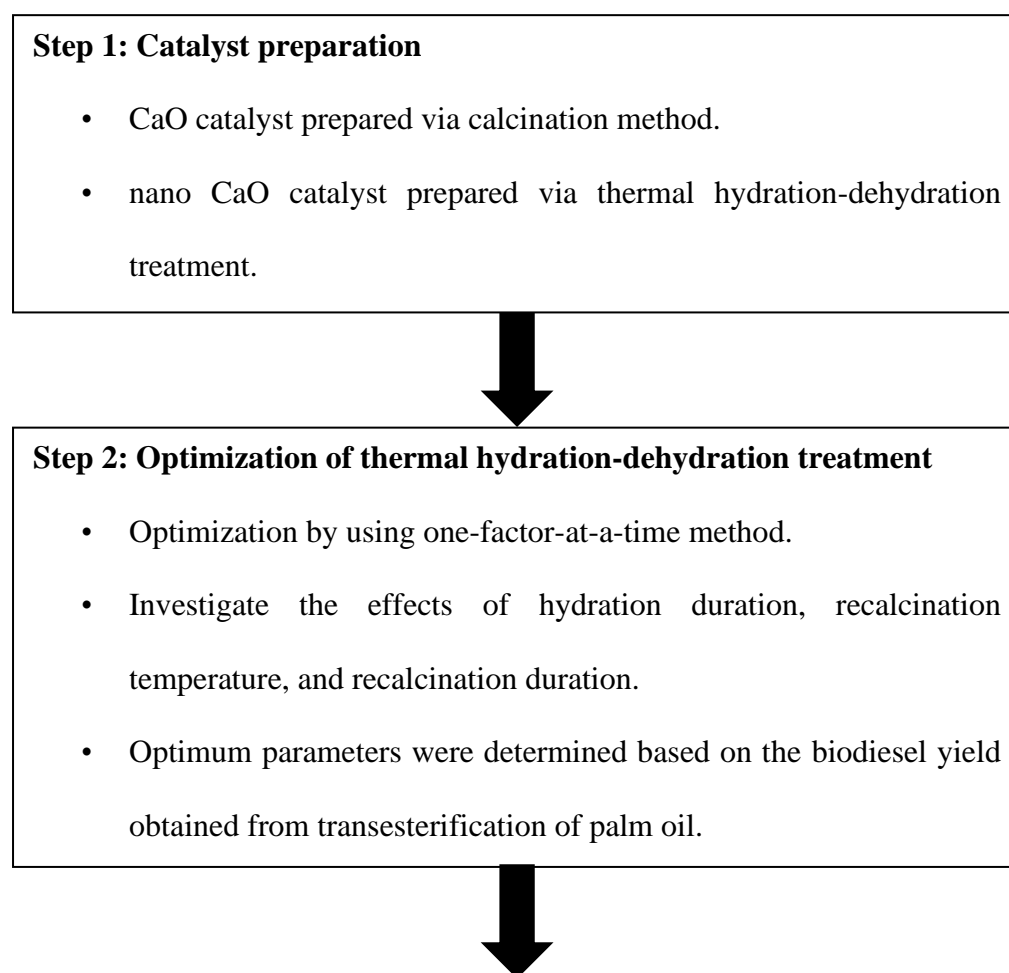
There is an optimum alcohol to oil feedstock molar ratio where the reaction time for transesterification will remain constant even though the number of molar ratio was further increased (Granados *et al.*, 2009), yet, the optimum ratio can be varied according to the reaction condition. According to Chen *et al.* (2016), the methanol to oil molar ratio was ranging from 3:1 to 18:1, and the biodiesel yields shows the increment gradually, then reach an equilibrium at the optimum point, 9:1 for the treated CaO catalyst. Besides, there would be difficulty to the purification of biodiesel product mixture if the methanol is in excess amount.

CHAPTER 3

METHODOLOGY AND WORK PLAN

3.1 Project Workflow

The overall project workflow had been summarized in the flowchart of Figure 3.1.



Step 3: Characterization of the physical and chemical properties of catalyst.

- TGA, FTIR, XRD, SEM – EDX, TPD
- BET, TEM



Step 4: Deduce kinetic mechanism for the transesterification reaction catalyzed by optimized nano CaO catalyst.

- Develop a kinetic model to study the transesterification reaction.
- Verification of kinetic model by using experimental data.
- Determine the activation energy of the transesterification reaction.

Figure 3.1: Research flow diagram

Firstly, the effects of important parameters related to thermal hydration and dehydration treatment such as hydration duration, recalcination temperature, recalcination duration were studied and optimized by using one-factor-at-a-time method. The developed nano CaO catalysts were used to run the transesterification of palm oil to biodiesel. The optimum catalytic performance of nano CaO catalyst was determined based on the biodiesel yield from the transesterification. The biodiesel yield was obtained from gas chromatography (GC) analysis, and, the catalytic performance of optimum nano CaO catalyst was compared with CaO catalyst.

After that, the range of calcination temperature for waste cockle shells and calcination temperature of hydrated CaO were analysed through

Thermogravimetric analysis (TGA). Then, the physical and chemical properties of samples including raw cockle shells, CaO catalyst prepared via calcination method, hydrated CaO and nano CaO catalyst prepared via thermal hydration-dehydration treatment were characterised and compared. The bonded chemicals in catalysts were analysed by using Fourier Transform Infrared Spectroscopy (FT-IR). The phases were predicted by using X-ray Diffraction (XRD). The surface morphologies of the catalysts were examined using scanning electron microscopy (SEM) and the elemental compounds were identified by Energy Dispersive X-ray (EDX). The basicity level of the catalyst was analyzed by using Temperature Programmed Desorption (TPD).

In addition, the surface area, pore volume and pore diameter of the CaO catalyst prepared via calcination method and nano CaO catalyst prepared via thermal hydration-dehydration treatment were determined by Brunner-Emmett-Teller (BET) while the particle size was estimated by using High Resolution Transmission Electron Microscopy (HRTEM).

Lastly, a kinetic mechanism was deduced and kinetic model was developed for the transesterification reaction catalysed by nano CaO catalyst. The proposed kinetic mechanism for the reaction was verified with the experimental data. The activation energy was identified by plotting the Arrhenius equation.

3.2 Materials and Equipment

The “Buruh” brand cooking oil as oil feedstock for transesterification reaction was purchased from the grocery shop, located in Bandar Sungai Long, Malaysia. Methanol (CH₃OH) and hexane (C₆H₁₄) of analytical grade with 99 % purity was procured from Merck, Malaysia Ltd. Methyl heptadecanoate of analytical grade with 99 % purity was purchased from Sigma Aldrich, Malaysia Ltd and it was used as internal standard for gas chromatography (GC) analysis. Materials and equipment that required in this research were summarized and tabulated in Table 3.1 and Table 3.2, respectively.

Table 3.1: Materials for biodiesel production

Material	Composition	Origin
Buruh Brand Palm Cooking Oil		Grocery shop
Waste Cockle Shell		Hawker stalls
Methanol	99.9 %	Merck, Malaysia Ltd
Hexane	99.9 %	Merck, Malaysia Ltd
Methyl Heptadecanoate (Internal standard)	99.9 %	Sigma Aldrich, Malaysia Ltd

Table 3.2: Equipment needed for the research

Equipment	Brand	Model
X-ray diffractometer	Shimadzu	XRD-6000
Thermogravimetric & Differential Thermal Analyser (TGS/DTA)	Perkin Elmer	STA 8000
Scanning electron microscopy (SEM)	Hitachi	S-3400N

Table 3.2 (Continued): Equipment needed for the research

Energy Dispersive X-ray (EDX)	Hitachi	S-3400N
Temperature-programmed desorption (TPD)	Thermo Scientific	TPDRO 1100
Gas Chromatograph (GC)	Perkin Elmer	Clarus 500
Programmable Furnace	Wise Therm	FP-03
Oven	Memmert	-

3.3 Catalyst Preparation

3.3.1 CaO catalyst prepared via calcination treatment

Initially, the waste cockle shells were washed then rinsed with tap water. The cleaned cockle shells were dried in an oven at 80 °C overnight to remove the remaining water and moisture. The cockle shells were then crushed into small pieces by using hammer and placed in the crucible with lid for first calcination at 900 °C for 3 h under atmospheric pressure. To ensure the completion of thermal decomposition, a 70 ml crucible was only filled with 20 g of waste cockle shell crushed pieces. The calcined cockle shell powder was kept in a container and placed in dessicator to ensure the dryness of the powder.

3.3.2 Catalyst prepared via thermal hydration and dehydration method

The waste cockle shells were washed then rinsed with tap water. The cleaned cockle shells were dried in an oven at 80 °C and left overnight to remove the water content. The cockle shells were then crushed into small pieces and it was ready to be treated with thermal hydration and dehydration. The crushed cockle shells were first calcined in the furnace at 900 °C for 3 h. After the thermal treatment, the CaO powder was then refluxed with distilled water at 60 °C for 3 h. During the hydration, only maximum 15 g of CaO catalyst prepared via calcination treatment powder were added into 600 ml of distilled water. The precipitate was then filtered and dried overnight in the oven at 80 °C to remove the remaining water content. The hydrated CaO was recalcined in the furnace at 650 °C for 2 h. After the dehydration stage, a fined white powder of nano CaO catalyst was synthesized. Figure 3.2 shows the flow of catalyst preparation from cockle shell to CaO catalyst prepared via calcination treatment then nano CaO catalyst prepared via thermal hydration-dehydration treatment.



Figure 3.2: Catalyst preparation from cockle shell to CaO catalyst prepared via calcination treatment and then nano CaO catalyst prepared via thermal hydration-dehydration treatment

3.4 Optimization of thermal-hydration-dehydration treatment

The effects of important parameters related to thermal hydration and dehydration treatment such as hydration duration, recalcination temperature, recalcination duration were studied and optimized by using one-factor-at-a-time method. The effect of hydration duration was first optimized with the duration varied at 3 h, 4 h, 5 h, and 6 h. The others parameter of recalcination temperature and recalcination duration were constant at 650 °C and 3 h respectively. After the optimum hydration duration was determined, the recalcination temperature was varied at 650 °C, 750 °C, 850 °C and 950 °C. while the recalcination duration was constant at 3 h. Lastly, the recalcination duration effect was studied at various values of 2 h, 3 h, 4 h, 5 h.

The levels of each parameter for the study and the experimental runs were tabulated in Table 3.3. The developed nano CaO catalyst prepared via thermal hydration-dehydration treatment was used to run the transesterification with palm oil as feedstock. The catalytic performance of nano CaO catalyst prepared via thermal hydration-dehydration treatment was determined based on the biodiesel yield from the transesterification.

Table 3.3: Denotation of the catalyst samples

Catalyst	Hydration duration(h)	Recalcination temperature(°C)	Recalcination duration (h)
Optimization for duration of hydration treatment			
3_650_3	3	650	3
4_650_3	4	650	3
5_650_3	5	650	3
6_650_3	6	650	3
Optimization for recalcination temperature			
6_650_3	6	650	3
6_750_3	6	750	3
6_850_3	6	850	3
6_950_3	6	950	3
Optimization for recalcination duration			
6_650_2	6	650	2
6_650_3	6	650	3
6_650_4	6	650	4
6_650_5	6	650	5

3.5 Transesterification reaction of palm oil

Catalytic activity of CaO catalyst in transesterification reaction was evaluated based on the biodiesel yield achieved. The transesterification reaction was performed in a 250 mL round bottomed flask equipped with condenser column approximately 150 mL of cooking oil was mixed with methanol at 8:1 methanol to oil molar ratio and the mixture was stirred at 350 rpm (Chen *et al.*,

2016),. The reaction was operated at 60 °C operating temperature and catalysed with 3 wt% CaO catalyst (Kumar *et al.*, 2012; Zhao *et al.*, 2013). The biodiesel sample was collected at every 1 hour with total duration of 5 h (Latchubugata *et al.*, 2018). The biodiesel sample was centrifuged to separate biodiesel layer from mixture solution. 1 mL of biodiesel sample was collected and diluted by 3 mL of n-hexane. Table 3.4 had summarized the reaction condition for the biodiesel production. The experimental set-up was showed in Figure 3.3.

Table 3.4: Reaction condition for biodiesel production

Condition	Unit	Specification	References
Temperature	°C	60	(Kumar <i>et al.</i> , 2012)
Duration	min	300	(Latchubugata <i>et al.</i> , 2018)
Methanol: Palm oil ratio	mol/mol	8:1	(Chen <i>et al.</i> , 2016)
Stirring speed	rpm	400	(Chen <i>et al.</i> , 2016)
Catalyst loading	wt %	3	(Zhao <i>et al.</i> , 2013)

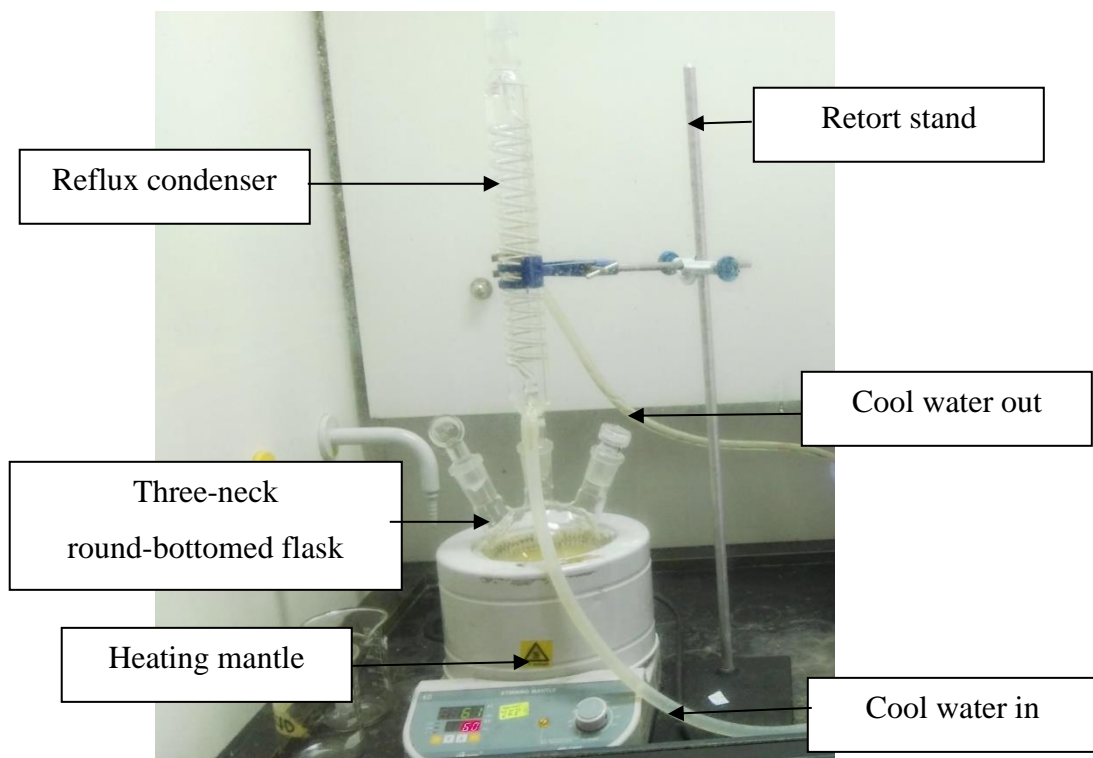


Figure 3.3: Experimental set-up for biodiesel production

3.6 Gas chromatography analysis for biodiesel

The biodiesel that derived from palm oil were the mixtures of different FAME, methyl linoleate, methyl oleate, methyl palmitate, and methyl stearate. The concentration of biodiesel produced was analysed by using gas chromatography (Perkin-Elmer Clarus 500 GC). The gas chromatography was equipped with Nukol™ FUSED SILICA (with dimensions of 30 m × 0.53 mm × 0.5 μm) and connected to flame ionization detector. The temperature of the oven was specified at 220 °C with ramping rate of 10 °C/minute. Helium was selected as the carrier gas for analysis with flowrate of 3 mL/minute.

250 μL of the internal standard, methyl heptadecanoate was added into 250 μL of diluted FAME mixture. 1 μL of the mixtures was then injected into

the GC for analysis. The objective of this step was to determine the peak location of methyl ester. The retention time of the peak location for each of the methyl esters were tabulated in Table 3.5. The calibration curve of the internal standard and external standard mixture were plotted in appendix A.

Table 3.5: Type of FAME and their retention time

Types of FAME	Molecular Weight (g/mol)	Retention Time (min)
Methyl Heptadecanoate (IS)	284.48	13.27
Methyl Linoleate	294.47	15.88
Methyl Oleate	296.49	15.02
Methyl Palmitate	270.45	12.17
Methyl Stearate	298.50	14.65

1 mL of FAME sample from biodiesel production was diluted with 3 mL of hexane. Then, 100 μ L of diluted FAME sample was mixed with 200 μ L internal standard, methyl heptadecanoate with concentration of 10 g/L. Next, 1 μ L of the mixture was injected into GC. The concentration of the respective methyl ester present in the sample was then calculated by comparing the ratio of methyl esters peak area to internal standard peak area. Biodiesel yield was calculated based on equation (3.1) and a sample calculation was shown in appendix E and F.

Biodiesel Yield=

$$Dilution\ factor \times \frac{M_{Palmitic} + M_{Stearic} + M_{Oleate} + M_{Linoleate}}{3(M_{Palm\ oil})} \times 100\% \quad (3.1)$$

where

M_{Palmitic} = Moles of methyl palmitic

M_{Stearic} = Moles of methyl stearic

M_{Oleate} = Moles of methyl oleate

$M_{\text{Linoleate}}$ = Moles of methyl linoleate

$M_{\text{Palm oil}}$ = Moles of palm oil

3.7 Characterisation of catalyst

Numerous characterisation studies had been carried out to determine the physical and chemical properties of waste cockle shell, CaO catalyst prepared via calcination method, hydrated CaO and the nano CaO catalyst prepared via thermal hydration-dehydration treatment. The samples were characterised by thermogravimetric analysis (TGA), Fourier Transformed Infrared Spectroscopy (FTIR), X-ray diffraction (XRD), Scanning Electron Microscopy (SEM), Energy-Dispersive X-ray spectroscopy (EDX), Temperature-Programmed Desorption (TPD) of CO₂. Then, the sintering effects of nano CaO were studied by using Brunauer–Emmett–Teller (BET), and High-Resolution Transmission Electron Microscopy (HRTEM) analyses.

3.7.1 Thermogravimetric & Differential Thermal Analyser (TGS/DTA)

The trend of raw cockle shell decomposition and dehydration of calcium hydroxide were investigated by using Thermogravimetric analysis (TGS/DTA). These analyses were performed by using Perkin Elmer STA

8000 with the heating rate of 20 °C/min starting from 40 °C to 1000 °C under the flow of nitrogen gas.

3.7.2 Fourier Transform Infrared (FT-IR)

FT-IR analysis was used to determine the functional groups and the bonding that presence in the sample. This was performed by using Thermo Scientific Nicolet iS10 FT-IR Spectrometer. The range of the FT-IR spectrum were initiated from 400 cm⁻¹ to 4000 cm⁻¹.

3.7.3 X-ray Diffraction (XRD)

X-ray Diffraction was used to identify the phases and species of the samples. First, a piece of flat glass was applying pressure to the powdered sample to ensure the sample was packed uniformly and its surface completely flat on the sample holder. Analysis of XRD was conducted through the Shimadzu XRD-6000 X-ray diffractometer which uses Cu K α radiation with 1.54 Å to create diffraction patterns at 40 kV. The catalyst sample was scanned with a range of wavelength from 0.5 to 2.0 Å and 2 θ from 20° to 80° at the scanning rate of 2° per minute.

3.7.4 Scanning Electron Microscopy (SEM) and Energy Dispersive X-ray (EDX)

Scanning electron microscopy was used to examine the surface morphology of the sample. The sample was coated with palladium and gold by placing the sample holder in the sputter coater. The accelerating voltage of the SEM was set at 15 kV. Micrographs of the sample (CaO nano catalyst) at different magnifications, i.e., 1000x, 5000x, 10000x ,20000x, were captured by the electron detector. Energy dispersive X-ray (EDX) spectroscopy was conducted as well to study the presence of elements and its composition (at % or wt %) in the sample. This analysis was based on the fact that every element exhibits a unique irradiation which constituted to different sets of peaks. Both of the SEM analysis and EDX analysis were done by using the Hitachi S-3400N SEM.

3.7.5 Temperature Programmed Desorption (TPD)

The basicity and the basic strength distribution of nano CaO were analysed using temperature-programme desorption of CO₂. Before the analysis, the catalysts were pre-treated with nitrogen. The pre-treatment nitrogen stream was set at a temperature 120 °C and was allowed to pre-treat for 30 min. Temperature was increased linearly at a rate of 10 °C per minute and a nitrogen flow of 20 mL per minute. The temperature was then brought down to room temperature before a stream of pure CO₂ was introduced into the reactor. The pure CO₂ flow was held for 120 minutes with a flow rate of 20

mL per minute followed by the flushing of N₂ to the system for 60 minutes. After that, the desorption process of CO₂ was carried out under helium flow at a flow rate of 20 mL per minutes. Temperature was set to climb steadily at a rate of 10 °C per minute from 30 °C to 900 °C. The TPD analysis of CO₂ was done by operating Thermo Electron TPDRO 1100.

3.7.6 Brunauer-Emmett-Teller (BET) analysis

The surface area of the CaO catalyst was investigated by using Brunauer-Emmett-Teller (BET) analysis. There are two major steps to conduct BET analysis which are degassing and sample analysis. The model of BET equipment used for this research work was Micromeritics 3 Flex Version 5.02. Initially, the sample was undergone degassing at 90 °C for 1 hour and 200 °C for 8 h. The actual sample mass was obtained at the end of the degas process. The degassed sample was inserted into the transducer for further sample analysis.

3.7.7 High Resolution Transmission Electron Microscopy (HRTEM)

HRTEM is used to estimate the particle size and investigate the arrangement of particle in the nano CaO. Four samples (6_650_3, 6_950_3, 6_650_5, CaO catalyst prepared via calcination treatment) were sent to SIRIM (Kulim branch) for analysis. Before the analysis, sample preparation was done by using isopropanol. The samples were analysed by using Philips Tecnai 2.0 HRTEM and carried out on 29/1/2020.

3.8 Experimental work for verification of kinetic model

Experimental data for transesterification reaction catalysed by optimized nano CaO catalyst was obtained. The transesterification reaction was performed in a 250 mL round bottomed flask equipped with condenser column approximately 150 mL of cooking oil was mixed with methanol to form a mixture of triglycerides at concentration of 0.4 mol/dm^3 and the mixture was stirred at 350 rpm. The reaction was operated at $60 \text{ }^\circ\text{C}$ operating temperature and catalysed with 2 grams of optimized nano CaO catalyst. The biodiesel sample was collected at every 15 minutes with total duration of 1 h. The biodiesel sample was centrifuged to separate biodiesel layer from mixture solution. Four points (15 minutes, 30 minutes, 45 minutes, and 60 minutes) were collected and tried to fit with the developed kinetic equation. The rate constant was obtained from the plots. The activation energy and pre-exponential factor of the kinetic model was identified by plotting Arrhenius equation based on the variation of temperature from $45 \text{ }^\circ\text{C}$ to $60 \text{ }^\circ\text{C}$ with $5 \text{ }^\circ\text{C}$ step size. Table 3.6 had summarized the reaction condition for the kinetic study.

Table 3.6: Reaction condition for kinetic studies

Condition	Unit	Specification
Temperature	$^\circ\text{C}$	60
Duration	min	60
Stirring speed	rpm	350
Catalyst loading	g	2

CHAPTER 4

RESULTS AND DISCUSSION

4.1 Catalyst Characterization

4.1.1 Thermogravimetric (TGA) analysis

Figure 4.1 shows the result of decomposition test of waste cockle shells. A sudden decline weight of waste cockle shell is observed at 650 °C and the weight loss eventually reached plateau at 875 °C. It can be observed from Figure 4.2 that the highest weight decrement was at 875 °C, with -8.24 % per min.

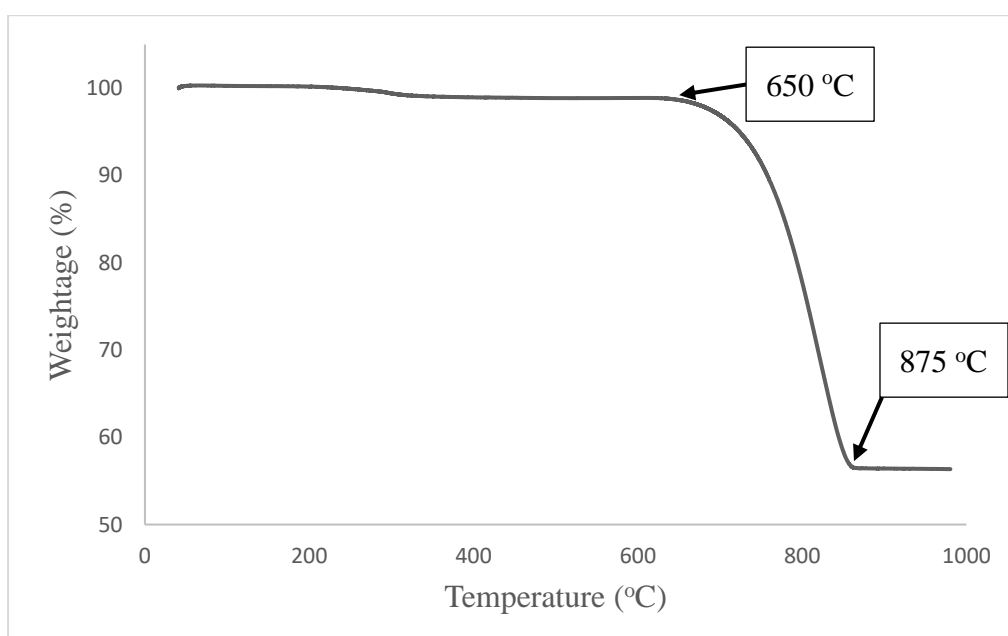


Figure 4.1: Decomposition of cockle shell

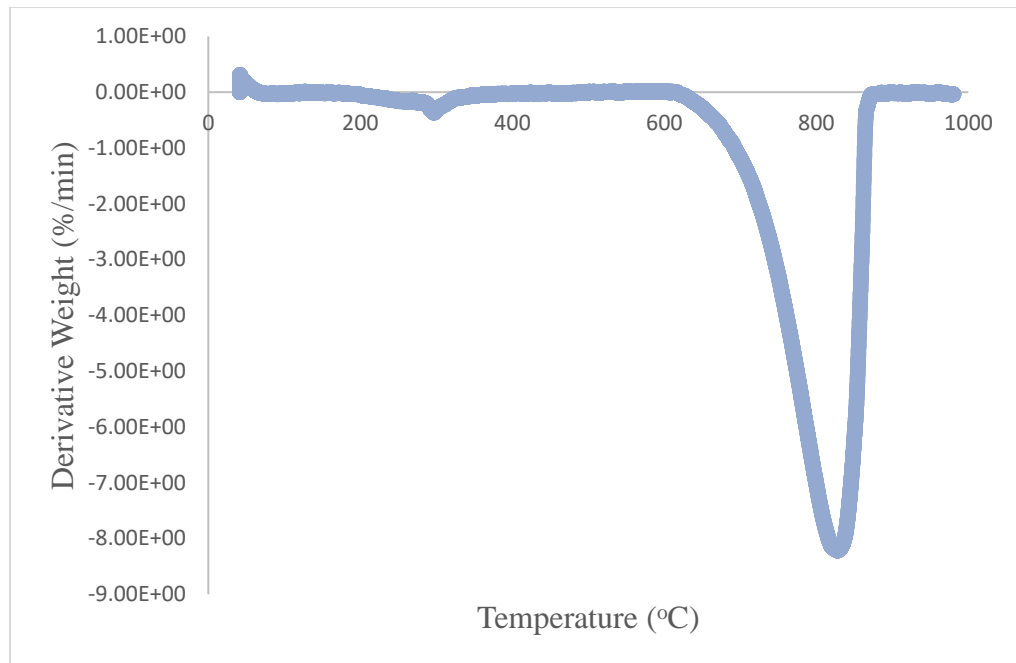


Figure 4.2: Derivative weight for decomposition of cockle shell

The mass loss of raw cockle shell during the calcination stage was related to the released of carbon dioxide (CO₂) from the calcium carbonate (CaCO₃) content (Ljupkovic *et al.*, 2014). The chemical equation (4.1) shows the decomposition of calcium carbonate during calcination stage:



Figure 4.3 shows the results of the decomposition of hydrated CaO. It was observed that hydrated CaO shows two decay steps of mass of hydrated CaO due to the heat decomposition of hydrated CaO. Based on Figure 4.3, there was a weight gain at the initial stage of thermogram from 41.56 °C to 434.07 °C. This may due to the adsorption of impurities in the air flow by calcium hydroxide during the TGA analysis (Vujicic *et al.*, 2010).

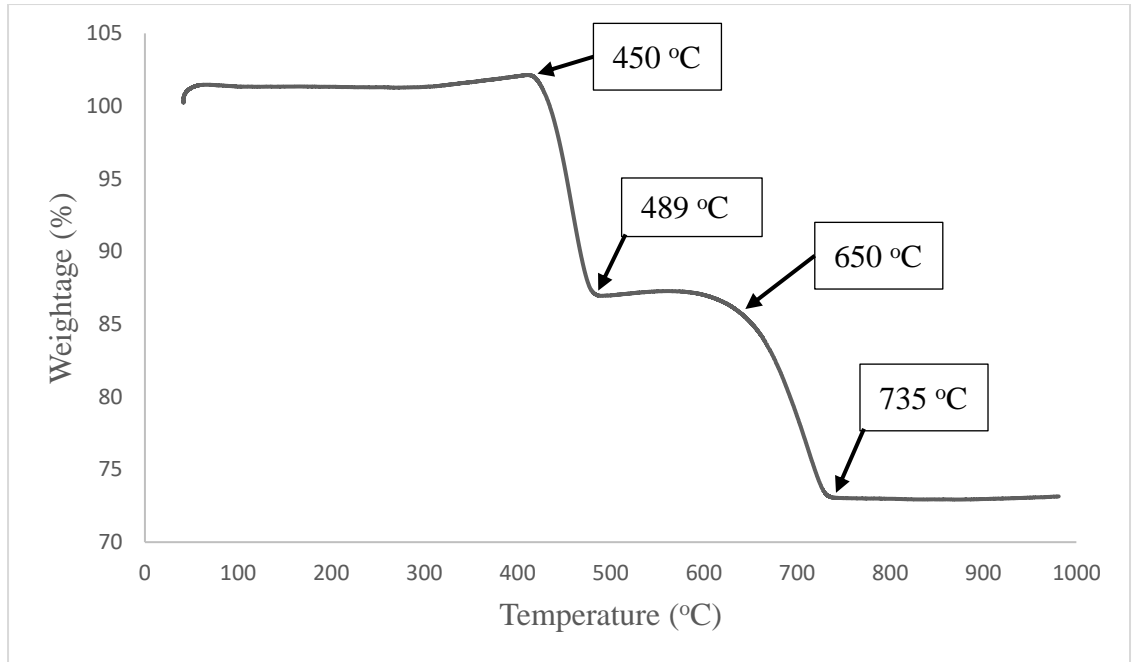


Figure 4.3: Decomposition of hydrated CaO

Figure 4.4 shows the derivative weight of hydrated CaO during thermal decomposition.

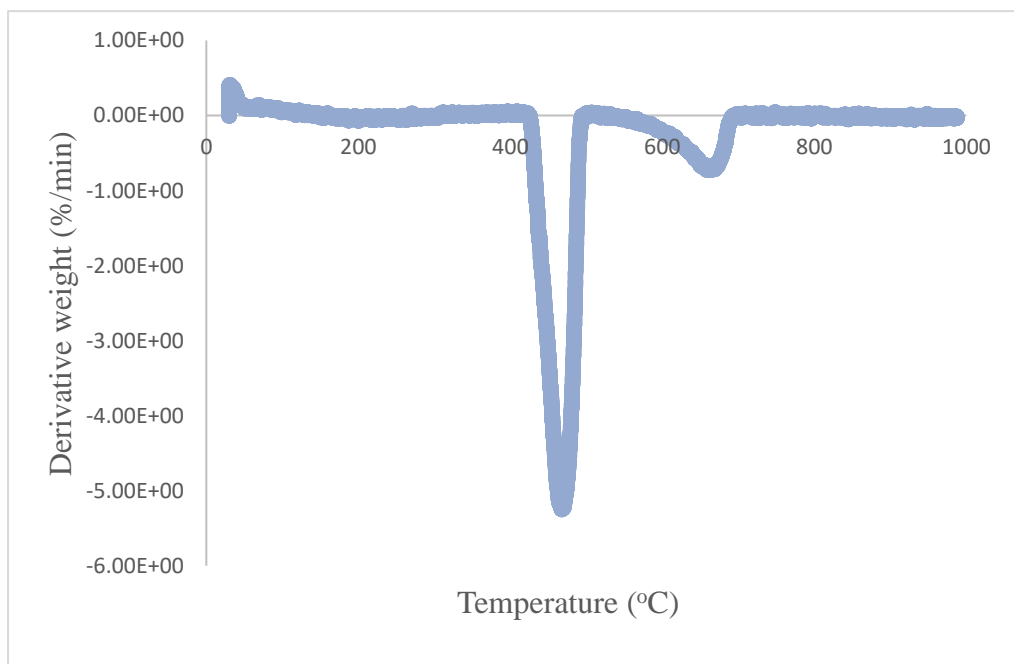


Figure 4.4: Derivative weight for thermal decomposition of hydrated CaO

The first mass decay step was occurred between 450 °C to 489 °C with derivative weight of -5.317 %/min and second decay step started from 650 °C to 735 °C with derivative weight of -0.777 %/min. The calcium hydroxide break into the calcium hydroxide-calcium oxide interphase followed by the evolution of the water molecules during the first endothermic process. The chemical equation (4.2) shows the formation of calcium hydroxide-calcium oxide CaO interphase and chemical equation (4.3) show evolution of water during first endothermic decay:



The decomposition of carbonaceous materials of CO₂ from the catalyst was occurred in second endothermic process (Micic *et al.*, 2015). In summary, the desire calcination temperature for waste cockle shell was at 880 °C and above as to completely transform CaCO₃ to active phase of CaO. Whereas the desire recalcination temperature for hydrated CaO was at 735 °C and above as to completely dehydrate the particle.

4.1.2 Fourier Transform Infrared (FT-IR) Analysis

FTIR analysis was used to identify the catalyst structure and bonded chemical compounds. Figure 4.5 shows the results of raw cockle shell, CaO catalyst prepared via calcination treatment, hydrated CaO and nanosized CaO.

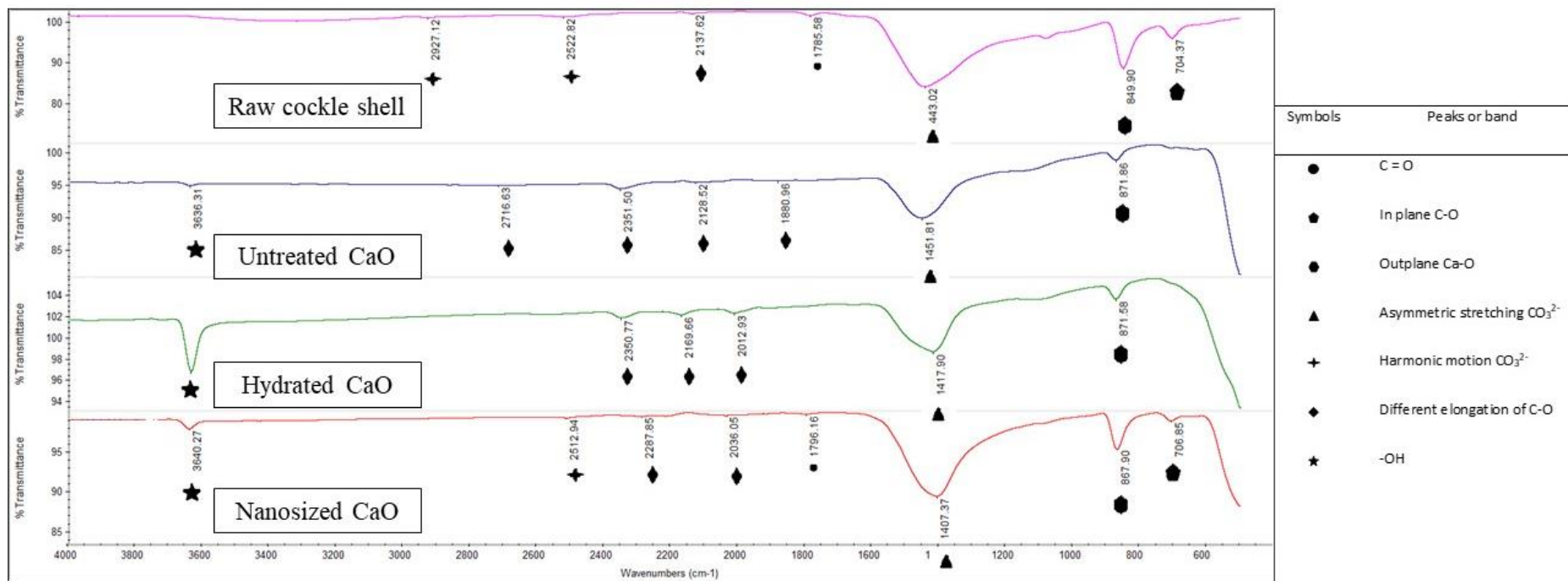


Figure 4.5: FT-IR spectra of (a) raw cockle shell, (b) CaO catalyst prepared via calcination treatment, (c) hydrated CaO and (d) nanosized CaO catalyst prepared via thermal hydration-dehydration treatment

Calcium carbonate content was found in the waste cockle shell. The existence of great peak at 1443 cm^{-1} which belongs to asymmetric stretching of carbonate ions (Wang *et al.*, 2010). The minor bands at 850 cm^{-1} and 704 cm^{-1} were responding to the out-of-plane band and in-plane band vibration modes of carbonate (CO_3^{2-}) group, correspondingly (Maneerung *et al.*, 2016). The bands presented at 2927 cm^{-1} , 2523 cm^{-1} and 704 cm^{-1} were corresponding to harmonic vibration of C-O elongation modes while the intense band at 1786 cm^{-1} is associated to the carbonate C=O double bonds (Rodriguez-garcia, 2009).

Additionally, the peaks intensity at 704 cm^{-1} , 850 cm^{-1} , 1443 cm^{-1} , 2523 cm^{-1} and 2927 cm^{-1} that related to CO_3^{2-} group in waste cockle shell were reduced in CaO catalyst prepared via calcination method and nano CaO catalyst prepared via thermal hydration-dehydration treatment. This indicated the decomposition of CaCO_3 into CaO with the released of CO_2 during the calcination treatment. The band from 867 cm^{-1} to 872 cm^{-1} corresponds to Ca—O bonds (Rodriguez-garcia, 2009).

CaO catalyst prepared via calcination method and nano CaO catalyst prepared via thermal hydration-dehydration treatment had the similar FT-IR spectra. The peaks that related to carbonate (CO_3^{2-}) group were reduced compared to the waste cockle shell's spectra. The band at 872 cm^{-1} for hydrated CaO and the band at 868 cm^{-1} for nano CaO catalyst prepared via thermal hydration-dehydration treatment correspond to Ca-O bonds. According to Rodriguez-garcia (2009), the band at 872 cm^{-1} was found in CaO

catalyst prepared via calcination method. This indicated the successful decomposition of calcium carbonate, CaCO_3 into CaO during the calcination.

The hydrated CaO had a peak located at 3640 cm^{-1} and it was referred to the formation of hydroxide ions between CaO and water molecules during hydration treatment at $60\text{ }^\circ\text{C}$ (Putra *et al.*, 2017). The peak located at 3636 cm^{-1} and 3640 cm^{-1} in spectra of CaO catalyst and nano CaO catalyst respectively were referred to the hydroxide ions which formed when CaO catalyst contacted to water vapour in the atmosphere (Putra *et al.*, 2017). The band at 1796 cm^{-1} in nano CaO catalyst's spectra corresponds to $\text{C}=\text{O}$ bonds.

In summary, the FT-IR analysis showed that waste cockle shell contained high amount of calcium carbonate, CaCO_3 . The CaCO_3 content in cockle shell was then transformed to CaO during the calcination treatment. The presence of the hydroxide ions in hydrated CaO showed that the hydration reaction between water and CaO catalyst was successfully carried out. The reduction of the intensity peak of hydroxide ions in nano CaO catalyst suggested with the removal of water molecules during recalcination or dehydration treatment.

4.1.3 X-ray Diffraction (XRD) Analysis

X-ray Diffraction was used to identify the phases, crystal structure and average crystallite size of the CaO catalysts. The diffractogram for waste cockle shell, CaO catalyst prepared via calcination method, hydrated CaO and

nano CaO catalyst prepared via thermal hydration-dehydration treatment were shown in Figure 4.6. The best nano CaO catalyst, 6_650_3 was selected for comparison.

The sharp peaks formation indicated the formation of highly crystalline materials. Figure 4.6a shows the diffractogram of waste cockle shell, the peaks with 2θ values at 26.2° , 27.2° , 33.1° , 36.2° , 37.9° , 38.4° , 42.9° , 45.8° , 50.2° , 52.5° , and 52.9° can be indexed to basal planes (111), (021), (012), (200), (112), (130), (211), (220), (221), (132), and (113) for aragonite crystalline form of CaCO_3 (Chong *et al.*, 2014).

The 2θ peak of CaO at 32.2° , 37.3° , 53.8° , 64.1° , and 67.3° can be index to the basal planes of (111), (200), (220), (311), and (222) respectively were found in the CaO catalyst prepared via calcination method (Figure 4.6b) and nano CaO catalyst prepared via thermal hydration-dehydration treatment (Figure 4.6d) (Cho *et al.*, 2009; Lesbani *et al.*, 2016). This again indicated that the decomposition of calcium carbonate and calcium hydroxide in nano CaO catalyst were accomplished during thermal hydration-dehydration treatment (Roschat *et al.*, 2018). However, the diffractogram of CaO catalyst prepared via calcination treatment and nanosized CaO showed a low intensity of peaks that belongs to impurities such as calcium carbonate and calcium hydroxide. These impurities were resulted from the reaction with carbon dioxide and water vapour in the atmosphere (Maneerung *et al.*, 2016).

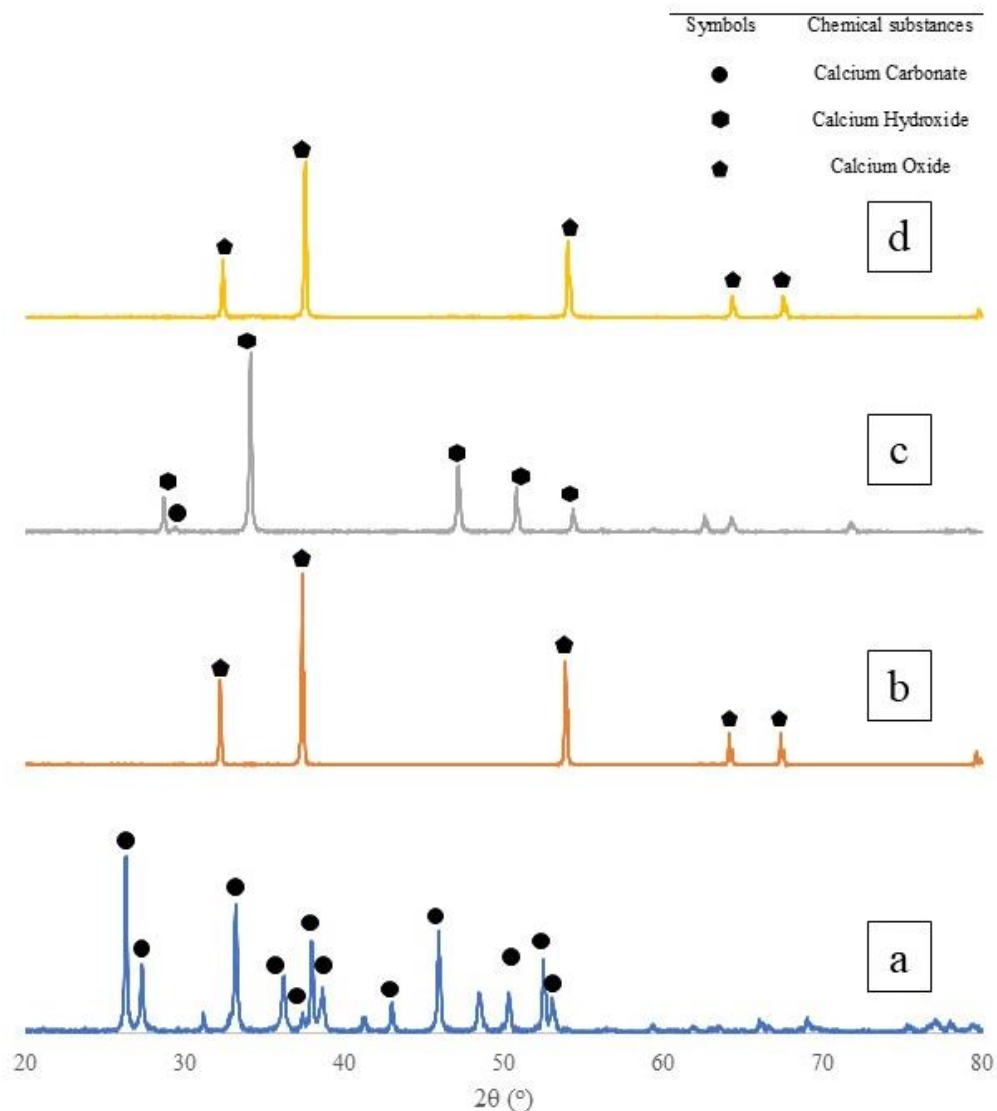


Figure 4.6: XRD analysis of (a) raw cockle shell, (b) CaO catalyst prepared via calcination treatment, (c) hydrated CaO and (d) nano CaO catalyst prepared via thermal hydration-dehydration treatment

Figure 4.6(c) shows the present of calcium hydroxide peaks at 2θ values 28.7° , 34.1° , 47.1° , 50.8° , 54.3° , 59.4° , 62.6° and 71.8° with corresponding basal planes of (001), (101), (102), (110), (111), (021), (013), and (022) in hydrated CaO was due to the reaction of calcium oxide with water during hydration process (Saoud *et al.*, 2014; Micic *et al.*, 2015).

The average crystallite size of nano CaO catalyst was calculated by using the Debye-Scherrer equation. Table 4.1 shows the average crystalline

size of four samples (waste cockle shell, CaO catalyst prepared via calcination method, hydrated CaO and nano CaO catalyst prepared via thermal hydration - dehydration treatment). The sample calculation for crystalline size was shown in Appendix G and the data to obtain average crystalline size for different samples were tabulated in Table H.3 (Waste cockle shell), Table H.4 (CaO catalyst prepared via calcination method), Table H.5 (Hydrated CaO) and Table H.6 (6_650_3) at Appendix H.

Table 4.1: Average crystalline size of different samples

Samples	Average crystalline size (nm)
Waste cockle shell	47.28
CaO catalyst prepared via calcination method	84.94
Hydrated CaO	55.44
Nano CaO catalyst prepared via thermal hydration-dehydration treatment	42.75

In brief, the compounds detected in XRD diffractogram for the cockle shell and CaO catalysts were in good agreement with FT-IR analysis which had further supported the present of calcium carbonate as aragonite phase in the waste cockle shell and absent in CaO catalyst prepared via calcination treatment and nano CaO catalyst prepared via thermal hydration-dehydration treatment.

4.1.3.1 XRD analysis: Nanocatalysts prepared under different hydration duration, recalcination temperature and recalcination duration

Nano CaO catalyst that developed under different parameters (hydration duration, recalcination temperature, and recalcination duration) were analysed by using XRD. As mentioned above, the 2θ peak for CaO at 32.2° , 37.3° , 53.8° , 64.1° , and 67.3° can be index to the basal planes of (111), (200), (220), (311), and (222) respectively were found in the nano CaO catalyst prepared under different parameters during thermal hydration-dehydration treatment (Cho *et al.*, 2009; Lesbani *et al.*, 2016). Figure 4.7 shows the diffractogram for nano CaO catalyst that developed under different hydration duration. Besides, Figure 4.8 shows the diffractogram for nano CaO catalyst that developed under different recalcination temperature, while Figure 4.9 shows the diffractogram for nano CaO catalyst that developed under different recalcination duration.

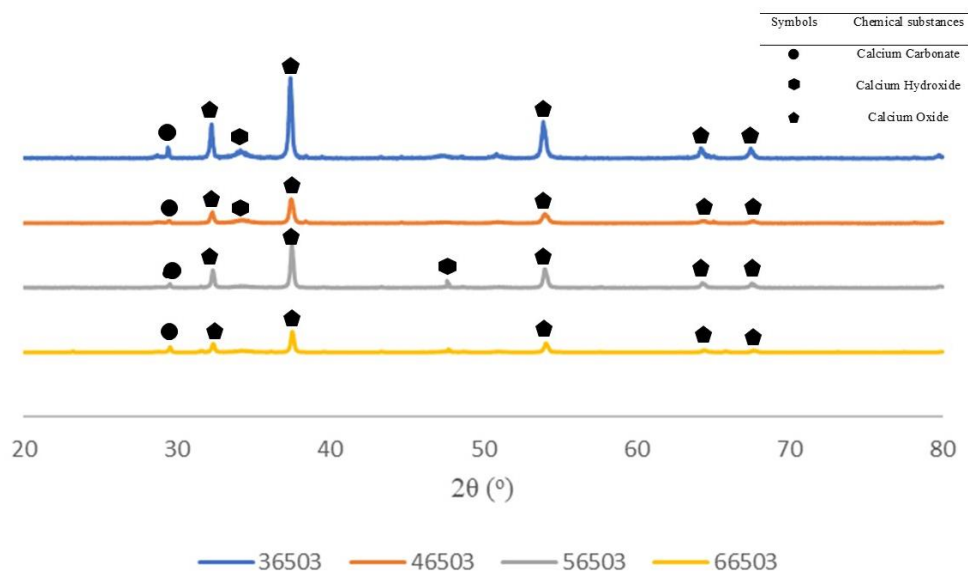


Figure 4.7: XRD analysis for effects of hydration duration

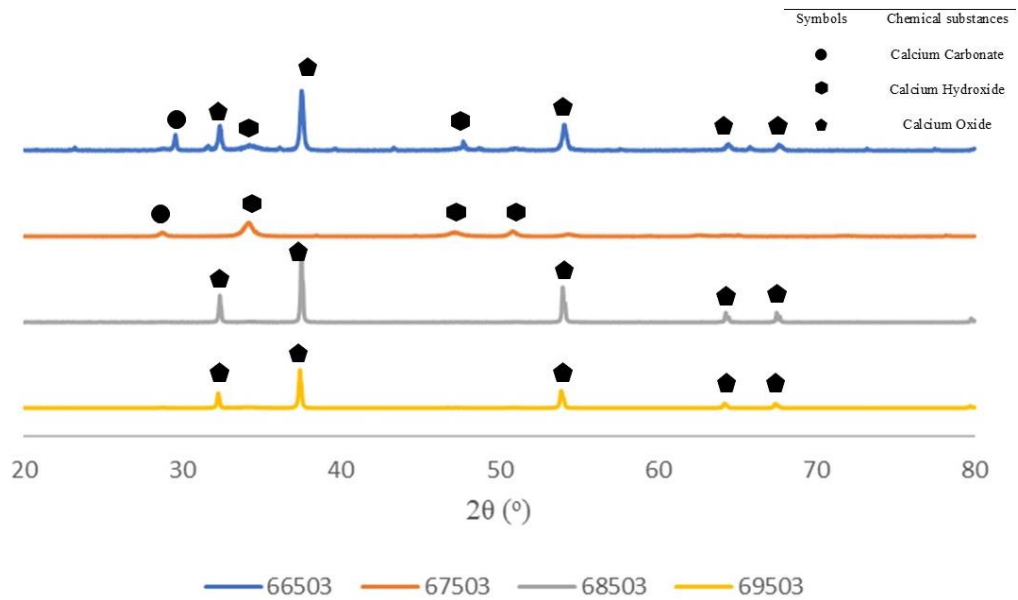


Figure 4.8: XRD analysis for effects of recalcination temperature

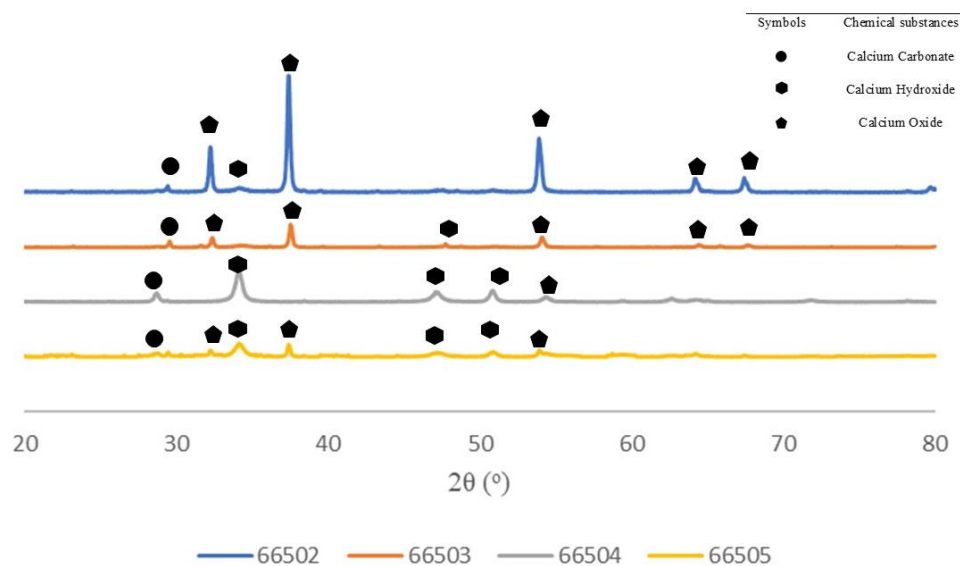


Figure 4.9: XRD analysis for effects of recalcination duration

Based on diffractograms, XRD analysis proved that nano CaO contain high amount of calcium oxide (CaO) compared to calcium hydroxide (Ca(OH)₂) and calcium carbonate (CaCO₃). From the XRD analysis, there were no significant difference in phases for different parameters (effects of hydration duration, recalcination temperature and recalcination duration).

Nevertheless, some of the nano CaO catalyst showed a low intensity of peaks that belongs to impurities such as calcium carbonate and calcium hydroxide. Part of the 2θ peaks that belongs to CaO were reduced in intensity or missing while the intensity for 2θ peaks of calcium carbonate and calcium hydroxide increased simultaneously. Based on Figure 4.7, among the different hydration hours samples, 66503 has the highest number of peaks that belongs to calcium oxide compared to other samples. The appearance of calcium hydroxide peaks instead of calcium oxide were found in 36503, 46503, and 56503 samples. This may due to the contamination of the water vapour in the atmospheric air (Maneerung *et al.*, 2016) or the long exposure of samples to the atmosphere during sample preparation for XRD analysis..

Besides that, Figure 4.8 showed the result of XRD analysis for different recalcination temperature. Samples 68503 and 69503 were only having the high number of peaks for calcium oxide while 66503 was having low number of impurities such as calcium hydroxide and calcium carbonate. Compared to 67503, it has the highest number of peaks for impurities and lowest number of peaks for calcium oxide. Similarly, the samples for 66503 and 67503 were contaminated with the water vapour and carbon dioxide in the atmospheric air (Maneerung *et al.*, 2016). This may due to the freshness of the catalyst during the XRD analysis. The samples for 68503 and 69503 were tested 2 days after it was produced while samples for 66503 and 67503 were tested 5 days after they were produced.

Moreover, Figure 4.9 showed the XRD analysis results for different recalcination duration. Among the four samples, high number of calcium oxide peaks with one calcium carbonate peaks were obtained by 66503 sample. The appearance of calcium hydroxide was obtained by 66502 sample. This may due to the incomplete decomposition of calcium hydroxide during the 2 hours recalcination. The samples for 66504 and 66505 were having highest number of impurities. This may due to the contamination of the water vapour and carbon dioxide in the atmospheric air (Maneerung *et al.*, 2016). And, the freshness of the catalyst during the XRD analysis may affect the appearance of the peaks belong to the impurities. The samples for 66504 and 66505 were tested 5 days after they were produced.

In short, the results from Figure 4.7 and Figure 4.9 showed that sample 66503 was having the highest number of peaks for calcium oxide compared to the impurities. Thus, the nano CaO catalyst obtained at 6 h hydration duration, recalcination temperature of 650 °C and recalcination duration of 3 h was expected to result in high FAME yield.

Table 4.2 shows the average crystalline size for nano CaO catalyst that developed under different parameters. The data to obtain the average crystalline size of nano CaO catalyst for different parameters were tabulated in Table 5.7 at Appendix H.

Table 4.2: Average crystalline size of different samples

Samples	Crystalline size (nm)
Effect of hydration duration	
3_650_3	37.58
4_650_3	41.80
5_650_3	38.64
6_650_3	35.19
Effect of recalcination temperature	
6_650_3	35.19
6_750_3	52.69
6_850_3	57.27
6_950_3	27.24
Effect of recalcination duration	
6_650_2	40.09
6_650_3	35.19
6_650_4	37.44
6_650_5	18.54

The crystalline size of nano CaO catalyst was calculated based on the 2θ peaks that belongs to CaO whereas the 2θ peaks that respect to impurities (calcium carbonate and calcium hydroxide) were ignored. The large crystalline size may indicate large particle size with low specific surface area. In other words, large average crystalline size may result in low biodiesel yield during transesterification of palm oil. Based on Table 4.2, the average crystalline size for effect of hydration duration in sequence of 6 h < 3 h < 5 h < 4 h. For effect of recalcination temperature, the sequence in 950 °C < 650 °C < 750 °C < 850 °C. And, the effect of recalcination duration had the sequence of 5 h < 3 h < 4 h < 2 h.

In summary, the small crystalline size of nano CaO catalyst obtained at 6 h hydration duration, recalcination temperature of 650 °C and recalcination duration of 5 h was expected to result in high FAME yield.

4.1.4 Scanning Electron Microscopy (SEM) analysis

The morphologies of raw cockle shell, CaO catalyst prepared via calcination method, hydrated CaO and nano CaO catalyst prepared via thermal hydration-dehydration treatment were shown in Figure 4.10.

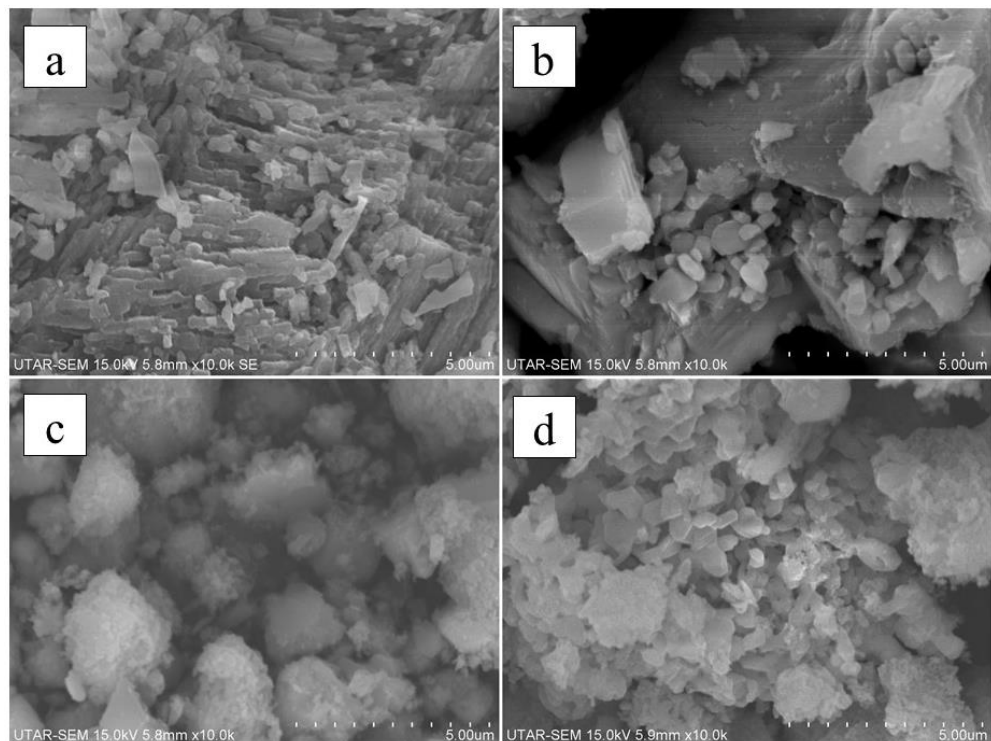


Figure 4.10: Structure of (a) raw cockle shell; (b) CaO catalyst prepared via calcination treatment; (c) hydrated CaO; and (d) nanosized CaO

The surface of raw cockle shell exhibits multiple layers of consistent rectangular shape with zero pores structures (Figure 4.10(a)). In Figure 4.10(b), the CaO catalyst derived from waste cockle shell via calcination at 900 °C

presented a rough and porous structure with inconsistent small particle sizes agglomerate. The formation of small particle sizes with porous structures have proved the formation of calcium oxide (Widayat *et al.*, 2017). The formation of porous channels can be attributed to the release of carbon dioxide during the thermal decomposition process (Tangboriboon *et al.*, 2012).

Figure 4.10(c) shows that hydrated CaO in sphere like shape that having uneven rough surface with low porosity. The porosities of CaO catalyst prepared via calcination method were reduced and its particle size were increased due to hydration reaction. When the CaO catalyst prepared via calcination method were refluxed in water, there was a transformation of oxide structures into hydroxide structures and increased the volume of the grains (Asikin-Mijan *et al.*, 2015). From Figure 4.10(d), the nano CaO catalyst prepared via thermal hydration-dehydration treatment shows a highly porosity and highly rough surface with the honey comb shape with sharp edges (Putra *et al.*, 2017). This is due to the immediate shrinkage of the expanded hydroxide structures during calcination that caused the cracking on the surface of the nano CaO catalyst prepared via thermal hydration-dehydration treatment catalyst (Yoosuk *et al.*, 2010). The highly porous structures helped to increase surface area which beneficial for achieving higher reaction rate.

In short, the transformation of the surface structure in calcium carbonate to CaO catalyst prepared via calcination treatment, then hydrated CaO and nano CaO catalyst prepared via thermal hydration-dehydration treatment were agree with the analyses in FT-IR, and X-ray Diffraction (XRD).

4.1.4.1 SEM analysis: Nanocatalysts prepared under different hydration duration, recalcination temperature and recalcination duration

The SEM images of catalysts prepared under different parameters such as hydration duration, recalcination temperature and recalcination duration were observed. Figure 4.11 shows the surface morphology of nanosized CaO that developed under different hydration duration. The SEM images for different hydration duration were captured under 5 k x magnification.

As the hydration h prolonged, the surface roughness and porosity of the nano CaO catalyst prepared by thermal hydration-dehydration treatment were increased. Nano CaO catalyst with 6 h hydration duration presented the non-uniform particle sizes, roughest surface with high number of sharp edges. Whereas rather smooth surfaces, bulky particles with minimum pores structures were discovered for nano CaO under 3 h hydration treatment. The prolonged hydration duration enhanced the formation of calcium hydroxide. The immediate water evaporation from hydrated catalyst during calcination had help to increase the formation of irregular sizes of particle with dense pores (Asikin-Mijan *et al.*, 2015). Thus, the catalytic properties of nano CaO catalyst were enhanced by prolong of hydration duration treatment.

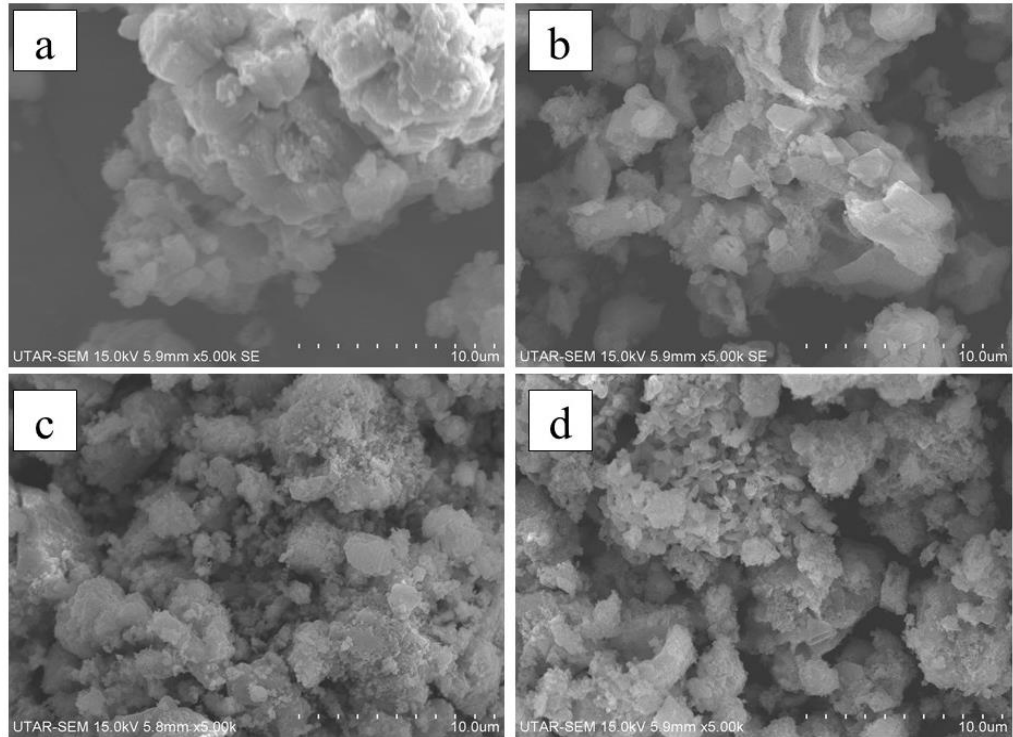


Figure 4.11: Effects of hydration duration (a) 3 h; (b) 4 h; (c) 5 h; and (d) 6 h to nano CaO catalyst

Figure 4.12 shows the surface morphologies of nano CaO catalysts prepared under different recalcination temperature treatment. The SEM images for catalysts different recalcination temperature were captured under 5 k x magnification. Nano CaO catalyst that developed under 950 °C calcination temperature had the smoothest surface while nano CaO catalyst recalcined at 650 °C had the roughest surface. As the recalcination temperature increased, the sharp edges start to accumulate and stack together which further reduce the surface roughness of nano CaO catalyst and the porous were demolished. This phenomena were interrelated to the sintering effects that were influenced by recalcination temperature (Smith *et al.*, 2013).

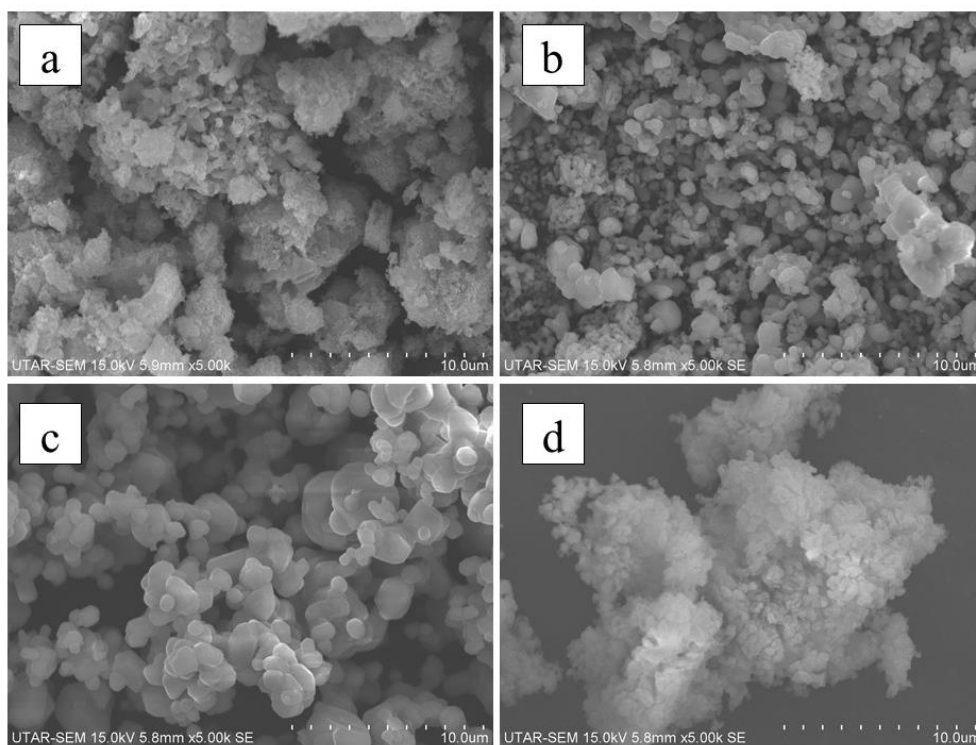


Figure 4.12: Effects of recalcination temperature (a) 650 °C; (b) 750 °C; (c) 850 °C; (d) 950 °C to nano CaO catalyst

Figure 4.13 shows the SEM images of nano CaO catalyst prepared under different recalcination duration. The SEM images for different recalcination duration were captured under 10 k x magnification. For nano CaO catalyst prepared under 2 h of recalcination, the surface structures were low in porosity and less surface roughness. Compared to 3 h of recalcination, the noticeable sharp edges and porous were observed. The sharp edges and pores on the surface of nano CaO catalyst were demolished gradually once the recalcination duration longer than 3 h. This phenomena was related to the sintering effects due to the prolonged recalcination duration (Micic *et al.*, 2015).

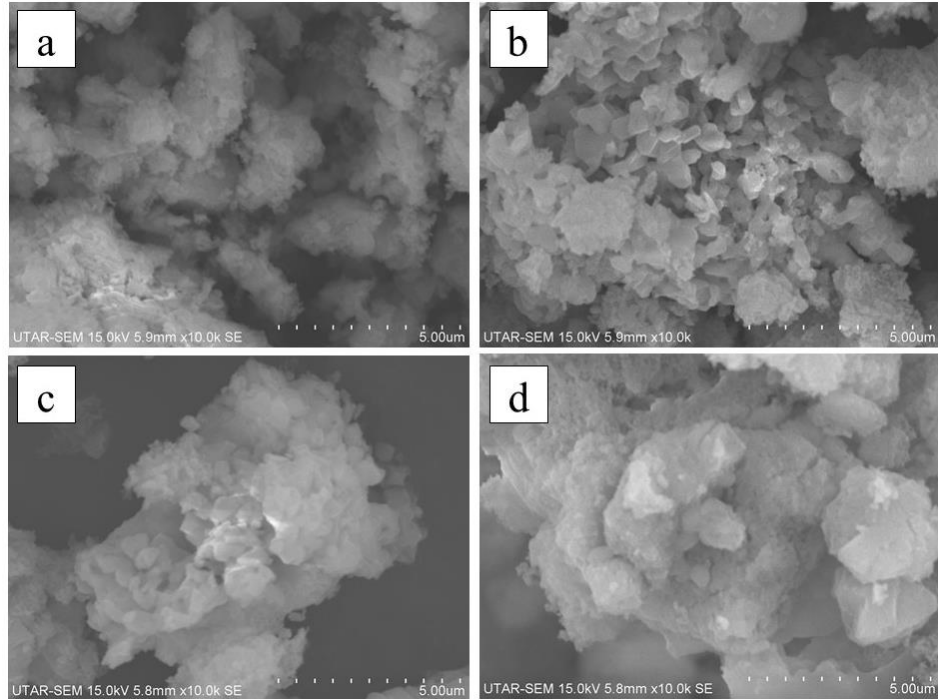


Figure 4.13: Effects of recalcination duration (a) 2 h; (b) 3 h; (c) 4 h and (d) 5 h to nano CaO catalyst

In summary, based on the surface morphologies observation, 6 h of hydration duration, 650 °C of recalcination temperature and 3 h recalcination duration were predicted as the optimum condition to develop nano CaO catalyst. This is because the irregular size of honey comb shape like small particles with high number of sharp edges and pores were found on the surface of 6_650_3 nano CaO catalyst.

4.1.5 Energy Dispersive X-ray (EDX) Analysis

Energy dispersive X-ray (EDX) spectroscopy was conducted to study the presence of elements and its composition (at % or wt %) in the sample. Four samples (waste cockle shell, CaO catalyst prepared via calcination method, hydrated CaO, and nano CaO catalyst prepared via thermal hydration-

dehydration treatment) were analysed. Table 4.3 shows the EDX results for the four different samples. The data to obtain average weightage of elemental compound for different samples were tabulated in Table I.8 (Waste cockle shell), Table I.9 (CaO catalyst prepared via calcination method), Table I.10 (Hydrated CaO) and Table I.11 (6_650_3) at Appendix I.

The elements that present in waste cockle shell were calcium, oxygen with trace amount of sodium, magnesium and carbon. (Mohamed *et al.*, 2012) reported the similar chemical composition of waste cockle shell. For CaO catalyst prepared via calcination method, calcium, oxygen with trace amount of sodium, silicone, and carbon.

Some of the elements was not detected in every samples. The absent of silicone in waste cockle shell may due to its surface structure. Based on SEM analyses, waste cockle shell was having rectangular shape stacking structure which may cover the elements from the detection of EDX analyses. Magnesium was not detected in CaO catalyst. Similarly, the trace amount of the elements (magnesium, silicone and sodium) was not detected in hydrated CaO and nano CaO catalyst prepared via thermal hydration-dehydration treatment. These phenomena may cause by the preparation of sample during EDX analyses. Only small amount of CaO catalyst powder was taken for EDX analyses and therefore, the low percentage, 0.60 % of magnesium was not detected.

For CaO catalyst prepared via calcination method, hydrated CaO and nano CaO catalyst prepared via thermal hydration-dehydration treatment, a reduction of carbon content which indicated that the removal of carbon dioxide was occurred during the calcination treatment. In CaO catalyst prepared via calcination treatment and nano CaO catalyst prepared via thermal hydration-dehydration treatment, major elements detected were calcium and oxygen which showed that the catalyst mostly occupied with CaO active sites and reflects its better catalytic activity. According to Rodriguez-garcia (2009), the presence of carbon atom in the catalyst was due to the contamination of the catalyst with CO₂ when the catalyst exposed to the atmosphere during the preparation of samples for EDX analyses.

Table 4.3: Average weightage of elemental compound in different samples

Samples	Average weightage (wt%)					
	C	O	Ca	Na	Si	Mg
Waste cockle shell	12.48	44.64	41.20	1.09	0.00	0.60
CaO catalyst prepared via calcination treatment	10.74	16.72	83.28	0.95	0.39	0.00
Hydrated CaO	4.23	35.31	60.47	0.00	0.00	0.00
Nano CaO catalyst prepared via thermal hydration-dehydration treatment	2.290	16.06	75.65	0.00	0.00	0.00

In summary, the raw cockle shell was decomposed into CaO catalyst prepared via calcination treatment during first calcination, followed by the reaction between CaO and water molecules during hydration process, then formation of nano CaO catalyst in recalcination. The results in EDX analysis were matched to the results in Thermogravimetric analysis, FT-IR analysis, and X-ray Diffraction (XRD) analysis.

4.1.5.1 EDX analysis: Nanocatalysts prepared under different hydration duration, recalcination temperature and recalcination duration

The nano CaO catalysts that developed under different parameters (hydration duration, recalcination temperature and recalcination duration) were undergone EDX analyses. Table 4.4 shows the average weightage of the elemental compound for different parameters. The data to obtain the average weightage of different parameters were tabulated in Table 5.11 at Appendix I.

Table 4.4: Average weightage of different parameters

Samples	Average weightage (wt %)		
	C	O	Ca
Effect of hydration h			
3_650_3	4.94	35.07	59.99
4_650_3	5.04	41.23	53.73
5_650_3	4.90	27.18	67.92
6_650_3	2.29	16.06	75.65
Effect of recalcination temperature			
6_650_3	2.29	16.06	75.65
6_750_3	5.25	39.29	55.32
6_850_3	4.70	41.87	53.44

Table 4.4 (Continued): parameters	Average	weightage	of different
6_950_3	3.67	28.93	67.40
Effect of recalcination duration			
6_650_2	3.18	33.31	63.51
6_650_3	2.29	16.06	75.65
6_650_4	5.30	29.94	64.76
6_650_5	3.02	40.45	56.53

As mentioned above, the trace amount of carbon atom in the catalyst was due to the contamination of the catalyst with CO₂ when the catalyst exposed to the atmosphere (Rodriguez-garcia, 2009). According to the theory, CaCO₃ compound has weightage composition of calcium, carbon and oxygen as 40%, 12 % and 48% respectively. Whereas the active phase of CaO compound should have 0% of carbon element and the weightage composition of calcium and oxygen as 71% and 28% respectively. From Table 4.4, the very low amount of carbon element (less than 6%) and high amount of Ca content (more than 55%) indicated high amount of CaO active sites available in the synthesized catalysts. This also reflected the better catalytic activity possessed by the catalysts.

Based on Table 4.4, the calcium content increased according to the sequence of hydration duration, 4 h < 3 h < 5 h < 6 h. This claimed that 6 h hydration may have great amount of CaO active sites. During the hydration treatment on CaO catalyst, hydroxylation reaction was occurred on the surface of CaO which promoted the formation of hydroxides. The long hour contact of CaO with water accelerated the growth of Ca (OH)₂ layers. This promoting the

formation of nano CaO catalyst (Yoosuk *et al.*, 2011) which may cause high calcium content was being detected during EDX analysis.

For recalcination temperature, the trend for weightage of calcium was $850\text{ }^{\circ}\text{C} < 750\text{ }^{\circ}\text{C} < 950\text{ }^{\circ}\text{C} < 650\text{ }^{\circ}\text{C}$. These results predicted that the optimized recalcination temperature was $650\text{ }^{\circ}\text{C}$. The sintering effects may occur on the surface of the nano CaO catalyst prepared as the recalcination temperature increases (Smith *et al.*, 2013). As the calcination temperature increased, the rough structure on the nano CaO catalyst surface was demolished gradually due to the agglomeration of small particles. Thus, low weightage of calcium was then detected as the recalcination temperature increases. Theoretically, the trend for weightage of calcium should be $950\text{ }^{\circ}\text{C} < 850\text{ }^{\circ}\text{C} < 750\text{ }^{\circ}\text{C} < 650\text{ }^{\circ}\text{C}$. However, recalcination temperature, $950\text{ }^{\circ}\text{C}$ sample obtained a higher weightage of calcium than $750\text{ }^{\circ}\text{C}$ and $850\text{ }^{\circ}\text{C}$ samples. When sintering effect was initiated, the active sites on the surface of the catalyst agglomerates randomly. The higher weightage of calcium in $950\text{ }^{\circ}\text{C}$ sample may due to the detection of calcium content with uneven agglomeration during the EDX analysis.

And lastly, the sequence of calcium weightage for recalcination duration was $5\text{ h} < 2\text{ h} < 4\text{ h} < 3\text{ h}$. The optimized recalcination duration was predicted as 3 hours. Similar to the recalcination temperature, sintering effects may occur on the surface of the nano CaO catalyst. The small particles on the surface of nano CaO was started to agglomerate and form a bigger particle. This indirectly causes a reduction to the amount of active site and the specific

surface area expose to the reaction environment (Reli *et al.*, 2012), hence, low calcium weightage was detected during EDX analysis. Based on the trend for recalcination duration, 2 h and 4 h samples were having similar calcium weightage which lower than the 3 h samples. For nano CaO that undergo 3 h recalcination, high calcium weightage proved that the nano CaO was fully activated with high number of active sites. In other word, 2 h recalcination duration sample was partially activated which having low number of active sites, thus low calcium weightage was detected. The decrease of calcium weightage in 4 h recalcination duration sample may due to the occurrence of sintering effect.

In summary, the optimized nano CaO catalyst was predicted to be developed under 6 h of hydration with recalcination temperature of 650 °C for 3 h.

4.2 Analysis on sintering effects

Sintering effects can be initiated by high calcination temperature or prolonged calcination duration at constant temperature. In this research, four samples were chosen for Temperature Programmed Desorption (TPD) analysis, Brunauer-Emmett-Teller (BET) analysis and High-Resolution Transmission Electron Microscopy (HRTEM) analysis.

The four samples were waste cockle shell, and CaO catalyst prepared via calcination treatment (6_650_3, 6_950_3 and 6_650_5). The best nano CaO catalyst, 6_650_3 was compared with waste cockle shell to differentiate

the effects of thermal hydration-dehydration treatment. Besides, the nano CaO 6_950_3 that developed under high temperature, 950 °C was compared with 6_650_3 to observe the effect of high calcination temperature. Lastly, the nano CaO 6_650_5 that calcined for 5 h was compared with 6_650_3 to study the effect of prolonged calcination duration.

4.2.1 Temperature Programmed Desorption (TPD) Analysis

The basicity of CaO catalyst prepared via calcination method and nano CaO catalyst prepared via thermal hydration-dehydration treatment were determined by using Temperature Programmed Desorption (TPD) Analysis. Table 4.5 shows the total basicity of both catalysts.

Table 4.5: Total basicity of catalysts

Catalyst	Total basicity ($\mu\text{mol CO}_2/\text{g}$)
CaO prepared via calcination method	462.62
nano CaO prepared via thermal hydration-dehydration treatment	
6_650_3	1046.46
6_950_3	849.98
6_650_5	241.53

The basicity of catalysts indicated the number of active sites available in the catalyst during the chemical reaction. In other words, catalyst with higher basicity had better catalytic performance compared to the catalyst with lower basicity (Asikin-Mijan *et al.*, 2015). Based on Table 5.5, nano CaO catalyst was having total basicity, 1046 $\mu\text{mol CO}_2/\text{g}$ which double of CaO catalyst total basicity, 463.62 $\mu\text{mol CO}_2/\text{g}$. This proved that the number of

active sites in nano CaO catalyst was greater than CaO catalyst. Thus, it concluded that the catalytic performance of CaO catalyst was enhanced by thermal hydration-dehydration treatment.

Besides that, the sintering effects may occur when recalcination temperature increased or recalcination duration prolonged. By comparing, the basicity of nano CaO developed under 650 °C, 1046.46 $\mu\text{mol CO}_2/\text{g}$ was higher than 950 °C, 849.98 $\mu\text{mol CO}_2/\text{g}$. And the basicity of nano CaO under recalcination for 5 hours, 241.53 $\mu\text{mol CO}_2/\text{g}$ was lower than recalcination for 3 hours. 1046.46 $\mu\text{mol CO}_2/\text{g}$. The trend shows that the high recalcination temperature and prolonged recalcination duration may initiate the sintering effects. This will further influence the catalytic performance of nano CaO catalyst during transesterification reaction of palm oil and reduce the biodiesel yield.

4.2.2 Brunauer-Emmett-Teller (BET) Analysis

The samples were undergoing BET analysis to estimate the multipoint BET surface area, total pore volume and the average of pore diameter. Four samples were chosen (CaO catalyst prepared via calcination treatment, 6_650_3, 6_950_3 and 6_650_5) for the analysis and further discuss. Table 4.6 summarized the BET data for the four samples.

According to Roschat *et al.* (2012), high value in BET surface area indicates higher basicity and catalytic performance of the nano CaO catalyst

which will further influence the biodiesel yield during transesterification. From Table 4.3, thermal hydration-dehydration method did enhance the performance of the CaO catalyst since nano CaO had obtained higher surface area than CaO catalyst prepared via calcination treatment.

Nano CaO that developed under calcination temperature of 650 °C had higher surface area and pore volume than calcination temperature of 950 °C. In contrast, the average pore diameter become larger from 39.55 nm to 40.65 nm as the calcination temperature increased. Similar trend was observed in Raj and Viswanathan (2009). They claimed that the surface area and pore volume of P25 sample had a decreasing trend with increasing of calcination temperature from 500 °C to 900 °C, yet, the pore size showed an increasing

Table 4.6: BET data for CaO catalyst prepared via calcination treatment, and nano CaO catalyst prepared via thermal hydration-dehydration treatment (6_650_3, 6_950_3 and 6_650_5)

Sample	Multipoint BET(m ² /g)	Total pore volume(cm ³ /g)	Average pore diameter(nm)	Biodiesel yield (%)
CaO catalyst prepared via calcination treatment	0.710 ± 0.004	0.00619	124	10
nano CaO catalyst prepared via thermal hydration-dehydration treatment				
6_650_3	13.9 ± 0.178	0.0318	33.2	82
6_950_3	10.2 ± 0.0758	0.0219	41.7	52
6_650_5	10.8 ± 0.132	0.0944	35.1	29

trend with the calcination temperature. These show that recalcination temperature plays important role during the synthesis of nano CaO, the critical high temperature can reduce the surface area and pore volume of the catalyst. In other words, sintering effect of the catalyst was happened where the porous structure will be eliminated and lowest BET surface area was obtained as the calcination temperature increased (Menad *et al.*, 2016).

A similar trend was found in the variation of recalcination duration. It gives the same effect to the nano CaO whereby calcination for 3 h was having surface area of 14.62 m²/g and pore volume of 0.1455 cm³/g higher than calcination for 5 h. At the same time, the average pore diameter increased from 39.55 nm to 44.01 nm as the calcination duration prolonged. These phenomena can be described by the sintering effect as the calcination duration prolonged, the active sites started to agglomerate and reduce the surface area of the nano CaO.

The size of porous on the nano CaO surface can affect the reaction rate of transesterification. According to Chang, H.J. and Crynes (1986), a smaller pore diameter may accumulate products inside the pore which can deactivate the active sites in the pores. This phenomenon can become rate limiting step for the reaction. However, rate of reaction may not affect by larger pore size due to the slow accumulation of products as well as increase the activity of catalyst. Based on Table 4.6, the increment of average pore diameter may not increase the rate of reaction. The rate limiting step that influence by the pores of nano CaO catalyst can be eliminated when the size of pore diameter falls within the range of 39.55 nm to 44.01 nm.

In addition, triglycerides in palm oil and methanol were the reactants in transesterification reaction. Four fatty acids were found in palm oil such as palmitic acid, stearic acid, oleic acid and linoleic acid. According to Shuit *et al.* (2015), palmitic acid has a spatial width of 0.372 nm, stearic acid was 0.25 nm, oleic acid was 0.72 nm and linoleic acid was 1.13 nm respectively. Besides, methanol molecule had a kinetic diameter around 0.39 nm (ten Elshof *et al.*, 2003). For the products from transesterification reaction, the molecular size of glycerol was around 0.1 nm while the molecular size of FAME was predicted within the range of 0.64 nm to 1.52 nm (Jahn *et al.*, 2016). Thus, the size of reactants and products were fall within the range of 0.25 nm to 1.52 nm which was accessible to the active sites available at the inner pore of nano CaO catalyst with average pore diameter of 39.55 nm.

In short, the surface structure of nano CaO catalyst sintered when recalcination temperature and recalcination duration increased. The results were interrelated with SEM analysis. Besides, the surface area of the nano CaO catalyst was the main factor that affecting the rate of reaction during transesterification of palm oil whereas pore volume and average pore diameter do not give a great influence.

4.2.3 High Resolution Transmission Electron Microscopy (HRTEM) analysis

Four sample (CaO catalyst prepared via calcination treatment, 6_650_3, 6_950_3, 6_650_5) were chosen to conduct HRTEM analysis to investigate the particle size and the arrangement of nano CaO. Figure 4.14 shows the HRTEM images of the four samples.

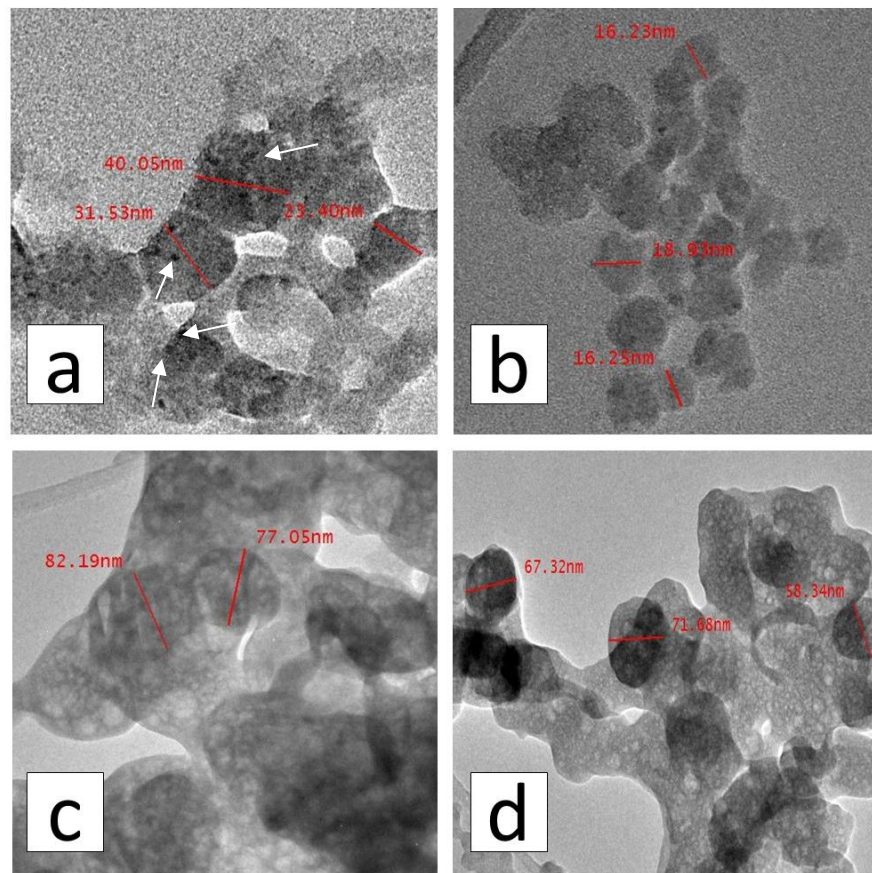


Figure 4.14: HRTEM analysis of (a) CaO catalyst prepared via calcination treatment, (b) 6_650_3, (c) 6_950_3 and (d) 6_650_5

Figure 4.14(b) has the consistent sphere like shape particle and it is monolayer arrangement, another three samples (Figure 4.14(a), Figure 4.14(c), and Figure 4.14(d)) have the mixing of rod and oval shapes with overlapping

arrangement. The different shape of the particles between Figure 4.14a and Figure 4.14b shows that thermal hydration- dehydration treatment had successfully carried out. Besides that, in Figure 4.14(a), there are some black spots that label by white arrows which size smaller than 5 nm. The black spot may due to multilayer arrangement of particles as the small particles (size < 5nm) may stack on the large particles (size range of 23 nm to 40 nm).

Figure 4.14b has smaller particle size range of 16 nm to 19 nm compared to Figure 4.14a with particle size range of 23 nm to 40 nm. This proved thermal hydration- dehydration treatment can help to further reduce the particle size of CaO catalyst and thus increase surface area and catalytic performance of nano CaO catalyst prepared via thermal hydration-dehydration treatment.

The particle grows larger with the overlapping arrangement as the calcination temperature increased. The morphologies of catalysts under prolonged calcination treatment resulted in the similar trend. These phenomena might due the existence of sintering effect. When sintering was introduced, the smaller particle may start to move and agglomerate to form a larger particle. The nano CaO catalyst prepared via thermal hydration-dehydration treatment was successfully developed with particle size fall within the range of 1 to 100 nm. The findings were in good agreement with BET analysis and the SEM analysis that support the existence of sintering effect at recalcination temperature of 950 °C.

In summary, the nano CaO catalyst prepared via thermal hydration-dehydration treatment was successfully developed with particle size fall within the range of 1 to 100 nm. The particles were increase in size and the arrangement of particles were overlapping when the calcination temperature increased and duration prolonged which proved the sintering was occurred. The result was agreed with the trend in BET and SEM analyses.

4.3 Optimization of thermal hydration-dehydration treatment

Each of the nano CaO catalysts that developed during the optimization of thermal hydration-dehydration treatment were undergone transesterification reaction. A preliminary run by using nano CaO that developed under 4 hours hydration and recalcination temperature at 650 °C for 3 hours was done to verify the total reaction time to achieve equilibrium. Figure 4.15 shows the trend of the transesterification reaction for 6 hours.

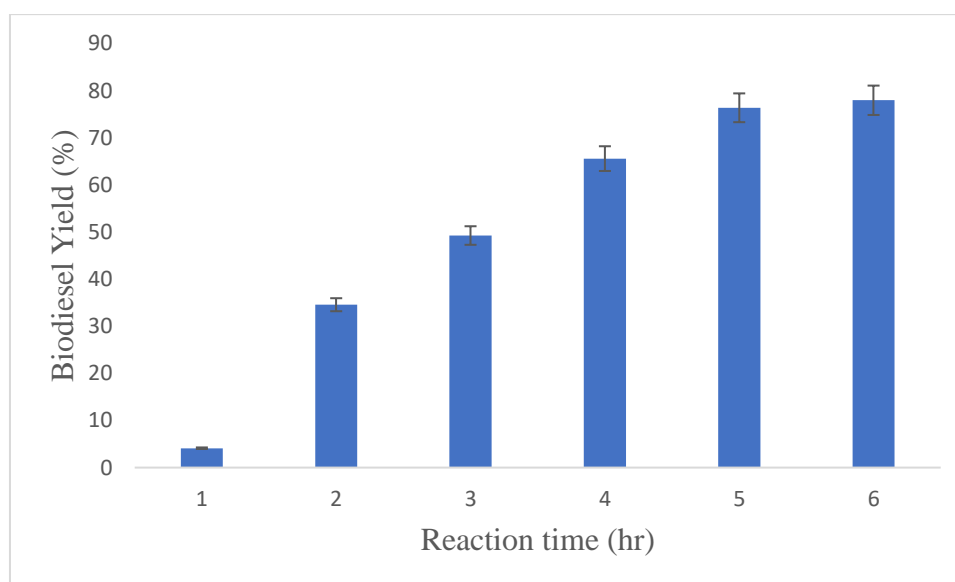


Figure 4.15: Preliminary run for transesterification reaction.

The equilibrium biodiesel yield of 76 % was achieved at 5 hours reaction time. Due to the reversibility nature of the transesterification reaction, a prolonged reaction time can shift the reaction to backward direction and decrease the biodiesel yield (Latchubugata et al., 2018). Thus, the total and optimum reaction time was set at 5 hours during the optimization study of key parameters related to catalyst performance with data collected in 2 hours step change (1 hour, 3 hours, and 5 hours). The biodiesel yield was obtained from the GC analysis and calculation by using equation 3.3. Three runs of transesterification reaction were conducted for each of the nano CaO catalyst that developed under different parameters. The percentage error for the data were fall in the range of 3 % to 5 %.

4.3.1 Effect of Hydration duration

The effect of hydration duration towards the catalytic performance of nano CaO prepared via thermal hydration-dehydration treatment was studied. Figure 4.16 shows the trend of biodiesel yield against the duration for hydration process.

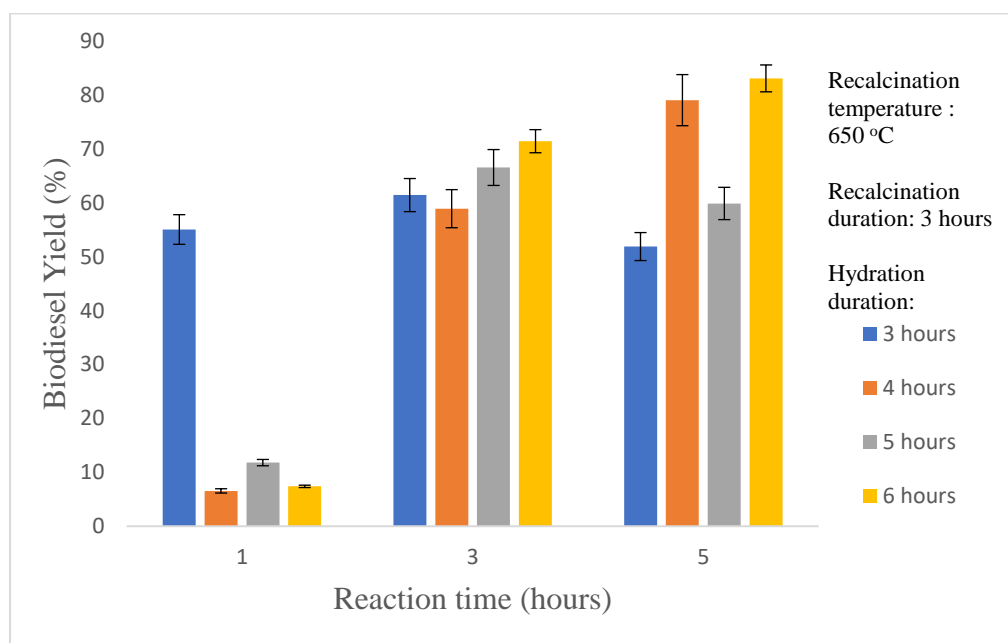


Figure 4.16: The relationship of biodiesel yield and the duration of hydration for 5 h reaction time

Based on Figure 4.16, the biodiesel yield increased with increased hydration duration. The biodiesel yield increased according to sequence of hydration duration 3 h < 4 h < 5 h < 6 h. The increasing trend of biodiesel yield with lengthy hydration duration was reported by Asikin-Mijan, Taufiq-Yap and Lee (2015).

During the hydration treatment on CaO catalyst, hydroxylation reaction was occurred on the surface of CaO which promoted the formation of hydroxides. The CaO catalyst with long hour contact with water accelerated the growth of Ca (OH)₂ layers. The heat decomposition of water molecules from the Ca(OH)₂ lattice structure during recalcination had led to the fractionation of crystallites into smaller particles' sizes, thus promoting high surface area, high porosity and pore volume (Yoosuk *et al.*, 2011).

Additionally, the hydration- dehydration treatment drastically improve the basicity by introducing Bronsted basic sites which increases the total basic sites and total basicity of the nano CaO (Yoosuk *et al.*, 2010). The results proved that the prolonged hydration duration enabled more hydroxide phases to form and increases the total basicity of the nano CaO, which correlates to the enhancement of active sites for the reaction leading to a higher biodiesel yield.

The morphologies observation of the catalysts has been discussed in SEM and BET analyses and both characterization results were in agreement with catalytic performance. The results proved that the prolonged hydration duration enhanced the catalytic activity of catalysts and thus lead to high biodiesel yield. 6 h was determined as the optimum hydration duration in the subsequent optimization studies.

4.3.2 Effect of Recalcination temperature

The experiment continues with 6 h hydration duration to optimize the recalcination temperature. The parameter was set at 650 °C, 750 °C, 850 °C and 950 °C for 3 h recalcination. Figure 4.17 shows the effects of recalcination temperature during the synthesise of nano CaO catalyst prepared via thermal hydration-dehydration treatment to the biodiesel yield.

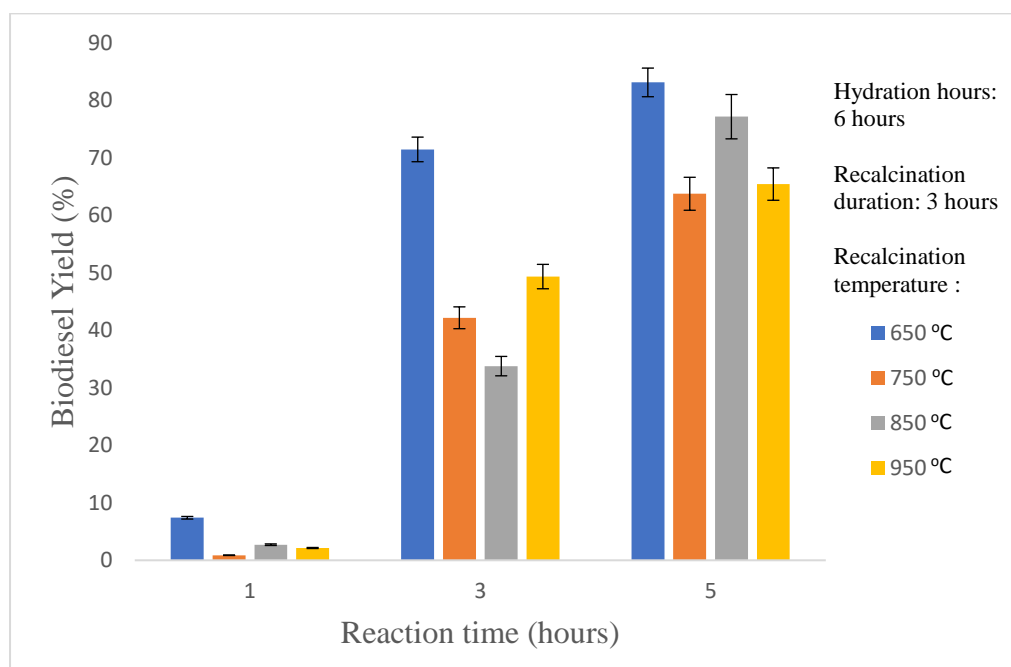


Figure 4.17: The relationship of biodiesel yield and the recalcination temperature for 5 h reaction time

For five-hour reaction, the highest biodiesel yield was achieved at 82 % for catalyst recalcined at temperature of 650 °C. The biodiesel yield reduced with the increased recalcination temperature where only 59 % biodiesel yield achieved for catalyst recalcined at 950 °C. The reason to this occurrence can be linked to the sintering effects on the surface of the nano CaO catalyst prepared via thermal hydration-dehydration treatment catalysts as the recalcination temperature increases (Smith *et al.*, 2013). As the calcination temperature increased, the rough structure on the nano CaO catalyst surface was demolished gradually due to the agglomeration of small particles. The morphologies observation of the catalysts has been discussed in SEM, TEM and BET analyses and both characterization results were in agreement with catalytic performance.

According to Smith *et al.* (2013), the highest biodiesel yield was obtained when the reaction was catalysed by catalyst prepared under 650 °C calcination temperature. As the calcination temperature of prepared catalyst gradually increased from 650 °C to 1100 °C, a decreasing trend of biodiesel yield was observed. In the current study, 650 °C was selected as the optimum recalcination temperature in the subsequent optimization study.

Thus, it proved that the recalcination temperature can affect the number of active sites available for reactant attachment and effectively vary the biodiesel yield. It is clearly concluded that the recalcination temperature of 650 °C was the optimum recalcination temperature which led to a biodiesel yield up to 72 % in 3 h reaction time.

4.3.3 Effects of Recalcination duration

Since recalcination temperature at 650 °C obtained the highest biodiesel yield, the temperature was carried forward for the optimization of recalcination duration. The duration for recalcination were set at 2 h, 3 h, 4 h and 5 h at 6 h hydration. Figure 4.18 reported the influence of the recalcination duration to the biodiesel yield.

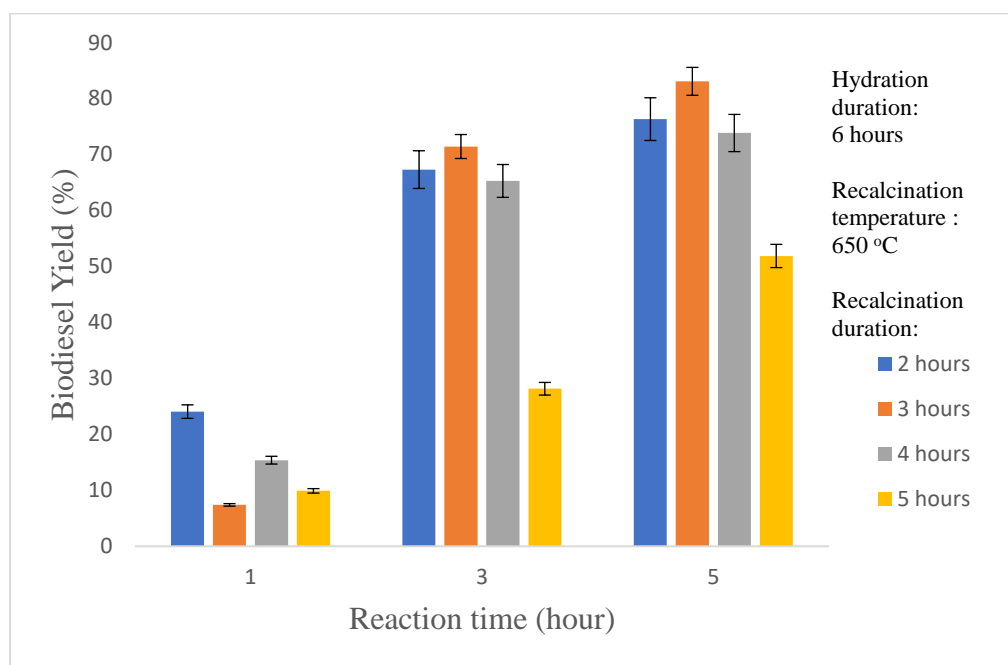


Figure 4.18: The relationship of biodiesel yield and the recalcination duration for 5 h reaction time.

Figure 4.18 shows that prolonged recalcination duration of more than 3 h can gradually reduce the biodiesel yield. For catalyst recalcined for 3 h, the highest biodiesel yield was achieved at 82 % for 5 h reaction time, followed by 4 h recalcination, 2 h recalcination, and the lowest biodiesel yield was only 49 % for 5 h recalcination. This is because the sintering effects was occurred on the surface of the nano CaO catalyst prepared via thermal hydration-dehydration treatment catalysts. The small particles on the surface of nano CaO was started to agglomerate and form a bigger particle. This indirectly causes a reduction to the amount of active site and the specific surface area of the nano CaO catalyst prepared via thermal hydration-dehydration treatment expose to the reaction environment (Reli *et al.*, 2012).

The morphologies observation of the catalysts has been discussed in SEM, TEM and BET analyses and both characterization results were in

agreement with catalytic performance. In the study, 3 h was selected as the optimum recalcination duration for the thermal hydration and dehydration treatment of CaO catalyst.

4.3.4 Optimization study

The treatment conditions used to develop nano CaO catalyst with good catalytic performance for transesterification reaction of palm oil were optimized. Table 4.7 shows the biodiesel yield that was obtained at 5 hours reaction time corresponding to the reaction time at equilibrium zone.

Based on Table 4.7, 3 out of 4 characterization studies were in good agreement with the biodiesel yield obtained during transesterification of palm oil. Thus, the optimized condition to develop the nano CaO catalyst via thermal hydration-dehydration treatment was 6 h hydration, recalcination under 650 °C for 3 h.

Table 4.7: Optimized condition based on the characterization studies and biodiesel yield obtained at 5 h reaction time

Types of characterization studies	Optimum nanocatalyst			Biodiesel FAME yield (%)
	Hydration duration (h)	Recalcination temperature (°C)	Recalcination duration (h)	
XRD	6	650	5	52
SEM	6	650	3	82
EDX	6	650	3	82
TPD-CO ₂	6	650	3	82
GC	6	650	3	82

As shown in Table 4.7, the optimum condition based on XRD results was disproportion with the biodiesel yields obtained in transesterification reaction. In section 4.1.3.1, the small crystalline size of nano CaO catalyst obtained at 6 h hydration duration, recalcination temperature of 650 °C and recalcination duration of 5 h was expected to result in high FAME yield. According to Rabiei *et al.* (2020), the estimation of crystalline size (summarized in Table 4.2) by using Debye-Scherrer equation may inaccurate. The prediction on the trend of biodiesel yields based on particle size should refer to the characterization studies by using SEM, BET and TEM analyses. Hence, the expectation to obtain high biodiesel yield by nano CaO catalyst based on crystalline size in Table 4.2 was invalid.

4.3.5 Comparison of optimized nano CaO catalyst (6_650_3) with literature

The catalytic performance of optimized nano CaO catalyst (6_650_3) was compared with the similar catalysts from other researchers. Table 4.8 summarized the catalysts, transesterification condition, and biodiesel yield obtained by different catalysts with palm oil as oil feedstock.

Based on literature, CaO catalyst that derived from *A. cristatum shell* undergone transesterification of palm oil with the same reaction condition (8 :1 alcohol to oil molar ratio, 3 wt% of catalyst loading and 60 °C operating temperature) as nano CaO catalyst synthesized in the current study. A greater

biodiesel yield of 93 % was obtained from *A. cristatum shell* derived CaO catalyst compared to current study with 82 %. However, the time spent of 5 hours for nano CaO (in the current study) to achieve 82% equilibrium yield was shorter than *A. cristatum shell* derived CaO catalyst with 6 hours reaction time spent to achieve 93% biodiesel yield. This shows that nano CaO has competitive performance with advantage of shorter reaction time. In addition, the lower biodiesel yield, 82 % obtained in the current study can be further improved by optimizing the operating conditions (catalyst dosage, methanol to oil ratio, operating temperature) for the transesterification of palm oil that catalysed by the nano CaO catalyst.

Table 4.8: Comparison of optimized nano CaO catalyst with catalyst synthesized by other researchers with palm oil as feedstock

Catalyst	Alcohol to oil molar ratio	Weight of catalyst (wt %)	Process temperature (°C)	Process duration (h)	Yield (%)	Reference
nano CaO	8:1	3	60	5	82	Current study
CaO derived from <i>A. cristatum shell</i>	8:1	3	60	6	93	(Suryaputra <i>et al.</i> , 2013)
CaO supported by activated carbon	15:1	5.50	190	1.50	81	(Wan <i>et al.</i> , 2011)
CaO loaded ZnO	30:1	10	60	1	>94	(Ngamcharussrivichai <i>et al.</i> , 2008)
KOH supported by activated carbon	24:1	30	64	1	98	(Baroutian <i>et al.</i> , 2009)

According to Wan *et al.* (2011), CaO supported by activated carbon catalyst reached a biodiesel yield of 81 % with reaction time of 1.5 hours. However, the operating temperature for the reaction was 190 °C, three times higher than the operating temperature (60 °C) of the reaction catalysed by nano CaO catalyst. This shows that high amount of heat energy was needed to supply to the transesterification catalysed by activated carbon catalyst and it is not a cost-effective reaction system. Thus, nano CaO catalyst developed by thermal hydration-dehydration was preferable with low process temperature of 60 °C.

CaO loaded ZnO catalyst achieved a biodiesel yield of more than 94 % in only 1 hour reaction time, however, the alcohol to oil molar ratio used was 30 :1 (Ngamcharussrivichai *et al.*, 2008). In other word, the usage of methanol for the reaction catalysed by CaO loaded ZnO catalyst was 4 times greater than nano CaO catalyst. A high alcohol to oil molar ratio may favourable transesterification reaction as it can shift the equilibrium toward the product (Chen *et al.*, 2016), however the excess alcohol molecules can compete and detach biodiesel molecules from the catalyst surface (Kaur *et al.*, 2014). Nevertheless, there would be difficulty to the purification of biodiesel product mixture if the methanol is in over excess amount (Chen *et al.*, 2016). Hence, nano CaO catalyst with moderate methanol to oil molar ratio (8:1) is preferable as the purification of biodiesel molecules from the mixture of product and unreacted methanol was easier compared to CaO loaded ZnO catalyst.

A high biodiesel yield, 98 % can be obtained by using KOH supported by activated carbon catalyst in 1 hour reaction time (Baroutian *et al.*, 2009). High amount of catalyst dosage, 30 wt% was needed for KOH supported by activated carbon catalyst to achieve high biodiesel yield compared to 3 wt% nano CaO catalyst to achieve 81% biodiesel yield. Even though high biodiesel yield can be achieved in a very short reaction time for KOH supported by activated carbon catalyst, the high catalyst loading required may increase the operating cost of the transesterification reaction. Therefore, nano CaO catalyst was preferable.

In summary, nano CaO catalyst was preferable as relatively mild reaction condition (operating temperature, alcohol to oil molar ratio and catalyst loading). was required for the reaction compared to other types of CaO based catalysts synthesised by other researchers Besides, the optimization of transesterification reaction operating conditions catalysed by nano CaO is suggested in future to further enhance the biodiesel yield.

4.4 Kinetic mechanism of transesterification reaction catalysed by optimized nano CaO catalyst

Kinetic study was carried out on transesterification reaction catalysed by nano catalyst derived from waste cockle shell. The kinetic mechanism of the nano CaO catalyst prepared via thermal hydration-dehydration treatment was deduced followed by the development of kinetic model. Stoichiometrically, one unit of triglycerides (TG) reacts with three units of methanol (M) to obtain

three moles of biodiesel (FAME) and one mole of glycerol (G). The reaction steps for biodiesel production were listed as below:



$$r_a = k_a C_{TG} C_S - k_{-a} C_{TG.S} \quad (3.1)$$

- where r_a = Reaction rate of adsorption
 k_a = Rate constant of forward reaction
 k_{-a} = Rate constant of backward reaction
 C_{TG} = Concentration of triglycerides
 C_S = Number of vacant sites

Given that $K_a = \frac{k_a}{k_{-a}}$, ratio of rate constant of forward reaction to rate constant of backward reaction,

$$r_a = k_a \left(C_{TG} C_S - \frac{C_{TG.S}}{K_a} \right) \quad (3.2)$$



$$r_s = k_s C_{TG.S} C_M - k_{-s} C_{FAME.S} C_G \quad (3.3)$$

- where r_s = Reaction rate of surface reaction
 k_s = Rate constant of forward reaction

- k_{-s} = Rate constant of backward reaction
 C_M = Concentration of methanol
 $C_{TG.S}$ = Concentration of triglycerides attached to vacant sites
 $C_{FAME.S}$ = Concentration of FAME attached to vacant sites
 C_G = Concentration of glycerol

Given that $K_s = \frac{k_s}{k_{-s}}$, ratio of rate constant of forward reaction to rate constant of backward reaction,

$$r_s = k_s(C_{TG.S}C_M - \frac{C_{FAME.S}C_G}{K_s}) \quad (3.4)$$

Desorption: $FAME.S \rightleftharpoons FAME + S$

$$r_d = k_d C_{FAME.S} - k_{-d} C_{FAME} C_S \quad (3.5)$$

- where r_d = Reaction rate of desorption
 k_d = Rate constant of forward reaction
 k_{-d} = Rate constant of backward reaction

Given that $K_d = \frac{k_d}{k_{-d}}$, ratio of rate constant of forward reaction to rate constant of backward reaction,

$$r_d = k_d(C_{FAME.S} - \frac{C_{FAME}C_S}{K_d}) \quad (3.6)$$

4.4.1 Derivation of kinetic rate equation:

Some assumptions were made before the derivation of kinetic rate equation.

The assumptions were listed below:

1. Triglycerides was limiting reactant whereas methanol was excess reactant.
2. Triglycerides molecules were attached to the active sites and reacted with free moving methanol molecules.
3. The glycerol was free moving after the transesterification while FAME molecules were remained attached to the vacant sites.
4. The surface reaction was assumed as rate limiting step.

Given that surface reaction is rate limiting step, $r_a = r_d = 0$, thus, equation (3.2) and equation (3.5) were simplified as:

$$C_{TG.S} = K_a C_{TG} C_S \quad (3.7)$$

$$C_{FAME.S} = \frac{C_{FAME} C_S}{K_d} \quad (3.8)$$

The vacant site of nano CaO catalyst can be derived by balancing the total active sites (C_t):

$$C_t = C_S + C_{TG.S} + C_{FAME.S} \quad (3.9)$$

$$C_t = C_S + K_a C_{TG} C_S + \frac{C_{FAME} C_S}{K_d} \quad (3.10)$$

$$C_t = C_S \left(1 + K_a C_{TG} + \frac{C_{FAME}}{K_d} \right) \quad (3.11)$$

$$C_S = \frac{C_t}{1 + K_a C_{TG} + \frac{C_{FAME}}{K_d}} \quad (3.12)$$

Substitute equation (3.7), equation (3.8) and equation (3.12) into equation (3.3),

$$r_s = k_s C_{TG.S} C_M - k_{-s} C_{FAME.S} C_G \quad (3.13)$$

$$r_s = k_s K_a C_{TG} C_S C_M - k_{-s} \left(\frac{C_{FAME} C_S}{K_d} \right) C_G \quad (3.14)$$

$$r_s = \frac{C_t k_s K_a C_{TG} C_M}{1 + K_a C_{TG} + \frac{C_{FAME}}{K_d}} - k_{-s} \left[\frac{C_t C_{FAME}}{K_d \left(1 + K_a C_{TG} + \frac{C_{FAME}}{K_d} \right)} \right] C_G \quad (3.15)$$

Given that the methanol is in excess, the transesterification is assumed irreversible, the backward reaction can be ignored. As triglycerides are limiting reactant, the low concentration makes $1 + K_a C_{TG} \approx 1$. The FAME and glycerol detach from the active site in rapid rate, the ratio of C_{FAME} to K_d is approximately to zero, thus, equation (3.15) is simplified to:

$$r_s = k C_{TG} \quad (3.16)$$

where

$$k = C_t k_s K_a C_M$$

Given that $r_s = kC_{TG}$

$$-\frac{dC_{TG}}{dt} = kC_{TG} \quad (3.17)$$

With the limit $C_{TG} = C_{TG0}$ at $t = 0$ gives

$$\ln \frac{C_{TG0}}{C_{TG}} = kt \quad (3.18)$$

Consequently, the slope of a plot of $\ln \frac{C_{TG0}}{C_{TG}}$ as a function of time is linear with slope k .

4.4.2 Verification of kinetic equation with experimental data

Figure 4.19 shows a series of experimental data was obtained from the transesterification of palm oil catalysed by nano CaO prepared via thermal hydration-dehydration treatment.

The data was fit into the kinetic equation developed. The reaction rate constant, k value of the transesterification of palm oil catalysed by nano CaO prepared via thermal hydration-dehydration treatment was 0.0007 min^{-1} with R^2 value of 0.9049. This shows that the kinetic mechanism deduced based on

the Langmuir-Hinshelwood kinetics that involving adsorption reaction, surface reaction and desorption reaction was well described the catalytic mechanism of nano CaO catalyst in converting triglycerides into biodiesel.

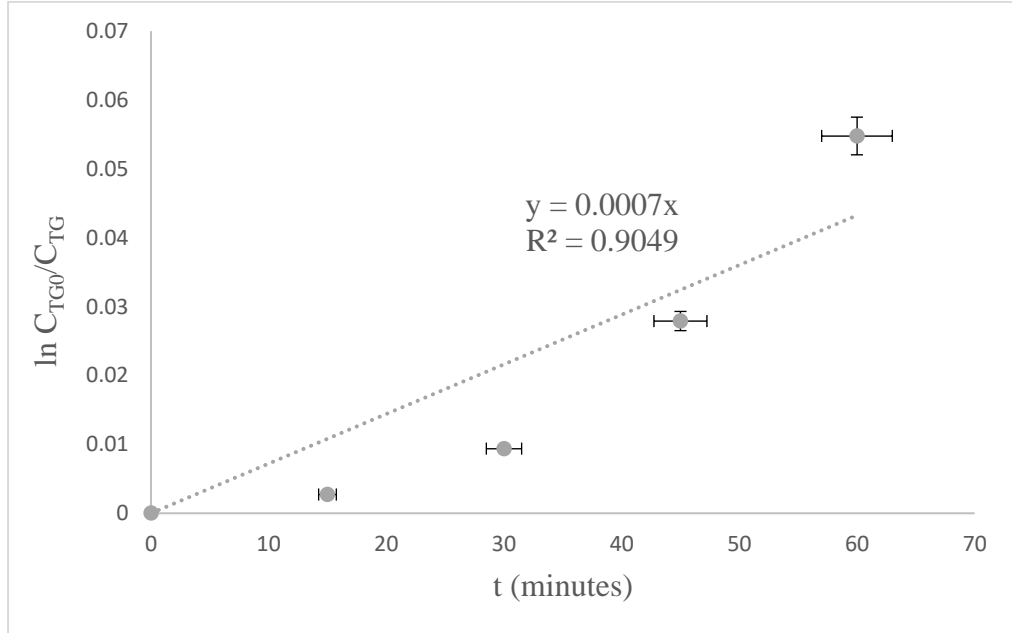


Figure 4.19: Plot of $\ln \frac{C_{TG0}}{C_{TG}}$ versus time

However, the slow reaction rate had been observed in the first 15 mins and 30 mins of the reaction. This is due to the presence of significant mass transfer limitation effects between the boundary layers as the reaction is carried out in three phases of methanol phase, palm oil phase and solid catalyst phase (Carroll *et al.*, 2009; Halim *et al.*, 2009). Besides that, the immiscibility of methanol phase with oil phase (the mixture of palm oil and biodiesel) would change with reaction time due to the reduced concentration of methanol (Patil *et al.*, 2009), hence, the reaction rate increased after 30 mins till the end of the reaction time.

Thus, the investigation and the incorporation of mass transfer factor into the proposed kinetic model were suggested to improve the accuracy of kinetic model for the reaction.

4.4.3 Activation energy and pre-exponential factor

In order to investigate the activation energy and the pre-exponential constant of the transesterification reaction catalysed by nano CaO. The Arrhenius equation was plotted. The derivation of Arrhenius equation into linear equation was shown below:

$$k = Ae^{\frac{-E_a}{RT}} \quad (3.22)$$

Taking the logarithmic form of Eq. (3.22) the equation can be expressed as:

$$\ln k = \ln A - \frac{E_a}{RT} \quad (3.23)$$

where k represents rate, constants derived from the kinetic model, A is the pre-exponential constant, R is the universal gas constant (8.314 J/mol. K), T is the absolute temperature in kelvin and E_a is the activation energy. The Arrhenius equation was plotted in Figure 4.20.

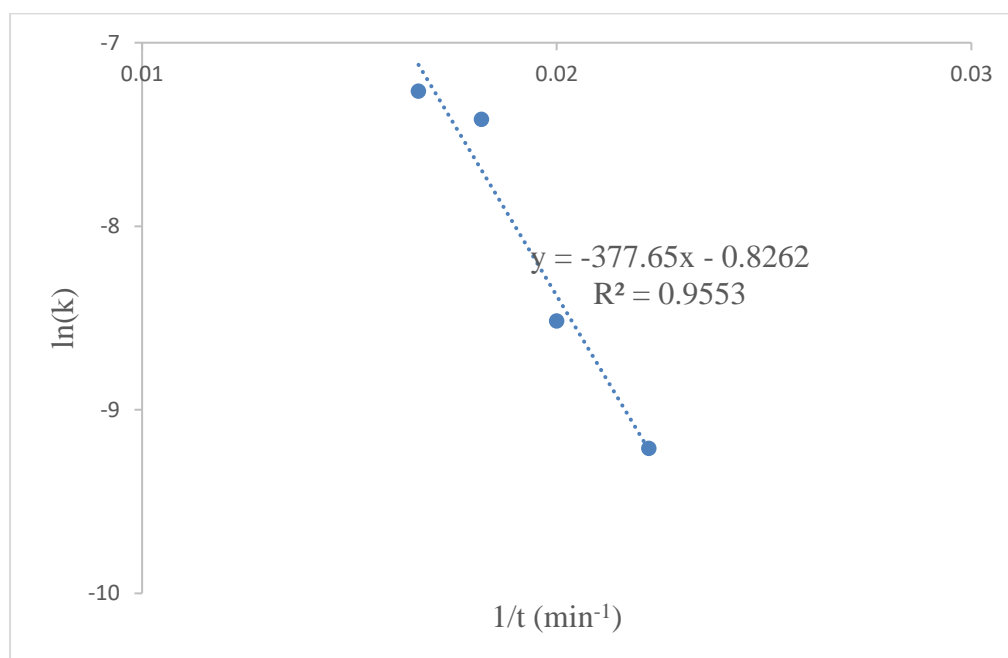


Figure 4.20: Arrhenius plot of transesterification reaction catalysed by nano CaO catalyst

Figure 4.20 shows the Arrhenius plot for transesterification reaction of palm oil at 45 °C, 50 °C, 55 °C and 60 °C. By obtaining the values from the linear equation, the activation energy was 3787 J/mol and the exponential constant is 1.677 min⁻¹. Freedman *et al.* (1986) claims that the activation energy is normally fall in the range of 33.6–84.0 kJ mol⁻¹ for base-catalysed transesterification reactions. Nevertheless, the activation energy for transesterification reaction of palm oil catalysed by nano CaO in the current study was lower than the activation energy for base-catalysed transesterification reactions.

The low activation energy denoted that the reaction can be initiated at relatively low operating temperature due to the low energy barrier requirement for the onset of reaction. The biodiesel yield obtained in the current study is lower than the yield reported in literature mainly due to the key parameters

related to the reaction (catalyst dosage, operating temperature, methanol to oil ratio) were not optimized in the current study. Thus, the biodiesel yield can be further enhanced by optimizing the key parameters related to reaction and this is suggested for future research work.

In summary, the nano CaO catalyst has been successfully synthesized with favour catalytic properties of low activation energy that lead to high reaction rate of 27.3% FAME yield / hr. The low operating temperature, 60 °C that applied in this study was favourable to the transesterification forward reaction. The investigation of mass transfer controlled is suggested as future research work.

CHAPTER 5

CONCLUSION AND RECOMMENDATION

5.1 Conclusion

Nano CaO catalyst was successfully developed from waste cockle shell via thermal hydration-dehydration treatment. The optimum condition for the thermal hydration-dehydration treatment were at 6 h of hydration duration, 650 °C of recalcination temperature and 3 h of recalcination duration. 82 % of biodiesel yield was obtained at 5 h reaction time from the transesterification of palm oil that catalysed by the nano CaO.

The FT-IR spectra, the XRD diffractogram and elemental results from EDX analysis confirmed the formation of CaCO₃ in waste cockle shell to CaO catalyst during the thermal hydration-dehydration treatment. BET results and TEM images proved the existence of sintering effect on the nano CaO catalyst when pre-treated under high recalcination temperature of 950 °C.

For kinetic mechanism, surface reaction is the rate limiting step for transesterification of palm oil catalysed by nano CaO catalyst. The rate constant of the reaction was 0.0007 min⁻¹ with R² value of 0.9047. Based on the Arrhenius equation, the activation energy was 3790 J/mol and the exponential constant is 1.677 min⁻¹. The activation energy for

transesterification reaction of palm oil catalysed by nano CaO in the current study was lower than the activation energy for base-catalysed transesterification reactions. It can be concluded that the nano CaO catalyst synthesized with properties of lower activation energy offered have resulted in higher reaction rate of 27.3% FAME yield / hr. The low operating temperature, 60 °C that applied in this study was favourable to the transesterification forward reaction with mass transfer controlled.

5.2 Recommendation

There are some recommendations for future study in transesterification of palm oil that catalysed by nano CaO catalyst. Firstly, the optimization of the reaction conditions for transesterification of palm oil can further investigate to maximize the performance of the nano CaO catalyst. Besides, the performance of nano CaO catalyst will affect by the oil feedstock, crude palm oil can be used as oil feedstock in future study instead of cooking oil from the market. Moreover, the investigation and the incorporation of mass transfer factor into the proposed kinetic model were suggested to improve the accuracy of kinetic model for the reaction. Lastly, the transesterification of palm oil in the mode of batch reaction can be further transform into continuous reaction.

REFERENCES

Adib REN, R., Folkecenter, M., Eckhart Mohamed El-Ashry David Hales Kirsty Hamilton Peter Rae, M., and Bariloche, F. (2018) *Report Renewable Energy*. Available at: www.ren21.net.

Agarwal, M., Chauhan, G., Chaurasia, S. P., and Singh, K. (2012) 'Study of catalytic behavior of KOH as homogeneous and heterogeneous catalyst for biodiesel production', *Journal of the Taiwan Institute of Chemical Engineers*, 43(1), pp. 89–94. doi: <https://doi.org/10.1016/j.jtice.2011.06.003>.

Ahmad, A. L., Yasin, N. H. M., Derek, C. J. C., and Lim, J. K. (2011) 'Microalgae as a sustainable energy source for biodiesel production: A review', *Renewable and Sustainable Energy Reviews*, 15(1), pp. 584–593. doi: [10.1016/j.rser.2010.09.018](https://doi.org/10.1016/j.rser.2010.09.018).

Amini, G., Najafpour, G. D., Rabiee, S. M., and Ghoreyshi, A. A. (2013) 'Synthesis and characterization of amorphous nano-alumina powders with high surface area for biodiesel production', *Chemical Engineering and Technology*, 36(10), pp. 1708–1712. doi: [10.1002/ceat.201300102](https://doi.org/10.1002/ceat.201300102).

Asikin-Mijan, N., Lee, H. V., Juan, J. C., Noorsaadah, A. R., Abdulkareem-Alsultan, G., Arumugam, M., and Taufiq-Yap, Y. H. (2016) 'Waste clamshell-derived CaO supported Co and W catalysts for renewable fuels production via cracking-deoxygenation of triolein', *Journal of Analytical and Applied Pyrolysis*, 120, pp. 110–120. doi: [10.1016/j.jaap.2016.04.015](https://doi.org/10.1016/j.jaap.2016.04.015).

Asikin-Mijan, N., Taufiq-Yap, Y. H., and Lee, H. V. (2015) 'Synthesis of clamshell derived Ca(OH)₂nano-particles via simple surfactant-hydration treatment', *Chemical Engineering Journal*, 262, pp. 1043–1051. doi: [10.1016/j.cej.2014.10.069](https://doi.org/10.1016/j.cej.2014.10.069).

Atabani, A. E., Silitonga, A. S., Anjum, I., Mahlia, T. M. I., Masjuki, H. H., and Mekhilef, S. (2012) 'A comprehensive review on biodiesel as an alternative energy resource and its characteristics', *Renewable and Sustainable Energy Reviews*, 16(4), pp. 2070–2093. doi: [10.1016/j.rser.2012.01.003](https://doi.org/10.1016/j.rser.2012.01.003).

Atadashi, I. M., Aroua, M. K., Abdul Aziz, A. R., and Sulaiman, N. M. N. (2013) 'The effects of catalysts in biodiesel production: A review', *Journal of Industrial and Engineering Chemistry*, 19(1), pp. 14–26. doi: [10.1016/j.jiec.2012.07.009](https://doi.org/10.1016/j.jiec.2012.07.009).

Atadashi, I. M., Aroua, M. K., and Aziz, A. A. (2011) 'Biodiesel separation and purification: A review', *Renewable Energy*. Pergamon, pp. 437–443. doi: [10.1016/j.renene.2010.07.019](https://doi.org/10.1016/j.renene.2010.07.019).

- Badriyah (2018) ‘Sustainable Energy- The Complete Equation’, *The institution of Engineers, Malaysia*, September, pp. 7–11.
- Bai, H. X., Shen, X. Z., Liu, X. H., and Liu, S. Y. (2009) ‘Synthesis of porous CaO microsphere and its application in catalyzing transesterification reaction for biodiesel’, *Transactions of Nonferrous Metals Society of China (English Edition)*, 19(SUPPL. 3), pp. s674–s677. doi: 10.1016/S1003-6326(10)60130-6.
- Balat, M. (2007) ‘Production of biodiesel from vegetable oils: A survey’, *Energy Sources, Part A: Recovery, Utilization and Environmental Effects*, 29(10), pp. 895–913. doi: 10.1080/00908310500283359.
- Banković–Ilić, I. B., Miladinović, M. R., Stamenković, O. S., and Veljković, V. B. (2017) ‘Application of nano CaO–based catalysts in biodiesel synthesis’, *Renewable and Sustainable Energy Reviews*, 72(January), pp. 746–760. doi: 10.1016/j.rser.2017.01.076.
- Baroutian, S., Aroua, M. K., Raman, A. A., and Sulaiman, N. M. (2009) ‘Rbd palm olein-based methyl/ethyl esters’, *Journal of Oil Palm Research*, 21(DECEMBER), pp. 659–666.
- Bensebaa, F. (2013) ‘Nanoparticle Fundamentals’, *Interface Science and Technology*, 19, pp. 1–84. doi: 10.1016/B978-0-12-369550-5.00001-X.
- Bhuiya, M. M. K., Rasul, M. G., Khan, M. M. K., Ashwath, N., and Azad, A. K. (2016) ‘Prospects of 2nd generation biodiesel as a sustainable fuel - Part: 1 selection of feedstocks, oil extraction techniques and conversion technologies’, *Renewable and Sustainable Energy Reviews*. Pergamon, pp. 1109–1128. doi: 10.1016/j.rser.2015.04.163.
- Birla, A., Singh, B., Upadhyay, S. N., and Sharma, Y. C. (2012) ‘Kinetics studies of synthesis of biodiesel from waste frying oil using a heterogeneous catalyst derived from snail shell’, *Bioresource Technology*, 106, pp. 95–100. doi: 10.1016/j.biortech.2011.11.065.
- Borges, M. E. and Díaz, L. (2012) ‘Recent developments on heterogeneous catalysts for biodiesel production by oil esterification and transesterification reactions: A review’, *Renewable and Sustainable Energy Reviews*. Pergamon, pp. 2839–2849. doi: 10.1016/j.rser.2012.01.071.
- Borugadda, V. B. and Goud, V. V. (2012) ‘Biodiesel production from renewable feedstocks: Status and opportunities’, *Renewable and Sustainable Energy Reviews*. Pergamon, pp. 4763–4784. doi: 10.1016/j.rser.2012.04.010.
- Boz, N., Degirmenbasi, N., and Kalyon, D. M. (2009) ‘Conversion of biomass to fuel: Transesterification of vegetable oil to biodiesel using KF loaded nano- γ -Al₂O₃ as catalyst’, *Applied Catalysis B: Environmental*, 89(3), pp. 590–596. doi: <https://doi.org/10.1016/j.apcatb.2009.01.026>.

- Canakci, M. and Gerpen, J. Van (1999) 'B p a c', *Society*, 42(1984), pp. 1203–1210.
- Cao, W., Han, H., and Zhang, J. (2005) 'Preparation of biodiesel from soybean oil using supercritical methanol and co-solvent', 84, pp. 347–351. doi: 10.1016/j.fuel.2004.10.001.
- Carroll, K. C., Taylor, R., Gray, E., and Brusseau, M. L. (2009) 'The impact of composition on the physical properties and evaporative mass transfer of a PCE-diesel immiscible liquid', *Journal of hazardous materials*. 2008/09/07, 164(2–3), pp. 1074–1081. doi: 10.1016/j.jhazmat.2008.09.003.
- Chang, H.J. and Crynes, B. L. (1986) 'Effect of Catalyst Pore and Pellet Sizes on Deactivation in SRC Oil Hydrotreatment', 32(2), pp. 224–232.
- Cheirsilp, B. and Louhasakul, Y. (2013) 'Industrial wastes as a promising renewable source for production of microbial lipid and direct transesterification of the lipid into biodiesel', *Bioresource Technology*, 142, pp. 329–337. doi: 10.1016/j.biortech.2013.05.012.
- Chen, G.-Y. Y., Shan, R., Yan, B.-B. B., Shi, J.-F. F., Li, S.-Y. Y., and Liu, C.-Y. Y. (2016) 'Remarkably enhancing the biodiesel yield from palm oil upon abalone shell-derived CaO catalysts treated by ethanol', *Fuel Processing Technology*, 143, pp. 110–117. doi: 10.1016/j.fuproc.2015.11.017.
- Chen, G., Shan, R., Shi, J., and Yan, B. (2014) 'Ultrasonic-assisted production of biodiesel from transesterification of palm oil over ostrich eggshell-derived CaO catalysts', *Bioresource Technology*, 171, pp. 428–432. doi: 10.1016/j.biortech.2014.08.102.
- Cho, Y. B., Seo, G., and Chang, D. R. (2009) 'Transesterification of tributyrin with methanol over calcium oxide catalysts prepared from various precursors', *Fuel Processing Technology*, 90(10), pp. 1252–1258. doi: 10.1016/j.fuproc.2009.06.007.
- Chong, K. Y., Chia, C. H., and Zakaria, S. (2014) 'Polymorphs calcium carbonate on temperature reaction', *AIP Conference Proceedings*, 1614(February 2015), pp. 52–56. doi: 10.1063/1.4895169.
- Chongkhong, S., Tongurai, C., and Chetpattananondh, P. (2009) 'Continuous esterification for biodiesel production from palm fatty acid distillate using economical process', *Renewable Energy*, 34(4), pp. 1059–1063. doi: 10.1016/j.renene.2008.07.008.
- Clark, S., Wagner, L., Piennaar, P., Boshoff, B., Hugo, F., Fuls, J., Hawkins, C., Walt, An., and Engelbrecht, A. (1981) 'Hour Screening Test for Alternate Fuels in Energy Notes for , Variables Affecting the Yields of Fatty Esters from Transesterified Vegetable Oils 1', *American Society of Agricultural Engineers*, 2(10), pp. 385–390. doi: 10.1007/BF02541649.

Darnoko, D. and Cheryan, M. (2000) 'Kinetics of palm oil transesterification in a batch reactor', *Journal of the American Oil Chemists' Society*, 77(12), pp. 1263–1267. doi: 10.1007/s11746-000-0198-y.

Degirmenbasi, N., Coskun, S., Boz, N., and Kalyon, D. M. (2015) 'Biodiesel synthesis from canola oil via heterogeneous catalysis using functionalized CaO nanoparticles', *Fuel*, 153, pp. 620–627. doi: 10.1016/j.fuel.2015.03.018.

Dehkhoda, A. M., West, A. H., and Ellis, N. (2010) 'Biochar based solid acid catalyst for biodiesel production', *Applied Catalysis A: General*, 382(2), pp. 197–204. doi: 10.1016/j.apcata.2010.04.051.

Dwivedi, G., Jain, S., and Sharma, M. P. (2011) 'Impact analysis of biodiesel on engine performance - A review', *Renewable and Sustainable Energy Reviews*. Pergamon, pp. 4633–4641. doi: 10.1016/j.rser.2011.07.089.

Ejikeme, P. M., Anyaogu, I. D., Ejikeme, C. L., Nwafor, N. P., Egbuonu, C. A. C., Ukogu, K., Ibemesi, J. A., Chemistry, I., and Polytechnic, F. (2010) 'Catalysis in Biodiesel Production by Transesterification Processes-An Insight', 7(4), pp. 1120–1132.

El-Sayed, M. A. (2004) 'Small is different: Shape-, size-, and composition-dependent properties of some colloidal semiconductor nanocrystals', *Accounts of Chemical Research*, 37(5), pp. 326–333. doi: 10.1021/ar020204f.

ten Elshof, J. E., Abadal, C. R., Sekulić, J., Chowdhury, S. R., and Blank, D. H. A. (2003) 'Transport mechanisms of water and organic solvents through microporous silica in the pervaporation of binary liquids', *Microporous and Mesoporous Materials*, 65(2–3), pp. 197–208. doi: 10.1016/j.micromeso.2003.08.010.

Enweremadu, C. C. and Mbarawa, M. M. (2009) 'Technical aspects of production and analysis of biodiesel from used cooking oil-A review', *Renewable and Sustainable Energy Reviews*. Pergamon, pp. 2205–2224. doi: 10.1016/j.rser.2009.06.007.

Ezebor, F., Khairuddean, M., Abdullah, A. Z., and Boey, P. L. (2014) 'Oil palm trunk and sugarcane bagasse derived solid acid catalysts for rapid esterification of fatty acids and moisture-assisted transesterification of oils under pseudo-infinite methanol', *Bioresource Technology*, 157, pp. 254–262. doi: 10.1016/j.biortech.2014.01.110.

Feyzi, M. and Shahbazi, E. (2015) 'Catalytic performance and characterization of Cs-Ca/SiO₂-TiO₂ nanocatalysts for biodiesel production', *Journal of Molecular Catalysis A: Chemical*, 404–405, pp. 131–138. doi: 10.1016/j.molcata.2015.04.018.

Freedman, B., Butterfield, R. O., and Pryde, E. H. (1986) 'Transesterification kinetics of soybean oil 1', *Journal of the American Oil Chemists' Society*,

63(10), pp. 1375–1380. doi: 10.1007/BF02679606.

Garrigue, P., Delville, M. H., Labrugère, C., Cloutet, E., Kulesza, P. J., Morand, J. P., and Kuhn, A. (2004) ‘Top-down approach for the preparation of colloidal carbon nanoparticles’, *Chemistry of Materials*, 16(16), pp. 2984–2986. doi: 10.1021/cm049685i.

Granados, M. L., Alonso, D. M., Sádaba, I., Mariscal, R., and Ocón, P. (2009) ‘Leaching and homogeneous contribution in liquid phase reaction catalysed by solids: The case of triglycerides methanolysis using CaO’, *Applied Catalysis B: Environmental*, 89(1–2), pp. 265–272. doi: 10.1016/j.apcatb.2009.02.014.

Halim, S. F. A., Kamaruddin, A. H., and Fernando, W. J. N. (2009) ‘Continuous biosynthesis of biodiesel from waste cooking palm oil in a packed bed reactor: Optimization using response surface methodology (RSM) and mass transfer studies’, *Bioresource Technology*, 100(2), pp. 710–716. doi: <https://doi.org/10.1016/j.biortech.2008.07.031>.

Han, H. and Guan, Y. (2009) ‘Synthesis of biodiesel from rapeseed oil using $K_2O/\gamma-Al_2O_3$ as nano-solid-base catalyst’, *Wuhan University Journal of Natural Sciences*, 14(1), pp. 75–79. doi: 10.1007/s11859-009-0116-x.

Harsha, H. H. R., Math, M. C., and Yatish, K. V (2017) ‘AC’. doi: 10.1016/j.energy.2017.10.118.This.

Hattori, H. (1995) ‘<Heterogeneous Basic Catalysis.pdf>’. doi: 10.1021/cr00035a005.

Islam, N. and Miyazaki, K. (2007) ‘Nanotechnology systems of innovation: Investigation of scientific disciplines’ fusion trend into nanotech’, *Portland International Conference on Management of Engineering and Technology*, pp. 2922–2931. doi: 10.1109/PICMET.2007.4349636.

Jahn, D. A., Wong, J., Bachler, J., Loerting, T., and Giovambattista, N. (2016) ‘Glass polymorphism in glycerol-water mixtures: I. A computer simulation study’, *Physical Chemistry Chemical Physics*, 18(16), pp. 11042–11057. doi: 10.1039/c6cp00075d.

Kapil, A., Wilson, K., Lee, A. F., and Sadhukhan, J. (2011) ‘Kinetic modeling studies of heterogeneously catalyzed biodiesel synthesis reactions’, *Industrial and Engineering Chemistry Research*, 50(9), pp. 4818–4830. doi: 10.1021/ie101403f.

Karmakar, A., Karmakar, S., and Mukherjee, S. (2010) ‘Properties of various plants and animals feedstocks for biodiesel production’, *Bioresource Technology*, 101(19), pp. 7201–7210. doi: 10.1016/J.BIORTECH.2010.04.079.

Kaur, M. and Ali, A. (2014) ‘Potassium fluoride impregnated CaO/NiO: An efficient heterogeneous catalyst for transesterification of waste cottonseed oil’,

European Journal of Lipid Science and Technology, 116(1), pp. 80–88. doi: 10.1002/ejlt.201300213.

Keera, S. T., El Sabagh, S. M., and Taman, A. R. (2018) ‘Castor oil biodiesel production and optimization’, *Egyptian Journal of Petroleum*. doi: 10.1016/j.ejpe.2018.02.007.

Kesic, Z., Lukic, I., Zdujic, M., Mojovic, L., and Skala, D. (2016) ‘Calcium oxide based catalysts for biodiesel production: A review’, *Chemical Industry and Chemical Engineering Quarterly*, 22(4), pp. 391–408. doi: 10.2298/CICEQ160203010K.

Khachani, M., Hamidi, A. El, Halim, M., and Arsalane, S. (2014) ‘Non-isothermal kinetic and thermodynamic studies of the dehydroxylation process of synthetic calcium hydroxide $\text{Ca}(\text{OH})_2$ ’, (January).

Kouzu, M., Kasuno, T., Tajika, M., Sugimoto, Y., Yamanaka, S., and Hidaka, J. (2008) ‘Calcium oxide as a solid base catalyst for transesterification of soybean oil and its application to biodiesel production’, *Fuel*, 87(12), pp. 2798–2806. doi: 10.1016/J.FUEL.2007.10.019.

Kumar, D. and Ali, A. (2012) ‘Nanocrystalline K–CaO for the transesterification of a variety of feedstocks: Structure, kinetics and catalytic properties’, *Biomass and Bioenergy*, 46, pp. 459–468. doi: 10.1016/J.BIOMBIOE.2012.06.040.

Kumar, D. and Ali, A. (2013) ‘Transesterification of Low-Quality Triglycerides over a Zn/CaO Heterogeneous Catalyst: Kinetics and Reusability Studies’, *Energy & Fuels*, 27(7), pp. 3758–3768. doi: 10.1021/ef400594t.

Kumar, N., Varun, and Chauhan, S. R. (2013) ‘Performance and emission characteristics of biodiesel from different origins: A review’, *Renewable and Sustainable Energy Reviews*, 21, pp. 633–658. doi: 10.1016/J.RSER.2013.01.006.

Kumar Naik, M., Charan Meher, L., Kumar Dalai, A., and Narayan Naik, S. (2008) ‘Biodiesel Production Using Karanja(*Pongamia pinnata*) and Jatropha (*Jatropha curcas*) Seed Oil’, *Handbook of Plant-Based Biofuels*, (September), pp. 255–266. doi: 10.1201/9780789038746.ch18.

Lam, M. K. and Lee, K. T. (2011) *Production of biodiesel using palm oil*. 1st edn, *Biofuels*. 1st edn. Elsevier Inc. doi: 10.1016/B978-0-12-385099-7.00016-4.

Lam, M. K., Lee, K. T., and Mohamed, A. R. (2010) ‘Homogeneous, heterogeneous and enzymatic catalysis for transesterification of high free fatty acid oil (waste cooking oil) to biodiesel: A review’, *Biotechnology Advances*, 28(4), pp. 500–518. doi: 10.1016/J.BIOTECHADV.2010.03.002.

Latchubugata, C. S., Kondapaneni, R. V., Patluri, K. K., Virendra, U., and Vedantam, S. (2018) 'Kinetics and optimization studies using Response Surface Methodology in biodiesel production using heterogeneous catalyst', *Chemical Engineering Research and Design*, 135, pp. 129–139. doi: 10.1016/j.cherd.2018.05.022.

Lesbani, A., Okta, S., Sitompul, C., Mohadi, R., and Hidayati, N. (2016) 'Characterization and Utilization of Calcium Oxide (CaO) Thermally Decomposed from Fish Bones as a Catalyst in the Production of Biodiesel from Waste Cooking Oil', 20(3), pp. 121–126. doi: 10.7454/mst.v20i3.3066.

Leung, D. Y. C., Wu, X., and Leung, M. K. H. (2010) 'A review on biodiesel production using catalyzed transesterification', *Applied Energy*. Elsevier, pp. 1083–1095. doi: 10.1016/j.apenergy.2009.10.006.

Liu, K., Wang, R., and Yu, M. (2018) 'An efficient, recoverable solid base catalyst of magnetic bamboo charcoal: Preparation, characterization, and performance in biodiesel production', *Renewable Energy*, 127, pp. 531–538. doi: <https://doi.org/10.1016/j.renene.2018.04.092>.

Ljupkovic, R., Micic, R., Tomic, M., Radulovic, N., Bojic, A., and Zarubica, A. (2014) 'Significance of the structural properties of CaO catalyst in the production of biodiesel: An effect on the reduction of greenhouse gases emission', *Hemijaska industrija*, 68(4), pp. 399–412. doi: 10.2298/HEMIND130612063L.

Looney, B. (2020) *Statistical Review of World Energy, 2020 | 69th Edition, BP*. Available at: <https://www.bp.com/content/dam/bp/business-sites/en/global/corporate/pdfs/energy-economics/statistical-review/bp-stats-review-2020-full-report.pdf>.

Lotero, E., Liu, Y., Lopez, D. E., Suwannakarn, K., Bruce, D. A., and Goodwin, J. G. (2005) 'Synthesis of biodiesel via acid catalysis', *Industrial and Engineering Chemistry Research*, 44(14), pp. 5353–5363. doi: 10.1021/ie049157g.

Luo, H., Fan, W., Li, Y., and Nan, G. (2013) 'Biodiesel production using alkaline ionic liquid and adopted as lubricity additive for low-sulfur diesel fuel', *Bioresource Technology*, 140, pp. 337–341. doi: <https://doi.org/10.1016/j.biortech.2012.11.112>.

Mandolesi de Araújo, C. D., de Andrade, C. C., de Souza e Silva, E., and Dupas, F. A. (2013) 'Biodiesel production from used cooking oil: A review', *Renewable and Sustainable Energy Reviews*, 27, pp. 445–452. doi: 10.1016/J.RSER.2013.06.014.

Maneerung, T., Kawi, S., Dai, Y., and Wang, C. H. (2016) 'Sustainable biodiesel production via transesterification of waste cooking oil by using CaO catalysts prepared from chicken manure', *Energy Conversion and*

Management, 123, pp. 487–497. doi: 10.1016/j.enconman.2016.06.071.

Maneerung, T., Kawi, S., and Wang, C. H. (2015) ‘Biomass gasification bottom ash as a source of CaO catalyst for biodiesel production via transesterification of palm oil’, *Energy Conversion and Management*, 92, pp. 234–243. doi: 10.1016/j.enconman.2014.12.057.

Marchetti, J. M., Miguel, V. U., and Errazu, A. F. (2007) ‘Possible methods for biodiesel production’, *Renewable and Sustainable Energy Reviews*, 11(6), pp. 1300–1311. doi: 10.1016/J.RSER.2005.08.006.

Mekhmer, G. A. H. (1998) ‘Characterization of phosphated zirconia by XRD, Raman and IR spectroscopy’, *Colloids and Surfaces A: Physicochemical and Engineering Aspects*, 141(2), pp. 227–235. doi: [https://doi.org/10.1016/S0927-7757\(98\)00344-6](https://doi.org/10.1016/S0927-7757(98)00344-6).

Menad, K., Feddag, A., and Rubenis, K. (2016) ‘Synthesis and study of calcination temperature influence on the change of structural properties of the LTA zeolite’, *Rasayan Journal of Chemistry*, 9(4), pp. 788–797.

Micic, R. D., Bosnjak Kiralj, M. S., Panic, S. N., Tomic, M. D., Jovic, B. D., and Boskovic, G. C. (2015) ‘Activation temperature imposed textural and surface synergism of CaO catalyst for sunflower oil transesterification’, *Fuel*, 159, pp. 638–645. doi: 10.1016/J.FUEL.2015.07.025.

Mohamed, M., Yousuf, S., and Maitra, S. (2012) ‘Decomposition study of calcium carbonate in cockle shell’, *Journal of Engineering Science and Technology*, 7(1), pp. 1–10.

Mosaddegh, E. and Hassankhani, A. (2014) ‘Preparation and characterization of nano-CaO based on eggshell waste: Novel and green catalytic approach to highly efficient synthesis of pyrano[4,3-b]pyrans’, *Chinese Journal of Catalysis*, 35(3), pp. 351–356. doi: 10.1016/S1872-2067(12)60755-4.

Muciño, G. G., Romero, R., Ramírez, A., Martínez, S. L., Baeza-Jiménez, R., and Natividad, R. (2014) ‘Biodiesel production from used cooking oil and sea sand as heterogeneous catalyst’, *Fuel*, 138, pp. 143–148. doi: 10.1016/J.FUEL.2014.07.053.

Nadagouda, M. N. and Varma, R. S. (2006) ‘Green and controlled synthesis of gold and platinum nanomaterials using vitamin B2: Density-assisted self-assembly of nanospheres, wires and rods’, *Green Chemistry*, 8(6), pp. 516–518. doi: 10.1039/b601271j.

Ngamcharussrivichai, C., Totarat, P., and Bunyakiat, K. (2008) ‘Ca and Zn Mixed Oxide as a Heterogeneous Base Catalyst for Transesterification of Palm Kernel oil’, *Applied Catalysis A-general - APPL CATAL A-GEN*, 341, pp. 77–85. doi: 10.1016/j.apcata.2008.02.020.

Niju, S., Meera, K. M., Begum, S., and Anantharaman, N. (2014) 'Modification of egg shell and its application in biodiesel production', *Journal of Saudi Chemical Society*, 18(5), pp. 702–706. doi: 10.1016/J.JSCS.2014.02.010.

Nomura, K., Terwilliger, P., Bharadwaj, A. V. S. L. S., Singh, M., Niju, S., and Begum, K. M. M. S. (2019) 'Self-dual Leonard pairs Biodiesel production from rubber seed oil using calcium oxide derived from eggshell as catalyst – optimization and modeling studies a', pp. 430–442.

Nye, M. J., Williamson, T. W., Deshpande, W., Schrader, J. H., Snively, W. H., Yurkewich, T. P., and French, C. L. (1983) 'Conversion of used frying oil to diesel fuel by transesterification: Preliminary tests', *Journal of the American Oil Chemists' Society*, 60(8), pp. 1598–1601. doi: 10.1007/BF02666593.

Pandit, P. R. and Fulekar, M. H. (2017) 'Egg shell waste as heterogeneous nanocatalyst for biodiesel production: Optimized by response surface methodology', *Journal of Environmental Management*, 198, pp. 319–329. doi: 10.1016/J.JENVMAN.2017.04.100.

Patil, P. D. and Deng, S. (2009) 'Optimization of biodiesel production from edible and non-edible vegetable oils', *Fuel*, 88(7), pp. 1302–1306. doi: <https://doi.org/10.1016/j.fuel.2009.01.016>.

Philippot, K. and Serp, P. (2012) *Nanomaterials in Catalysis*. First. doi: 10.1002/9783527656875.ch1.

Putra, R. S., Liyanita, A., Arifah, N., Puspitasari, E., Sawaludin, and Hizam, M. N. (2017) 'Enhanced Electro-Catalytic Process on the Synthesis of FAME Using CaO from Eggshell', *Energy Procedia*, 105, pp. 289–296. doi: 10.1016/j.egypro.2017.03.316.

Rabiei, M., Palevicius, A., Monshi, A., Nasiri, S., Vilkauskas, A., and Janusas, G. (2020) 'Comparing methods for calculating nano crystal size of natural hydroxyapatite using X-ray diffraction', *Nanomaterials*, 10(9), pp. 1–21. doi: 10.3390/nano10091627.

Raj, K. J. A. and Viswanathan, B. (2009) '<Surface area p25.pdf>', 48(October), pp. 1378–1382. doi: 10.1152/ajpendo.00192.2014.

Reddy, C., Reddy, V., Oshel, R., and Verkade, J. G. (2006) 'Room-temperature conversion of soybean oil and poultry fat to biodiesel catalyzed by nanocrystalline calcium oxides', *Energy and Fuels*, 20(3), pp. 1310–1314. doi: 10.1021/ef050435d.

Reli, M., Kočí, K., Matějka, V., Kovář, P., and Obalová, L. (2012) 'Effect of calcination temperature and calcination time on the kaolinite/tio2 composite for photocatalytic reduction of CO2', *GeoScience Engineering*, 58(4), pp. 10–

22. doi: <https://doi.org/10.2478/v10205-011-0022-2>.

Rodriguez-garcia, M. E. (2009) 'Characterization of Calcium Carbonate , Calcium Oxide , and Calcium " This material may be downloaded for personal use only . Any other use requires prior permission of the American Society of Civil Engineers ." " Final draft "' , (November).

Roschat, W., Kacha, M., Yoosuk, B., Sudyoadsuk, T., and Promarak, V. (2012) 'Biodiesel production based on heterogeneous process catalyzed by solid waste coral fragment', *Fuel*, 98, pp. 194–202. doi: 10.1016/J.FUEL.2012.04.009.

Roschat, W., Phewphong, S., Thangthong, A., Moonsin, P., Yoosuk, B., Kaewpuang, T., and Promarak, V. (2018) 'Catalytic performance enhancement of CaO by hydration-dehydration process for biodiesel production at room temperature', *Energy Conversion and Management*, 165(January), pp. 1–7. doi: 10.1016/j.enconman.2018.03.047.

Sahani, S. and Sharma, Y. C. (2018) 'Economically viable production of biodiesel using a novel heterogeneous catalyst: Kinetic and thermodynamic investigations', *Energy Conversion and Management*, 171(April), pp. 969–983. doi: 10.1016/j.enconman.2018.06.059.

Samah, A. R. A. (2018) 'Sustainable Energy for Malaysia: An Exciting Journey Awaits', *The institution of Engineers, Malaysia*, pp. 13–19.

Santacesaria, E., Vicente, G. M., Serio, M. Di, and Tesser, R. (2020) 'Main technologies in biodiesel production : State of the art and future challenges', 195(2012), pp. 2–13. doi: 10.1016/j.cattod.2012.04.057.

Saoud, K., Ibala, I., Ladki, D., Ezzeldeen, O., and Saeed, S. (2014) *Microwave Assisted Preparation of Calcium Hydroxide and Barium Hydroxide Nanoparticles and Their Application for Conservation of Cultural Heritage*. doi: 10.1007/978-3-319-13695-0_33.

Schmidt, F. (2001) 'New catalyst preparation technologies—observed from an industrial viewpoint', *Applied Catalysis A: General*, 221(1), pp. 15–21. doi: [https://doi.org/10.1016/S0926-860X\(01\)00802-X](https://doi.org/10.1016/S0926-860X(01)00802-X).

Shankar, A. A., Pentapati, P. R., and Prasad, R. K. (2017) 'Biodiesel synthesis from cottonseed oil using homogeneous alkali catalyst and using heterogeneous multi walled carbon nanotubes: Characterization and blending studies', *Egyptian Journal of Petroleum*, 26(1), pp. 125–133. doi: <https://doi.org/10.1016/j.ejpe.2016.04.001>.

Sharma, Y. C. and Singh, B. (2008) 'Development of biodiesel from karanja, a tree found in rural India', *Fuel*, 87(8–9), pp. 1740–1742. doi: 10.1016/J.FUEL.2007.08.001.

Sharma, Y. C., Singh, B., and Korstad, J. (2011) 'Latest developments on application of heterogenous basic catalysts for an efficient and eco friendly synthesis of biodiesel: A review', *Fuel*, 90(4), pp. 1309–1324. doi: 10.1016/J.FUEL.2010.10.015.

Shuit, S. H., Ng, E. P., and Tan, S. H. (2015) 'A facile and acid-free approach towards the preparation of sulphonated multi-walled carbon nanotubes as a strong protonic acid catalyst for biodiesel production', *Journal of the Taiwan Institute of Chemical Engineers*, 52, pp. 100–108. doi: 10.1016/j.jtice.2015.02.018.

Singh, A. K. and Fernando, S. D. (2007) 'Reaction kinetics of soybean oil transesterification using heterogeneous metal oxide catalysts', *Chemical Engineering and Technology*, 30(12), pp. 1716–1720. doi: 10.1002/ceat.200700274.

Smith, S. M., Oopathum, C., Weeramongkhonlert, V., Smith, C. B., Chaveanghong, S., Ketwong, P., and Boonyuen, S. (2013) 'Transesterification of soybean oil using bovine bone waste as new catalyst', *Bioresource Technology*, 143, pp. 686–690. doi: 10.1016/j.biortech.2013.06.087.

Sun, C., Qiu, F., Yang, D., and Ye, B. (2014) 'Preparation of biodiesel from soybean oil catalyzed by Al-Ca hydrotalcite loaded with K₂CO₃ as heterogeneous solid base catalyst', *Fuel Processing Technology*, 126, pp. 383–391. doi: 10.1016/J.FUPROC.2014.05.021.

Sunita, G., Devassy, B. M., Vinu, A., Sawant, D. P., Balasubramanian, V. V., and Halligudi, S. B. (2008) 'Synthesis of biodiesel over zirconia-supported isopoly and heteropoly tungstate catalysts', *Catalysis Communications*, 9(5), pp. 696–702. doi: <https://doi.org/10.1016/j.catcom.2007.08.007>.

Suryaputra, W., Winata, I., Indraswati, N., and Ismadji, S. (2013) 'Waste capiz (*Amusium cristatum*) shell as a new heterogeneous catalyst for biodiesel production', *Renewable Energy*, 50, pp. 795–799. doi: 10.1016/j.renene.2012.08.060.

Talebian-Kiakalaieh, A., Amin, N. A. S., and Mazaheri, H. (2013) 'A review on novel processes of biodiesel production from waste cooking oil', *Applied Energy*, 104, pp. 683–710. doi: 10.1016/J.APENERGY.2012.11.061.

Tamilmagan, Maheswari, A., Priyabijesh, and Gopal, A. (2015) 'Biodiesel production from waste cooking oil using green synthesized nanoFe₂O₃ and CuO impregnated nanoFe₃O₄', *International Journal of ChemTech Research*, 8(5), pp. 90–96.

Tang, S., Wang, L., Zhang, Y., Li, S., Tian, S., and Wang, B. (2012) 'Study on preparation of Ca/Al/Fe₃O₄ magnetic composite solid catalyst and its application in biodiesel transesterification', *Fuel Processing Technology*, 95,

pp. 84–89. doi: 10.1016/J.FUPROC.2011.11.022.

Tangboriboon, N., Kunanuruksapong, R., and Srivat, A. (2012) ‘Mesoporosity and phase transformation of bird eggshells via pyrolysis’, *Journal of Ceramic Processing Research*, 13(4), pp. 413–419.

Thanh, L. T., Okitsu, K., Boi, L. Van, and Maeda, Y. (2012) ‘Catalytic Technologies for Biodiesel Fuel Production and Utilization of Glycerol: A Review’, pp. 191–222. doi: 10.3390/catal2010191.

Viriya-empikul, N., Krasae, P., Nualpaeng, W., Yoosuk, B., and Faungnawakij, K. (2012) ‘Biodiesel production over Ca-based solid catalysts derived from industrial wastes’, *Fuel*, 92(1), pp. 239–244. doi: 10.1016/J.FUEL.2011.07.013.

Vujicic, D., Comic, D., Zarubica, A., Micic, R., and Boskovic, G. (2010) ‘Kinetics of biodiesel synthesis from sunflower oil over CaO heterogeneous catalyst’, *Fuel*, 89(8), pp. 2054–2061. doi: 10.1016/J.FUEL.2009.11.043.

Wan, Z. and Hameed, B. H. (2011) ‘Transesterification of palm oil to methyl ester on activated carbon supported calcium oxide catalyst’, *Bioresource Technology*, 102(3), pp. 2659–2664. doi: <https://doi.org/10.1016/j.biortech.2010.10.119>.

Wang, Y., Moo, Y. X., Chen, C., Gunawan, P., and Xu, R. (2010) ‘Journal of Colloid and Interface Science Fast precipitation of uniform CaCO₃ nanospheres and their transformation to hollow hydroxyapatite nanospheres’, *Journal of Colloid And Interface Science*, 352(2), pp. 393–400. doi: 10.1016/j.jcis.2010.08.060.

WebBook, N. C. (2018) *Calcium carbonate (precipitated)*, U.S. Secretary of Commerce on behalf of the United States of America. Available at: <https://webbook.nist.gov/cgi/cbook.cgi?ID=C471341&Mask=80#Refs> (Accessed: 14 June 2019).

Wen, L., Wang, Y., Lu, D., Hu, S., and Han, H. (2010) ‘Preparation of KF/CaO nanocatalyst and its application in biodiesel production from Chinese tallow seed oil’, *Fuel*, 89(9), pp. 2267–2271. doi: 10.1016/J.FUEL.2010.01.028.

Widayat, W., Darmawan, T., Hadiyanto, H., and Rosyid, R. A. (2017) ‘Preparation of Heterogeneous CaO Catalysts for Biodiesel Production’, *Journal of Physics: Conference Series*, 877(1). doi: 10.1088/1742-6596/877/1/012018.

Yaakob, Z., Mohammad, M., Alherbawi, M., Alam, Z., and Sopian, K. (2013) ‘Overview of the production of biodiesel from Waste cooking oil’, *Renewable and Sustainable Energy Reviews*, 18, pp. 184–193. doi: 10.1016/J.RSER.2012.10.016.

Yadav, M., Upadhyay, S., and Sharma, Y. C. (2018) 'Process optimization, kinetics of production Jatropa curcus methyl ester, and its utilization in single cylinder diesel engine', *Energy Conversion and Management*, 160, pp. 364–374. doi: 10.1016/J.ENCONMAN.2017.12.072.

Yilmaz, B. and Müller, U. (2009) 'Catalytic Applications of Zeolites in Chemical Industry', *Topics in Catalysis*, 52(6), pp. 888–895. doi: 10.1007/s11244-009-9226-0.

Yoo, S. J., Lee, H., Veriansyah, B., Kim, J., Kim, J.-D., and Lee, Y.-W. (2010) 'Synthesis of biodiesel from rapeseed oil using supercritical methanol with metal oxide catalysts', *Bioresource Technology*, 101(22), pp. 8686–8689. doi: 10.1016/J.BIORTECH.2010.06.073.

Yoosuk, B., Udomsap, P., Puttasawat, B., and Krasae, P. (2010) 'Modification of calcite by hydration–dehydration method for heterogeneous biodiesel production process: The effects of water on properties and activity', *Chemical Engineering Journal*, 162(1), pp. 135–141. doi: 10.1016/J.CEJ.2010.05.013.

Yoosuk, B., Udomsap, P., and Puttasawat, B. (2011) 'Hydration–dehydration technique for property and activity improvement of calcined natural dolomite in heterogeneous biodiesel production: Structural transformation aspect', *Applied Catalysis A: General*, 395(1–2), pp. 87–94. doi: 10.1016/J.APCATA.2011.01.026.

Yusuf, N. N. A. N., Kamarudin, S. K., and Yaakub, Z. (2011) 'Overview on the current trends in biodiesel production', *Energy Conversion and Management*, 52(7), pp. 2741–2751. doi: 10.1016/J.ENCONMAN.2010.12.004.

Zabeti, M., Daud, W. M. A. W., and Aroua, M. K. (2010) 'Biodiesel production using alumina-supported calcium oxide: An optimization study', *Fuel Processing Technology*, 91(2), pp. 243–248. doi: 10.1016/J.FUPROC.2009.10.004.

Zahmakiran, M. and Özkar, S. (2011) 'Metal nanoparticles in liquid phase catalysis; From recent advances to future goals', *Nanoscale*, 3(9), pp. 3462–3481. doi: 10.1039/c1nr10201j.

Zhang, H., Aytun Ozturk, U., Wang, Q., and Zhao, Z. (2014) 'Biodiesel produced by waste cooking oil: Review of recycling modes in China, the US and Japan', *Renewable and Sustainable Energy Reviews*, 38, pp. 677–685. doi: 10.1016/J.RSER.2014.07.042.

Zhang, Y., Dubé, M. A., McLean, D. D., and Kates, M. (2003) 'Biodiesel production from waste cooking oil: 1. Process design and technological assessment', *Bioresource Technology*, 89(1), pp. 1–16. doi: 10.1016/S0960-8524(03)00040-3.

Zhao, L., Qiu, Z., and Stagg-Williams, S. M. (2013) 'Transesterification of canola oil catalyzed by nanopowder calcium oxide', *Fuel Processing Technology*, 114, pp. 154–162. doi: 10.1016/J.FUPROC.2013.03.027.

APPENDICES

Appendix A : Calibration curves and retention time of external standard
and internal standard

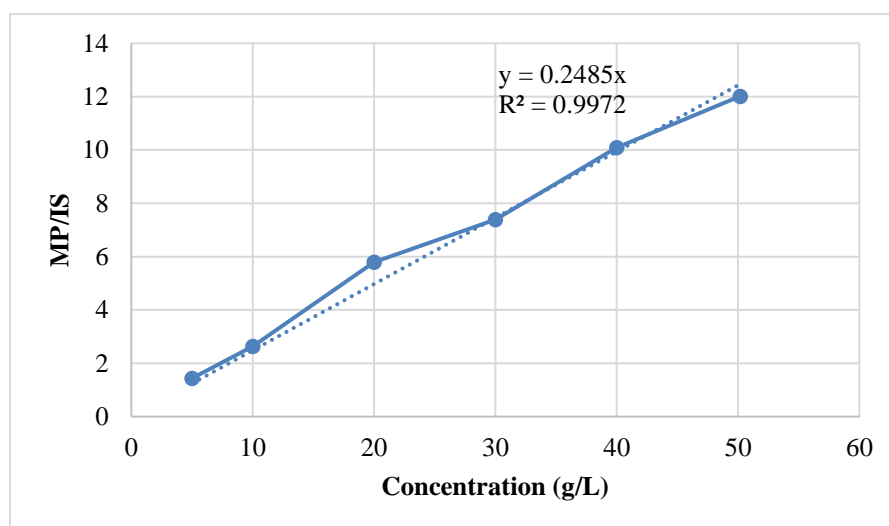


Figure A.1: Standard curve of methyl palmitate

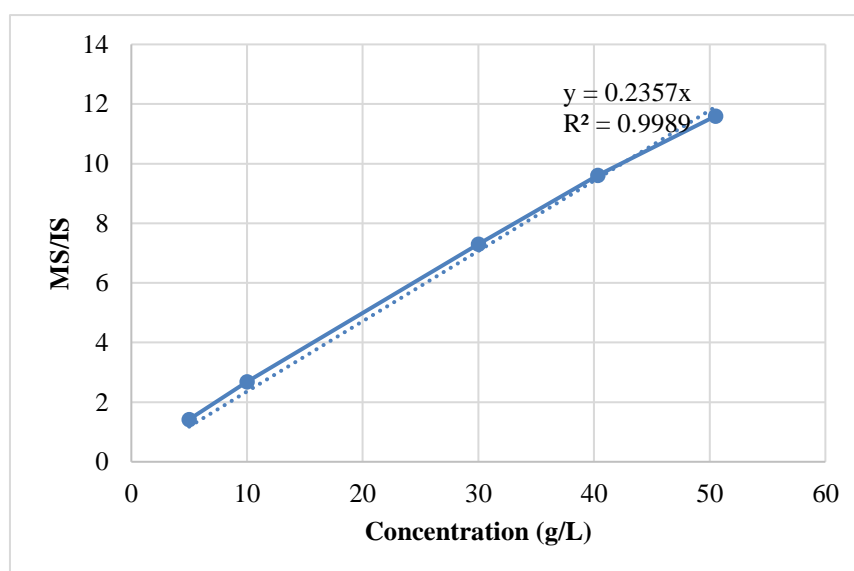


Figure A.2: Standard curve of methyl stearate

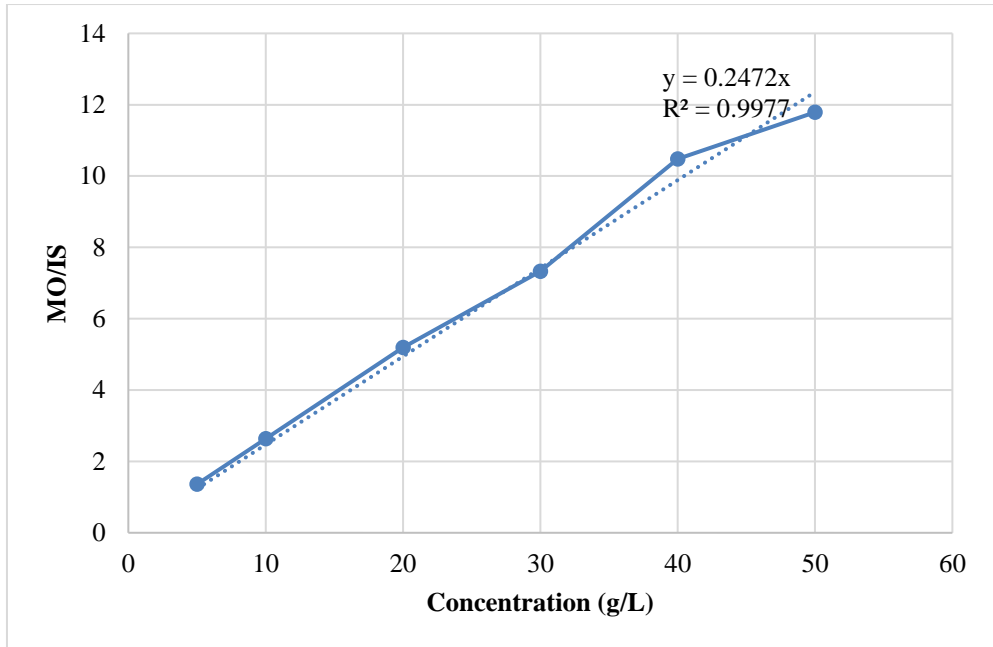


Figure A.3: Standard curve of methyl oleate

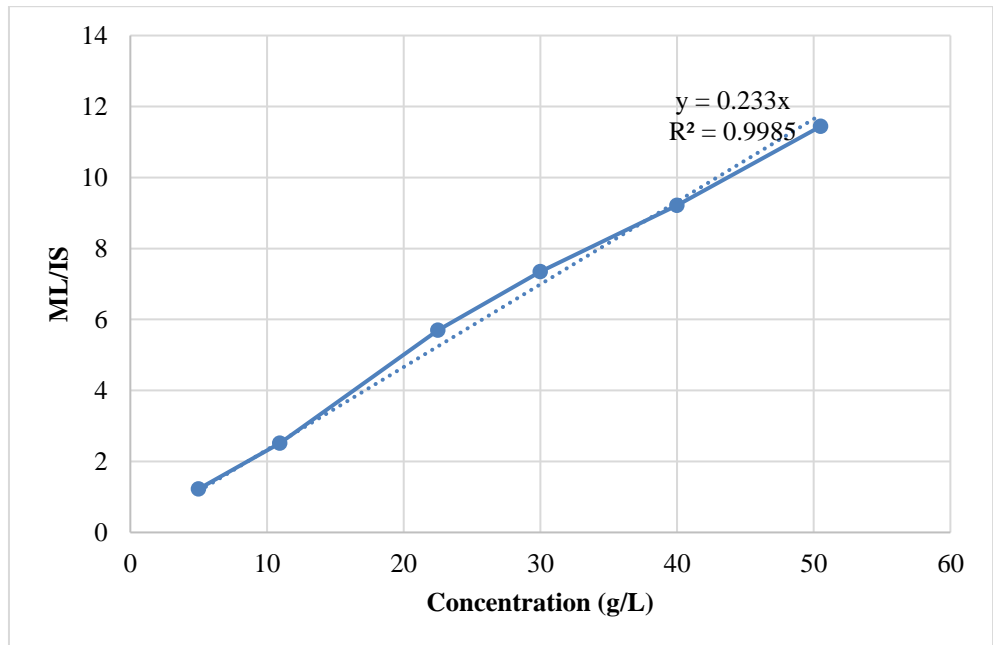


Figure A.4: Standard curve of methyl linoleate

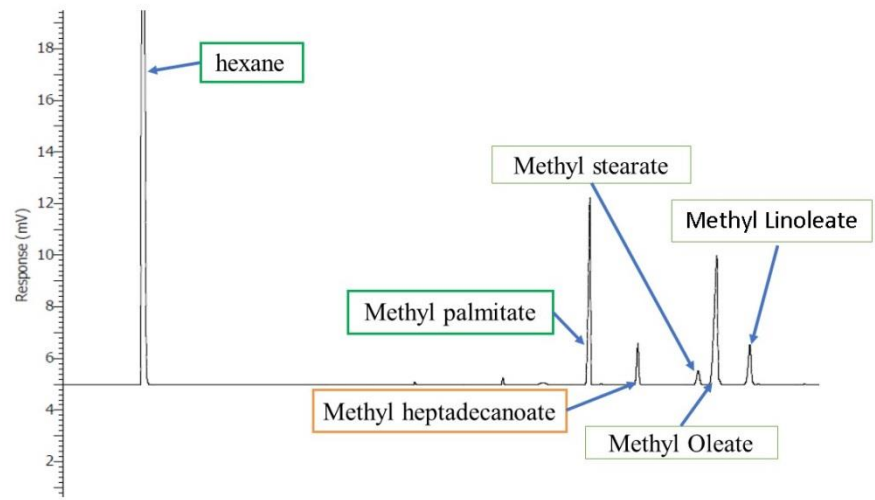


Figure A.5: Retention time of internal and external standard

Appendix B : Estimation of fatty acid methyl esters (FAMES)
molecular weight

Table B.1: Physical data of fatty acids (Lam *et al.*, 2011)

Fatty acids	Molecular weight of fatty acids (g/mol)	Composition in Palm oil
Palmitic	270.45	0.4176
Stearic	298.5	0.0373
Oleic	296.49	0.4386
Linoleic	294.47	0.1065

Average molecular weight of fatty acid methyl esters (FAMES)

$$= (270.45) (0.4176) + (298.5) (0.0373) + (296.49) (0.4386) + (294.47) (0.1065)$$

$$= 285.476 \text{ g/mol}$$

Appendix C : Calculation for methanol to oil molar ratio

Molecular weight of palm oil triglyceride estimated as 840.38 g/mol.

(Baroutian *et al.*, 2009)

Molarity of methanol is estimated as 32 g/mol

Density of palm oil is estimated as 0.924 g/cm³.

Density of methanol is estimated as 0.791 g/cm³

Given that the volume of palm oil is 150 cm³.

$$\begin{aligned}\text{Mass of palm oil} &= 150 \text{ cm}^3 \times 0.924 \text{ g/cm}^3 \\ &= 138.6 \text{ g}\end{aligned}$$

Assume 3 wt % of free fatty acids in the palm oil,

$$\begin{aligned}\text{Mole of palm oil} &= \frac{138.6 \text{ g}}{840.38 \text{ g/mol}} \times (1-0.03) \\ &= 0.15997763 \text{ mol} \\ &= 0.160\end{aligned}$$

$$\begin{aligned}\text{Mole of methanol required} &= 0.160 \text{ mol} \times 8 \\ &= 1.28 \text{ mol}\end{aligned}$$

$$\begin{aligned}\text{Mass of methanol required} &= 1.28 \text{ mol} \times 32 \text{ g/mol} \\ &= 40.96 \text{ g}\end{aligned}$$

$$\begin{aligned}\text{Volume of methanol required} &= \frac{40.96 \text{ g}}{0.791 \text{ g/cm}^3} \\ &= 51.7825537 \text{ cm}^3 \\ &= 52 \text{ cm}^3\end{aligned}$$

Appendix D : Weight of catalyst

Given that the weight percent of catalyst is 3 wt %,

$$\begin{aligned}\text{Weight of catalyst} &= 138.6 \text{ g} \times (1-0.03) \times 0.03 \\ &= 4.03326 \text{ g} \\ &= 4.033 \text{ g}\end{aligned}$$

Appendix E : Sample Calculation for Theoretical biodiesel yield

Molecular weight of palm oil triglyceride estimated as 840.38 g/mol.

Density of palm oil is estimated as 0.924 g/cm³.

Molecular weight of methyl ester estimated as 285.48 g/mol

Given that the volume of palm oil is 150 cm³

The volume of methanol is 52 cm³

$$\begin{aligned}\text{Mass of palm oil used} &= 150 \text{ ml} \times 0.924 \text{ g/cm}^3 \\ &= 138.6 \text{ g}\end{aligned}$$

Assume palm oil contain 3 wt % of free fatty acids,

$$\begin{aligned}\text{Molarity of palm oil} &= \frac{138.6 \text{ g}}{840.38 \text{ g/mol}} \times (1-0.03) \\ &= 0.15997763 \text{ mol} \\ &= 0.160 \text{ mol}\end{aligned}$$

Theoretically, 1 mole of palm oil will produce 3 mole of methyl ester,

$$\begin{aligned}\text{Molarity of methyl ester} &= 0.160 \text{ mol} \times 3 \\ &= 0.48 \text{ mol}\end{aligned}$$

$$\begin{aligned}\text{Mass of methyl ester} &= 0.48 \text{ mol} \times 285.48 \text{ g/mol} \\ &= 137.0304 \text{ g} \\ &= 137 \text{ g}\end{aligned}$$

$$\begin{aligned}\text{Theoretical concentration of methyl ester} &= \frac{\text{Mass of methyl ester}}{\text{total volume of reactants}} \\ &= \frac{137 \text{ g}}{0.202 \text{ L}} \\ &= 678.217822 \\ &= 678 \text{ g/L}\end{aligned}$$

Appendix F : Calculation for Experimental biodiesel yield

The peak area of the fatty acid methyl esters in the sample was acquired via the gas chromatography analysis. The ratio of FAME peak area to internal standard was obtained and the concentration of the FAME was computed using calibration curves.

Table F.2: GC data for 5_650_3 at 3 h reaction time

FAME	Area ($\mu\text{V} \cdot \text{s}$)	Concentration (g/L)
Palmitate	25048.99	17.80246559
Stearate	2640.5	1.978531267
Oleate	28737.04	20.53099015
Linoleate	7413.12	5.619031127
Internal std	5662.18	

Total FAMEs (diluted with internal standard) from Table X.X

$$= 17.80236559 + 1.978531267 + 20.53099015 + 5.619031127$$

$$= 45.93101813 \text{ g/L}$$

Total FAMEs (without internal standard)

$$= 45.93101813 \text{ g/L} \times 3$$

$$= 137.7930544 \text{ g/L}$$

Total FAMEs (without dilution by hexane)

$$= 137.7930544 \text{ g/L} \times 4$$

$$= 551.1722176 \text{ g/L}$$

$$\text{Biodiesel Yield} = \frac{551.1722176}{678} \times 100 \%$$

$$= 81.2938374$$

$$= 81.294 \%$$

Appendix G : Sample calculation for XRD crystalline size

The sample calculation below is reference to the hydrated calcium oxide. The average crystalline size of the calcium oxide is based on an average of peaks.

Table G.3: Peak data from XRD analysis for hydrated calcium oxide

Peak No	2 θ (°)	θ (°)	d-spacing(Å)	FWHM(°)
7	34.17	17.08	2.622	0.1574
11	47.20	23.60	1.924	0.1647
14	50.86	25.43	1.794	0.1487
16	54.42	27.21	1.685	0.1782
18	62.66	31.33	1.481	0.1629
19	64.33	32.17	1.450	0.1944
21	71.86	35.93	1.313	0.1605

The wavelength is firstly calculated using the Bragg's Law formula:

$$2d(\sin \theta) = \lambda$$

where,

d is lattice interplanar spacing of the crystal

θ is the x-ray incidence angle

λ is the x-ray wavelength

Thus, the wavelength λ of peak number 7 is

$$\begin{aligned}\lambda &= 2d(\sin \theta) \\ &= 2(2.622) (\sin 17.08) \\ &= 1.541 \text{ \AA}\end{aligned}$$

Therefore, the crystalline size of the catalyst using the Debye-Scherrer equation is,

$$\begin{aligned}L &= \frac{0.89\lambda}{\beta \cos\theta} \\ &= \frac{0.89 (1.541)}{0.0027 \cos 17.08} \\ &= 522.2 \text{ \AA}\end{aligned}$$

Given that $1 \text{ \AA} = 0.1 \text{ nm}$,

$$\begin{aligned}\text{Crystalline size (peak 7)} &= 522.2 (0.1 \text{ nm}) \\ &= 52.22 \text{ nm}\end{aligned}$$

Appendix H : XRD results

Table H.4: XRD results for waste cockle shell

No.	2theta(°)	theta(°)	d-spacing(Å)	wavenumber	FWHM(°)	L(Å)	Crystalline size (nm)
1	26.25	13.13	3.392	1.541	0.1602	503.5	50.35
2	27.26	13.63	3.268	1.541	0.1871	432.1	43.21
3	33.16	16.58	2.700	1.541	0.1761	465.5	46.55
4	36.14	18.07	2.484	1.541	0.2291	360.7	36.07
5	37.91	18.96	2.371	1.541	0.159	522.4	52.24
6	38.57	19.28	2.332	1.541	0.3072	270.9	27.09
7	42.95	21.47	2.104	1.541	0.1557	542.2	54.22
8	45.89	22.94	1.976	1.541	0.1643	519.2	51.92

Table H.4 (Continued): XRD results for waste cockle shell

9	50.28	25.14	1.813	1.541	0.1695	512.0	51.20
10	52.46	26.23	1.743	1.541	0.1664	526.3	52.63
11	53.01	26.50	1.726	1.541	0.1731	507.1	50.71
Average crystalline size							46.93

Table H.5: XRD results for CaO catalyst prepared via calcination method

No.	2theta(°)	theta(°)	d-spacing(Å)	wavenumber	FWHM(°)	L(Å)	Crystalline size (nm)
1	32.18	16.09	2.779	1.541	0.1024	798	79.8
2	37.34	18.67	2.406	1.541	0.1007	823.5	82.35
3	53.84	26.92	1.701	1.541	0.1068	825.0	82.50
4	64.14	32.07	1.451	1.541	0.1092	848.9	84.89
5	67.36	33.68	1.389	1.541	0.1061	889.8	88.98

Table H.5(Continued): XRD results for CaO catalyst prepared via calcination method

Average crystalline size 83.71

Table H.6: XRD results for hydrated CaO

No.	2theta(°)	theta(°)	d-spacing(Å)	wavenumber	FWHM(°)	L(Å)	Crystalline size (nm)
1	34.17	17.08	2.622	1.541	0.1574	522.2	52.22
2	50.86	25.43	1.794	1.541	0.1487	585.0	58.50
3	54.42	27.21	1.685	1.541	0.1782	495.7	49.57
4	62.66	31.33	1.481	1.541	0.1629	564.6	56.46
5	71.86	35.93	1.313	1.541	0.1605	604.5	60.45
Average crystalline size							55.44

Table H.7: XRD results for nano CaO catalyst prepared via thermal hydration-dehydration treatment.

No.	2theta(°)	theta(°)	d-spacing(Å)	wavenumber	FWHM(°)	L(Å)	Crystalline size (nm)
1	32.25	16.13	2.773	1.541	0.1839	444.7	44.47
2	37.41	18.70	2.402	1.541	0.1942	427.1	42.71
3	53.91	26.96	1.699	1.541	0.2094	420.9	42.09
4	64.20	32.10	1.450	1.541	0.2173	426.8	42.68
5	67.42	33.71	1.388	1.541	0.2258	418.2	41.82
Average crystalline size							42.75

Table H.8: XRD results for nano CaO catalyst prepared under different parameters.

No.	2theta(°)	theta(°)	d-spacing(Å)	wavenumber	FWHM(°)	L(Å)	Crystalline size (nm)
Effects of hydration h							
3_650_3							
1	32.27	16.14	2.772	1.541	0.2152	380.0	38.00
2	37.43	18.72	2.401	1.541	0.2218	374.0	37.40
3	53.94	26.97	1.698	1.541	0.2439	361.4	36.14
4	64.19	32.09	1.450	1.541	0.168	552.0	55.20
5	67.45	33.73	1.387	1.541	0.3895	242.5	24.3
6	79.82	39.91	1.201	1.541	0.2967	345.2	34.5
Average crystalline size							37.58
4h_650_3h							
1	32.19	16.09	2.779	1.541	0.2032	402.4	40.24

Table H.8 (Continued): XRD results for nano CaO catalyst prepared under different parameters

2	37.35	18.68	2.406	1.541	0.2209	375.4	37.54
3	53.84	26.92	1.701	1.541	0.185	476.3	47.63
Average crystalline size							41.80
<hr/>							
5h_650_3h							
1	32.32	16.16	2.767	1.541	0.2038	401.3	40.13
2	37.48	18.74	2.397	1.541	0.2023	410.1	41.01
3	54.01	27.00	1.696	1.541	0.2315	380.9	38.09
4	64.31	32.16	1.447	1.541	0.2503	370.7	37.07
5	67.54	33.77	1.386	1.541	0.2303	410.4	41.0
6	79.82	39.91	1.201	1.541	0.2967	345.2	34.5
Average crystalline size							38.64

6h_650_3h							
1	32.34	16.17	2.766	1.541	0.2205	371.0	37.10
2	37.51	18.76	2.396	1.541	0.2301	360.6	36.06
3	54.08	27.04	1.695	1.541	0.2315	381.0	38.10
4	64.42	32.21	1.445	1.541	0.28	331.6	33.16
5	67.63	33.81	1.384	1.541	0.3	315.2	31.5
Average crystalline size							35.19

Effects of recalcination temperature							
6h_650_3h							
1	32.34	16.17	2.766	1.541	0.2205	371.0	37.10
2	37.51	18.76	2.396	1.541	0.2301	360.6	36.06
3	54.08	27.04	1.695	1.541	0.2315	381.0	38.10
4	64.42	32.21	1.445	1.541	0.28	331.6	33.16

Table H.8(Continued): XRD results for nano CaO catalyst prepared under different parameters

5	67.63	33.81	1.384	1.541	0.3	315.2	31.5
Average crystalline size							35.19
6h_750_3h							
1	32.23	16.12	2.775	1.541	0.1643	497.7	49.77
2	37.38	18.69	2.404	1.540	0.1564	530.2	53.02
3	53.89	26.94	1.700	1.541	0.1686	522.7	52.27
4	64.19	32.10	1.450	1.541	0.1972	470.2	47.0
5	67.41	33.70	1.388	1.541	0.1683	561.1	56.1
6	79.69	39.84	1.202	1.541	0.1766	579.4	57.9
Average crystalline size							52.69
6h_850_3h							
1	32.23	16.12	2.775	1.541	0.1502	544.4	54.44

Table H.8: XRD results for nano CaO catalyst prepared under different parameters

2	37.39	18.69	2.403	1.541	0.1528	542.8	54.28
3	53.89	26.95	1.700	1.541	0.1502	586.7	58.67
4	64.19	32.09	1.450	1.541	0.1592	582.5	58.25
5	67.41	33.70	1.388	1.541	0.1539	613.6	61.4
6	79.69	39.84	1.202	1.541	0.1808	565.9	56.6
Average crystalline size							57.27
<hr/>							
6h_950_3h							
1	32.26	16.13	2.772	1.540	0.3265	250.4	25.04
2	37.42	18.71	2.401	1.540	0.3256	254.7	25.47
3	53.93	26.97	1.699	1.541	0.332	265.5	26.55
4	64.06	32.03	1.452	1.540	0.4964	186.6	18.66
5	67.45	33.73	1.387	1.540	0.2334	404.6	40.5

Table H.8 (Continued): XRD results for nano CaO catalyst prepared under different parameters

							Average crystalline size	27.24
Effects of recalcination duration								
6h_650_2h								
1	32.17	16.08	2.780	1.541	0.1903	429.6	42.96	
2	37.32	18.66	2.407	1.541	0.2002	414.2	41.42	
3	53.83	26.91	1.702	1.541	0.2138	412.1	41.21	
4	64.13	32.06	1.451	1.541	0.2113	438.7	43.87	
5	67.35	33.68	1.389	1.541	0.2593	364.1	36.4	
6	79.65	39.82	1.203	1.541	0.295	346.7	34.7	
							Average crystalline size	40.09
6h_650_3h								
1	32.34	16.17	2.766	1.541	0.2205	371.0	37.10	

Table H.8 (Continued): XRD results for nano CaO catalyst prepared under different parameters

2	37.51	18.76	2.396	1.541	0.2301	360.6	36.06
3	54.08	27.04	1.695	1.541	0.2315	381.0	38.10
4	64.42	32.21	1.445	1.541	0.28	331.6	33.16
5	67.63	33.81	1.384	1.541	0.3	315.2	31.5
Average crystalline size							35.19
<hr/>							
6h_650_4h							
86	32.26	16.13	2.773	1.541	0.2046	399.7	39.97
87	37.42	18.71	2.402	1.541	0.217	382.2	38.22
88	53.94	26.97	1.698	1.541	0.2701	326.4	32.64
89	64.25	32.13	1.448	1.541	0.2611	355.3	35.53
15	67.47	33.73	1.387	1.541	0.2667	354.2	35.42
16	79.76	39.88	1.201	1.541	0.239	428.4	42.84

Table H.8 (Continued): XRD results for nano CaO catalyst prepared under different parameters

							Average crystalline size	37.44
6h_650_5h								
95	32.24	16.12	2.774	1.541	0.4283	190.9	19.09	
96	37.38	18.69	2.404	1.541	0.376	220.6	22.06	
97	54.54	27.27	1.681	1.541	1	88.4	8.84	
98	64.17	32.08	1.450	1.541	0.496	186.9	18.69	
99	67.42	33.71	1.388	1.541	0.3933	240.1	24.0	
							Average crystalline size	18.54

Appendix I : EDX results

Table I.9: Average weightage of waste cockle shell

Samples	Average weightage (wt %)				
	C	O	Na	Mg	Ca
1	15.17	49.73	1.08	0.59	33.44
2	13.46	48.23	1.14	0.68	36.49
3	8.82	35.95	1.04	0.53	53.67
Average weightage	12.48	44.64	1.09	0.60	41.20

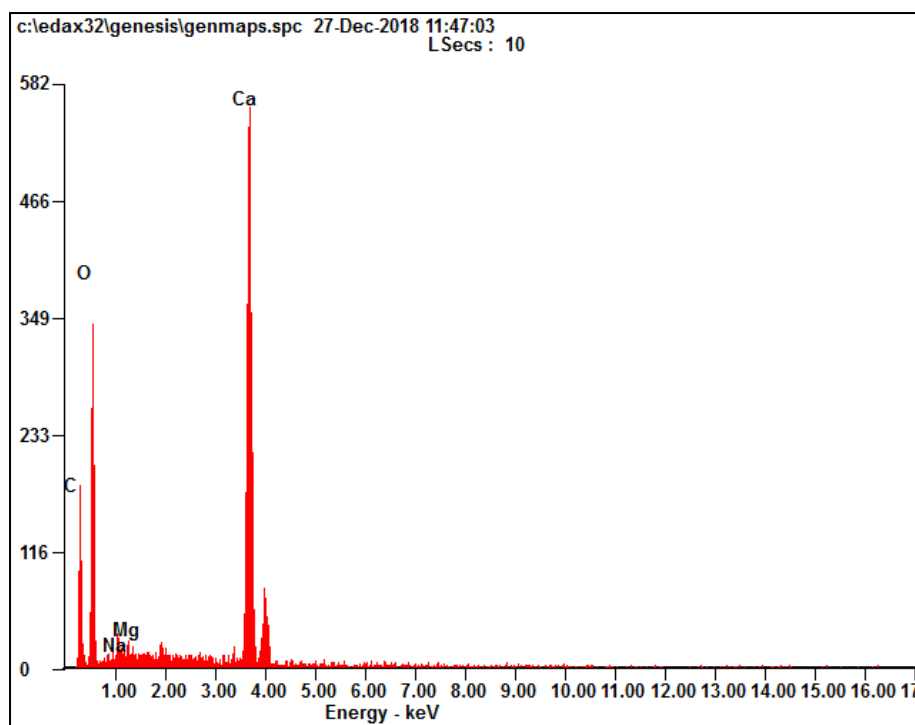


Figure I.6: Elemental compound available in waste cockle shell

Table I.10: Average weightage of CaO catalyst prepared via calcination method

Samples	Elemental weightage (wt %)					
	C	O	Na	Si	Al	Ca
1	6.93	30.50	1.25	0.50	0.75	60.06
2	6.58	32.55	1.61	0.68	0.88	57.69
3	18.71	30.95	0.00	0.00	0.75	47.67
Average weightage	10.74	31.33	0.95	0.39	0.79	55.14

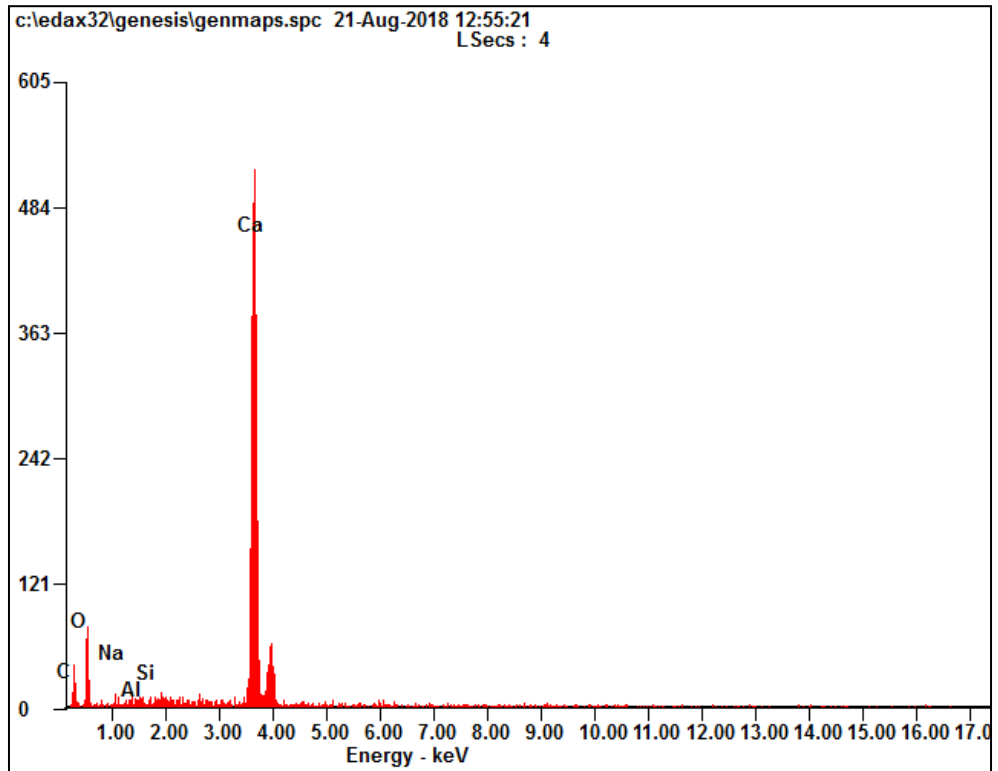


Figure I.7: Elemental compound available in CaO catalyst prepared via calcination method

Table I.11: Average weightage of hydrated CaO (6 h hydration)

Samples	Elemental weightage (wt %)		
	C	O	Ca
1	6.78	28.91	64.31
2	6.06	38.17	55.77
3	8.13	42.87	49.00
Average weightage	6.99	36.65	56.36

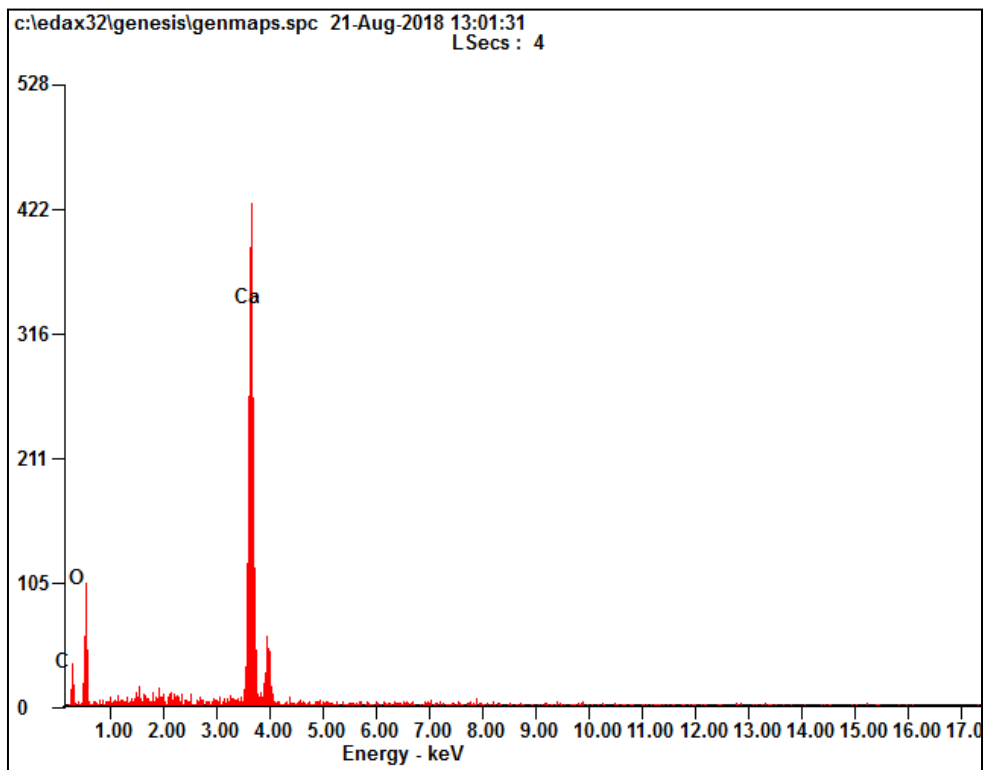


Figure I.8: Elemental compound available in hydrated CaO

Table I.12: Average weightage of different parameters

Samples	Elemental weightage (wt %)		
	C	O	Ca
Effect of hydration duration			
3_650_3			
1	4.99	25.97	69.04
2	4.06	40.30	55.64
3	5.76	38.95	55.29
Average weightage	4.94	35.07	59.99
4_650_3			
1	4.92	40.02	55.06
2	4.88	40.62	54.50
3	5.31	43.05	51.63
Average weightage	5.04	41.23	53.73
5_6503_			
1	5.77	26.48	67.75
2	4.42	24.64	70.94
3	4.52	30.42	65.06
Average weightage	4.90	27.18	67.92
6_650_3			
1	2.04	23.48	74.48
2	2.42	1.99	77.59
3	2.42	22.70	74.88
Average weightage	2.29	16.06	75.65

Table I.12 (Continued): Average weightage of different parameters

Effect of recalcination temperature

6_650_3

1	2.04	23.48	74.48
2	2.42	1.99	77.59
3	2.42	22.70	74.88
Average weightage	2.29	16.06	75.65

6_750_3

1	5.01	22.35	72.65
2	4.38	46.46	48.71
3	6.35	49.06	44.59
Average weightage	5.25	39.29	55.32

6_850_3

1	4.57	46.62	48.80
2	4.62	33.29	62.09
3	4.90	45.69	49.42
Average weightage	4.70	41.87	53.44

6_950_3

1	3.44	43.06	53.50
2	3.97	17.66	78.38
3	3.59	26.08	70.33
Average weightage	3.67	28.93	67.40

Effect of recalcination duration

6_650_2

Table I.12 (Continued): Average weightage of different parameters

1	3.39	31.28	65.33
2	3.36	39.80	56.84
3	2.78	28.85	68.36
Average weightage	3.18	33.31	63.51
<hr/>			
6_650_3			
1	2.04	23.48	74.48
2	2.42	1.99	77.59
3	2.42	22.70	74.88
Average weightage	2.29	16.06	75.65
<hr/>			
6_650_4			
1	5.48	26.65	67.87
2	4.97	29.04	65.99
3	5.44	34.12	60.43
Average weightage	5.30	29.94	64.76
<hr/>			
6_650_5			
1	3.06	42.34	54.60
2	3.32	31.50	65.18
3	2.68	47.50	49.82
Average weightage	3.02	40.45	56.53
